THE UNIVERSITY
of EDINBURGH

Understanding the Heterogeneity of Senescence and Ageing at the Single-Cell Level

Nattaphong Rattanavirotkul

Presented for the degree Doctor of Philosophy

University of Edinburgh

2019

PhD – The University of Edinburgh – 2019

Declaration

The data presented in this thesis was obtained in experiments carried out by research groups from three universities, the University of Edinburgh, the University of Glasgow and Brown University. I declare that this thesis is an original report of my research, has been written by me and has not been submitted for any previous degree. The experimental work is almost entirely my own work; the collaborative contributions have been indicated clearly and acknowledged. Due references have been provided on all supporting literatures and resources. I declare that this thesis was composed by myself, that the work contained herein is my own except where explicitly stated otherwise in the text, and that this work has not been submitted for any other degree or professional qualification.

…… Date ……12/12/2019……

Nattaphong Rattanavirotkul

Contents

Acknowledgements

In my journey to becoming a scientist, no challenge has ever been more formidable than what I encountered during this PhD. It was a rather shaky beginning, but with all the profound goodness that I received from Tamir Chandra, I managed to make it through to the end. To me, Tamir has been more than a supervisor. I benefited, and I still do, from his intellectual guidance as much as moral and personal support. I learned and I grew tremendously throughout my 4 years with him. The academic experience that I was fortunate enough to have would have been incomplete without him.

I also extend my sincere thanks to Professor Chris Ponting, who agreed to supervise me here at IGMM and is always kind and patient to me. Every meeting with him provided me with a thought-provoking discourse on how to work as a scientist.

My special thanks and gratitude must go to Kristina Kirschner, who had witnessed every stage of my PhD study. Working with and learning from her has been an inspiring and invaluable experience.

I would like to thank Jeanette Baran-Gale for her guidance and advice on the computational approaches employed in this thesis. The analysis of several single-cell data would have been impossible without her expertise and patience.

I was deeply touched by the supportive environment at IGMM, particularly members of the Advanced Imaging Team, who never hesitated to help out with microscopy techniques. I thank Harris Morrison, Laura Murphy, Matt Pearson and Ann Wheeler for their assistance in troubleshooting all the issues with microscopes.

Juan-Carlos Acosta and members of his lab, Nuria, Andrea and Priya, had always been sincerely generous, and I was most thankful and humbled to them, our close collaborators who kindly offered a variety of cell lines and lent me a helping hand in times of need.

A big and special thank you is due to all my friends and colleagues, past and present, whose names go unmentioned in this limited space. I owe a great debt to them all for their continuous encouragement and friendships, without which my life in the UK would have been empty and colourless.

I am forever indebted to the Sanger Institute, the Royal Thai Government and the Chandra lab for financially supporting me to the greatest extent of their capacities. A life without money is indeed impossible.

Lastly, my greatest gratitude and debt is owed to my wonderful parents, lovely younger brother and benevolent aunt. My parents know nothing about science, let alone the biology of ageing or senescence, but are very happy, excited and proud to have seen me pursue research in the UK and complete every study. And I, too, am very happy and grateful to have their unconditional love and support.

Lay Abstract

Cellular senescence is a common stress response in aged organs or malfunctioning cells, such as those that might became cancerous. Cellular senescence tries to prevent these cells from harming the organism, for example by preventing cancer. Once cells become senescent, they interact with surrounding cells and induce a "secondary" senescence response in them, spreading senescence within the tissue. However, if senescent cells persist or there are too many of them they can accelerate ageing and age-related disease. The discovery that senescent cells can be harmful has led to research and development in drugs that can specifically eliminate senescent cells, called senolytica. Examining the RNA in single-cells allowed, we have captured the complex interactions between senescent and non-senescent cells that get lost when measuring at the tissue level.

The first part of this research study shows that primary and secondary senescent cells are quite distinct from each other, and might fulfil different roles. These findings also raise the question of which cells are responsible for the negative effects seen in the persistence of senescent cells and whether this needs to be considered when developing new drugs (senolytica). The work has revealed an additional mechanism by which cells mediate secondary senescence after cancerous stress, called Notch signalling. Notch signalling relies on cells directly contacting each other. This study also highlights how diverse the senescence response is and how little we know about the role secondary senescence plays in health and disease.

In the second part of this research, we explored Hutchinson-Gilford progeria syndrome (HGPS). It is an early-onset form of a rare autosomal dominant genetic diseases characterised by clinical features of premature ageing and has been extensively studied as a model for the ageing process. We investigated the proportion of cells affected by the progeria condition in a mouse model, how these cells behaved phenotypically and transcriptionally. A better characterisation of phenotypes and transcriptional profiles of progeria cells could ultimately help improve our understanding of the ageing process per se, as well as open a window for safe and effective intervention.

Abstract

This thesis contains two main research projects, both of which demonstrate the power of single-cell approaches in the interrogation of complex biological systems. The first part of my studies focuses on cellular heterogeneity in oncogene-induced senescence (OIS).

Senescence is a cellular response triggered by diverse stresses. It can be beneficial, as a tumour suppressive response to oncogene activation, or detrimental as it drives inflammation and pathology of ageing. Senescence can be transmitted to neighbouring cells through secreted factors of the senescence associated secretory phenotype (SASP), a phenomenon known as secondary senescence. Thus far, primary and secondary senescence have been considered identical phenotypes. Here, I used single-cell transcriptomics in co-culture systems to decipher heterogeneity between primary and secondary Ras-induced senescence and observed two distinct transcriptional trajectories, one marked by Ras and the other by Notch. Furthermore, secondary senescence *in vitro* and *in vivo* were found to be driven by Notch, rather than by the SASP alone as previously thought. In conclusion, primary and secondary senescence showed functional diversification and were distinct molecular endpoints.

In the second part of this thesis, I explored cellular heterogeneity in Hutchinson-Gilford progeroid syndrome (HGPS), which represents a sporadic, rare, autosomal dominant genetic disease characterised by clinical features of premature ageing and has been extensively studied as a model for the ageing process.

Ageing remains indisputably the largest risk factor for the majority of prevalent human pathologies such as cancer, cardiovascular diseases and neurodegenerative disorders. An attractive interpretation of ageing is that cells age as a result of a 'toxic environment' created from damaged or defected cells, which then toxically impact on their healthy and normal neighbouring cells and tissues. Studies that lend support to this model reported that removal of senescent cells, namely stably non-proliferating cells induced by insulting stimuli, from mouse tissues can delay the onset of age-associated disorders in adipose tissues, skeletal muscles and eyes, as well as extend their healthy lifespan. Provided that persistent secretion of inflammatory cytokines and other systemic factors during chronic senescence can favour both degenerative and hyperplastic pathologies, it is plausible that accumulation of senescent cells might systematically promote an ageing environment and therefore the ensuing loss of cellular function. A study in mice whose cells were half progeria and half normal demonstrated that these mosaic mice age normally, with no overt abnormalities in the proliferative capacity in cell culture or increased levels of progeria markers, suggesting cell-extrinsic mechanisms in the pathogenesis of progeria. This finding further supports the interpretation of the toxic ageing model. Using confocal microscopy and single-cell technologies, I aimed to understand the heterogeneity in progeria by quantifying the proportion of progeria cells that were compromised phenotypically and transcriptionally. By combining the morphological profiles with the transcriptional profiles, I hope to dissect the disease state of progeria and propose a mechanism by which organismal ageing occurs. The molecular insight into the pathophysiology this premature ageing disease will help pave the way for novel development of therapeutic strategies against age-related disorders with the improvement of both lifespan and healthspan

Figures

Tables

Abbreviations

ATAC-Seq	Assay for Transposase-Accessible Chromatin using sequencing
BrdU	5-bromo-2'-deoxyuridine
C/EBPβ	CCAAT-enhancer-binding proteins
CCL2	C-C Motif Chemokine Ligand 2
Ccng2	Cyclin G2
CDK4	Cyclin-dependent kinase 4
CDK6	Cyclin-dependent kinase 6
CDKN1A	cyclin-dependent kinase 1a
CDKN2B	cyclin-dependent kinase inhibitor 2b
CIP1/WAF1	Wild type p53-activated fragment 1/Cdk-interacting protein 1
c-Myc	c-Master Regulator of Cell Cycle
D3E	Discrete Distributional Differential Expression
DAPI	4’-6-diamidine-2-phenyl indole
DDR	DNA damage response
DE	Differential Expression
DNA	Deoxyribonucleic acid
DNA-SCARS	DNA segments with chromatin alterations reinforcing senescence
dnMAML1	Dominant negative mastermind-like protein 1
DSB	Double-strand breaks
EdU	5-ethynyl-2′-deoxyuridine
EV	empty vector
FACS	Fluorescence-activated cell sorting
Fgf2	Fibroblast growth factor 2
FPKM	Fragments Per Kilobase Million
Gas1	Growth arrest-specific 1
GFP	Green Fluorescent Protein
GSEA	Gene Set Enrichment Analysis
H3K27me3	Histone H3 lysine 27 trimethylation
H3K9me3	Histone H3 lysine 9 trimethylation
HGPS	Hutchinson-Gilford progeria syndrome
IL-1	Interleukin-1
IL-1β	Interleukin-1 beta
IL-6	Interleukin-6
IL-8	Interleukin-8
IPA	Ingenuity Pathway Analysis
JAG1	Jagged1
Klf4	Kruppel-like factor 4
KO	Knockout
LMNA	Lamin A/C
LMNB1	Lamin B1

MAML1	Mastermind-like protein 1
MDM2	Mouse double minute 2
NF-κB	Nuclear factor kappa-light-chain-enhancer of activated B cells
Ngf	Nerve growth factor
NIS	Notch-induced senescence
NLRP3	NLR Family Pyrin Domain Containing 3
Oct-4	Octamer-binding transcription factor 4
OIS	Oncogene-induced senescence
PRC	Polycomb repressive complexes
QC	Quality control
RB	Retinoblastoma
RIS	Ras-induced senescence
RNA	Ribonucleic acid
SAHF	Senescence-associated heterochromatin foci
SASP	Senescence-associated secretory phenotype
SA-β-gal	Senescence-associated β-galactosidase
SC3	Single-cell Consensus Clustering
SCDE	Single-Cell Differential Expression
scRNA-seq	Single-cell RNA sequencing
Smad3	SMAD family member 3
Smart-Seq	Switching mechanism at 5′ end of RNA template sequencing
Sox2	Sex determining region Y
TGFβ	Transforming growth factor beta
UMI	Unique molecular identifier
VEGF	Vascular endothelial growth factor
WT	Wild-type
YFP	Yellow Fluorescent Protein
yH2AX	Gamma H2A histone family member X
Zmpste24	Zinc Metallopeptidase STE24
βNF	β-napthoflavone

Published, Presented and Submitted Work Relevant to This Thesis

Publication:

Teo, Yee Voan, Nattaphong Rattanavirotkul, Nelly Olova, Angela Salzano, Andrea Quintanilla, Nuria Tarrats, Christos Kiourtis, et al. 2019. "Notch Signaling Mediates Secondary Senescence." *Cell Reports* 27 (4): 997-1007.e5. https://doi.org/10.1016/j.celrep.2019.03.104.

Poster Presentation at the EMBO Conference on Cellular Signalling & Cancer Therapy

Secondary and a Subset of Primary Senescent Cells Result from Notch Signalling. Nattaphong Rattanavirotkul, Yee Voan Teo, Kristina Kirschner, Tamir Chandra.

Chapter 1: Introduction

1.1 Thesis Content

The main content of this thesis is based on the work published in *Cell Reports* titled "Notch Signalling Mediates Secondary Senescence" (Teo et al., 2019), of which I am a co-first author. The published article is available under the terms of the Creative Commons Attribution Licence (CC BY), which permits individuals to "copy and distribute the article, create extracts, abstracts and new works from the article, alter and revise the article, text or data mine the article and otherwise reuse the article commercially (including reuse and/or resale of the article) without permission from Elsevier." In each chapter of this thesis, I will give full credit to the original work and indicate any alterations made in figures or tables. The full references and relevant DOIs are also provided.

1.1.1 Thesis Statements and Questions

This thesis revolves around two research projects, both of which applied single-cell approaches to explore cellular heterogeneity within their respective contexts. The investigations were based on two thematic questions that have been framed and elaborated in what follows:

(1) Cellular senescence is characterised by an irreversible cell cycle arrest and has been implicated in tumour suppression, normal development, wound healing and ageing. Senescent cells differ from normal or quiescent cells in a prominent feature: the senescence-associated secretory phenotype (SASP), whose components include various signalling factors that affect surrounding cells and modify the microenvironment. These factors can serve to induce secondary senescence in neighbouring cells in a paracrine fashion. Meanwhile, secondary senescence can alternatively be triggered through cell-to-cell contact (juxtacrine). This leads to the first question: what mechanism dictates the induction of senescence through paracrine or juxtacrine communication? Differences between the transcriptional signatures of primary senescent cells and fully secondary senescent cells are also

understudied. Understanding the heterogeneity within the senescent population is a necessary task in order to fully understand secondary senescence and how it is induced.

(2) Hutchinson-Gilford progeria syndrome (HGPS) is an early-onset form of a rare autosomal dominant genetic disease characterised by clinical features of premature ageing. HGPS has been extensively used as a model to study human ageing, but the complete characterisation of phenotypic and transcriptional features of HGPS at the single-cell level remains a challenging task. The question here is: what is the proportion of HGPS cells that are compromised, phenotypically and transcriptionally? A better characterisation of phenotypes and transcriptional profiles of HGPS cells via the use of novel single-cell technologies could ultimately help improve our understanding of the disease state of HGPS and of the ageing process per se, as well as open a window for safe and effective intervention.

1.1.2 Thesis Aims

The aims of my studies can be seen as a single overarching theme: understanding the heterogeneity of senescence and ageing at the single-cell level. Overall, I aimed to address two sub-goals in this thesis:

(1) The first goal of this research was to investigate the heterogeneity within the oncogene-induced senescence (OIS) population using single-cell technologies.

(2) The second part of the thesis is dedicated to examining single-cell heterogeneity in HGPS through the use of single-cell technologies.

1.1.3 Thesis Structure

The thesis is divided into six chapters and covers two lines of research:

(1) Chapter 1 is the introductory chapter and deals with the preliminary background knowledge about cellular senescence and its mechanisms, modes of action and biological significance.

(2) Chapter 2 describes the research materials and methodologies employed to investigate the research problems.

(3) Chapter 3 describes the work on OIS as featured in our paper (Teo et al., 2019).

(4) Chapter 4 continues to discuss further and key experimental evidence, *in vitro* and *in vivo*, which brought the study of cellular heterogeneity in OIS to completion.

(5) Chapter 5 is devoted to a study of cellular heterogeneity in Hutchinson-Gilford progeria syndrome (HGPS). The chapter will contain a separate introductory section for HGPS and its relevance to human ageing and age-associated disorders.

(6) Chapter 6 presents the conclusions and implications derived from the two projects as well as future studies that need to be carried out.

1.2 Cellular Senescence and Ageing

1.2.1 Origin: the Biology of Telomeres

Cellular senescence refers to a process by which the cell cycle comes to a stable arrest accompanied by stereotyped phenotypic changes and implicated in various biological processes from cancer to ageing (van Deursen 2014). The origin of cellular senescence dates back to 1961, when Leonard Hayflick discovered that human diploid cells cease to proliferate after a limited number of passages in culture, a phenomenon called replicative senescence (Hayflick and Moorhead 1961). This finite capacity for cell division is still known as the 'Hayflick Limit', which since then has given rise to the speculation that replicative senescence plays a causal role in ageing at the cellular level. Studies of the end of the replicative lifespan have laid an important foundation for the theory that cellular senescence drives the ageing process in a cell-autonomous manner, exhausting replication resources required for tissue repair, regeneration and homeostasis.

The mechanism behind the maximum proliferative potential of cells is now well understood. In successive cell cycles, the telomeres, the chromosomal termini containing highly repetitive DNA sequences (TTAGGG repeats), are shortened as a result of the inability of DNA polymerases to completely replicate linear chromosomes (Olovnikov 1973; Watson 1972). Functional telomeric DNA is capped with a protective multiprotein complex known as shelterin, which together prevents chromosomal ends from being recognised as sites of DNA-double strand breaks from DNA damage response (DDR) proteins (de Lange 2005). Progressive telomere attrition, therefore, ultimately uncaps the protective ends, propagating persistent DNA damage signals and evoking DDR-mediated senescence (Fagagna et al., 2003). However, telomere erosion can be circumvented in cells that express telomerase, a reverse transcriptase specialised in replenishing and maintaining the length of telomeric regions. Most tumour cells, germ cells and embryonic stem cells are examples of telomerase-expressing cells with unlimited proliferative capacity. In fact, long-term maintenance of the telomeres and upregulation of telomerase activity represent one of the hallmarks of cancer, where replicative senescence is bypassed during malignant transformation (Hastie et al., 1990).

Given the roles of the telomeres in determining the trajectory of cellular replication and in maintaining genome integrity, much evidence has accrued to support the causative

association between telomere shortening and ageing. A lack of the telomerase gene in mice leads to premature ageing pathologies (H.-W. Lee et al., 1998). Such deterioration can be mitigated by transiently activating telomerase expression. Similarly, studies of telomere length in humans have presented evidence that supports the interpretation that shortened telomere length correlates with age-associated diseases and increased rates of mortality, and is therefore a potential biomarker of ageing (Harley, Futcher, and Greider 1990; Chang and Harley 1995; Rudolph et al., 2000; Cawthon et al., 2003). Yet the telomere theory of ageing has been received with scepticism and challenges in the past decade, as many cross-sectional and longitudinal studies failed to observe a significant relationship between telomere length and increased risk of mortality (Njajou et al., 2009; Bischoff et al., 2006; Martin-Ruiz et al., 2005). This is further complicated by reports from mouse models which do not conform to telomere-mediated replicative ageing and whose telomerase expression is not required for cellular immortalisation (Rudolph et al., 1999; Hande et al., 1999). It appears that the biological consequences of telomere dynamics on ageing diverge in different organisms and the exact reason for these contradictory results is still not revealed. A possible explanation is likely to involve factors beyond replicative senescence, which in itself offers only a partial glimpse into the many different contexts in which cellular senescence is established.

1.2.2 Molecular Basis: Molecular Players that Arrest Cells and Their Markers

The comprehensive model of cellular senescence is still in a nascent stage of development, but massive research efforts have contributed to a growing list of stimulators and our improved understanding of molecular mechanisms that underlie senescence-mediated cell arrest. In addition to and independent of telomere attrition, a variety of stressors (oncogene activation, oxidative damage, mitochondrial dysfunction and inflammation) and damaging agents (radiation and genotoxins) are canonically known to induce double-strand breaks (DSBs) and DNA lesions that are subsequently sensed by the DDR system [Figure 1.1]. DDR components exert their effects through activation of the p53 tumour suppressor, which in turn induces $p21^{CIP1/WAF1}$ (hereafter referred to as p21). Upregulation of p21 inhibits the formation of the cyclin-dependent kinases (CDK4 and CDK6), preventing the phosphorylation of the retinoblastoma tumour suppressor (RB) to become an active form, thereby inhibiting the subsequent progression of the G1 phase of the cell cycle.

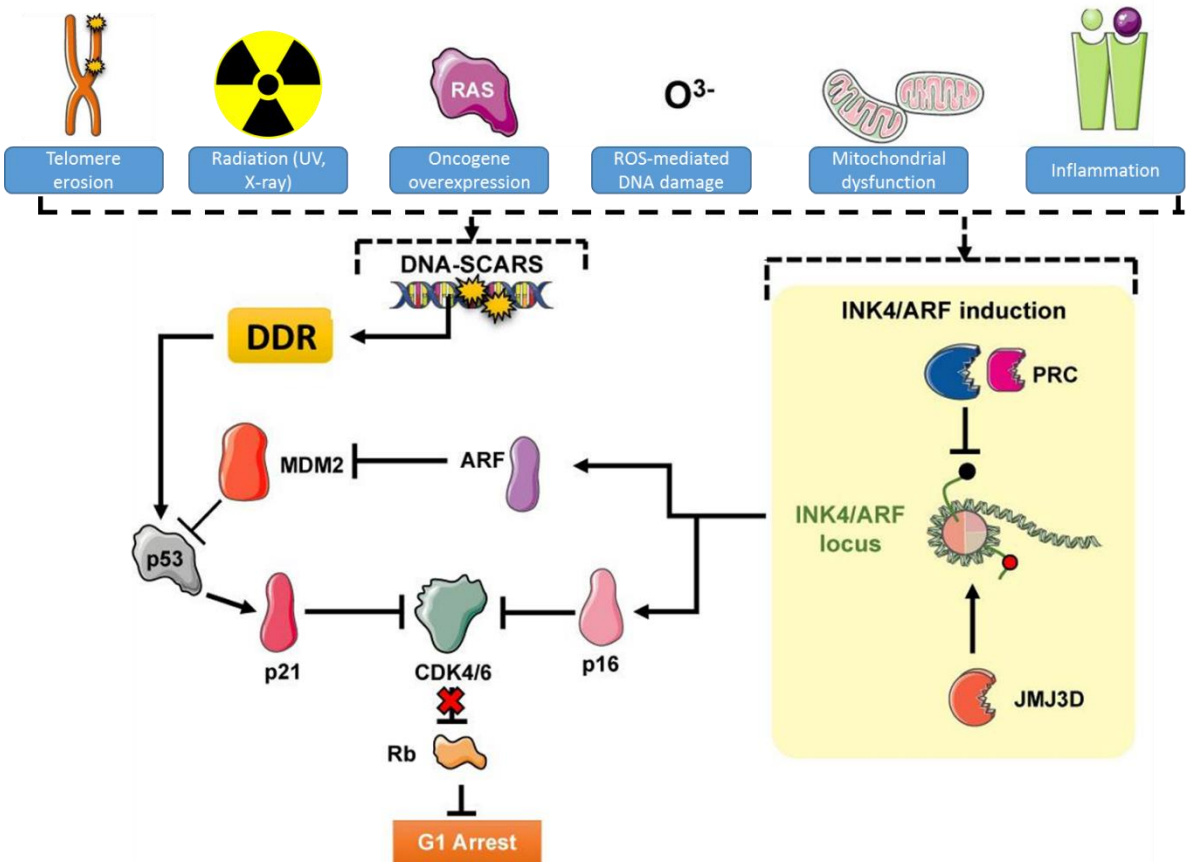

Figure 1.1: Molecular Pathways of Cellular Senescence; license number granted: 4663140192195 .

Taken and modified from McHugh and Gil 2018.

Regulation of the senescence growth arrest is achieved by two main pathways: p16INK4a/Rb and p53/p21CIP1, both of which converge on repression of CDK4/6. Under normal conditions, the INK4A/ARF locus is repressed by Polycomb repressive complexes (PRCs) and becomes activated during senescence. Activation of the p53/p21CIP1 pathway occurs downstream of the DNA damage response (DDR) from repair-resistant DNA segments with chromatin alterations reinforcing senescence (DNA-SCARS).

Alternatively, the $p16^{INK4a}$/RB tumour suppressor network presents a different means by which senescence establishment is independent of the DDR-p53 axis. The pathway mediates its anti-proliferative actions through the *INK4/ARF* locus, which encodes $p16^{INK4a}$ (hereafter referred to as p16) and ARF. The former serves directly to repress CDK4/6, while the latter cross-talks with the p53 pathway by inhibiting MDM2, a ubiquitin ligase for p53. The activation of the *INK4/ARF* locus is under epigenetic regulation by Polycomb repressive complexes (PRCs), histone modifiers that deposit repressive H3K27me3 marks to silence *INK4/ARF* gene expression. Triggers of senescence displace PRCs and remove the repressive marks to allow the onset of p16-mediated cell cycle arrest. For an additional layer of epigenetic control, p16 expression is also maintained in a permissive state by the histone demethylase JMJD3 during senescence.

While it is now clear that cellular senescence can be triggered by a plethora of stimuli, external and internal, senescent cells exhibit morphological changes and several markers that allow them to be detected and quantified. One of the gold-standard biomarkers frequently used to distinguish senescent cells from other non-dividing cells (quiescent or terminally differentiated cells) is senescence-associated β-galactosidase (SA-β-gal) activity, assayed at suboptimal pH (pH 6.0). This is believed to reflect the increased autophagy and lysosomal content during the execution of the senescence programme (Muñoz-Espín and Serrano 2014). Another canonical marker is elevated levels of p16, which indicate the activation of tumour suppressor networks. Senescent cells also secrete a panoply of extracellular proteins and pro-inflammatory factors, commonly known as the senescence-associated secretory phenotype (SASP), with potent effects on neighbouring cells. These SASP components point to the non-cell-autonomous function of cellular senescence, which will be discussed in depth later on.

Other notable features include the enlarged and flattened morphology, lack of the proliferation protein Ki67 or 5-bromodeoxyuridine (BrdU) incorporation, cessation of DNA

replication and presence of punctate DNA-dense, H3K9me3-rich senescence-associated heterochromatin foci (SAHF). However, given the heterogeneity of senescent cells, the application of these markers in defining the senescent state *in vitro* and *in vivo* remains limited and inconsistent. For example, a lack of SA-β-gal activity does not always compromise the ability of somatic cells to senesce (Lee et al., 2006). Likewise, the expression of p16, putatively the most reliable senescence biomarker, is absent in many forms of senescence such as telomere-mediated replicative senescence (Herbig et al., 2004; Beauséjour et al., 2003). These limitations imply that must the characterisation of senescence in any experimental model must be interpreted with caution and multiple markers should be used in combination.

Although none of these markers appears to be faithfully exclusive to or universally reliable for all types of senescence, it is generally accepted that most senescent cells display these characteristics reflecting the mechanistic relevance to the establishment and maintenance of the senescent state (S. Lee and Schmitt 2019). Overall, our molecular understanding of senescence demonstrates a complex and diverse nature of this phenomenon, with a collective phenotype resulting from multiple effectors and showing heterogeneous outcomes. As the field of senescence biology continues to evolve, *in vitro* and *in vivo* studies of senescence in the context of oncogenic signalling and tumour suppression pathways have greatly assisted in an ongoing search for a robust senescence signature and helped to reveal different levels of biological functionality of cellular senescence per se.

1.2.3 Oncogene-induced Senescence: Causes and Mechanisms

Oncogenic activation represents a dominant event that confers cancer cells the proliferative advantage critical for tumour growth and development. Oncogene-induced senescence (OIS) therefore refers to an irreversible state of proliferative arrest in response to oncogenic stimuli. OIS was first described in primary human lung fibroblasts IMR90 where expression of the oncogene $Hras^{V12}$, a mutational form of *Ras*, provoked cell cycle arrest phenotypically reminiscent of replicative senescence (Serrano et al., 1997). Unlike replicative senescence, OIS is independent of telomere attrition and requires the engagement of p16/RB and p53 pathways. Early studies have shown that inactivation of p53 or its regulator $p19^{Arf}$ in murine cells promotes Ras-induced malignant transformation, while the re-introduction of p53

expression regresses tumour growth and is accompanied by markers of cellular senescence (Kamijo et al., 1997; Ventura et al., 2007; Xue et al., 2007). OIS cells also express high levels of p16 and can escape from senescence and resume cell division if p16 expression is low (Rayess, Wang, and Srivatsan 2012). The accumulation of RB, which functions downstream of p16 by repressing E2F-target genes involved with DNA replication, is essential to the maintenance of OIS. This was shown in Ras-senescent cells that escape from cell arrest with the disruption of a p21-mediated cell cycle checkpoint following RB elimination (Chicas et al., 2010).

However, the important roles of p53 and p16 in OIS have faced contentious challenges from later studies which have demonstrated that loss of p16 does not bypass senescence and that p53 and p16 are dispensable for initiating and maintaining OIS. For instance, human melanocytes undergo OIS without requiring p53 or p16 (Zhuang et al., 2008). Discordant results have also been reported from other studies where abrogation of p16 did not affect Ras-induced senescence in melanocytes (Denoyelle et al., 2006). This is also the case in human mammary epithelial cells, which undergo p16- and p53-independent OIS in response to aberrant Ras activation that relies on TGF- β signalling (Cipriano et al., 2011). It appears the extent to which p53 and p16 contribute to the OIS programme varies from cell type to cell type. Unlike the well-documented triggers and components upstream of senescence cascades, little is known about how downstream mediators and effectors interact at the molecular level to enforce OIS.

A defined model of replicative senescence suggests a clear, linear signalling cascade whose stressors (telomere erosion) activates the DNA damage response (DDR) machinery (sensors), which then engages p53 and p21 (effectors) to manifest the senescent phenotype (Muñoz-Espín and Serrano 2014). For OIS, the prevailing view until now is that persistent DNA damage and the ensuing gross genomic abnormalities are the intrinsic requirements for OIS establishment and maintenance [Figure 1.2] (Di Micco et al., 2006; Bartkova et al., 2006). It was shown that H-RAS^{V12} activation induces robust DDR signalling, which then causes senescence (Di Micco et al., 2006). Cells undergoing OIS displayed increased phosphorylation of DDR elements that are associated with DNA damage in different cell cycle stages, whereas inactivation of these DDR gene products abolished OIS. It was next revealed that senescence was preceded by a hyper-proliferative phase in which activation of the H-RAS oncogene was followed by an increase in the number of simultaneously active DNA replication origins. Increased activity of origin firing was associated with fork progression asymmetry and higher

rates of fork stalling. An additional alteration in DNA replication observed was re-firing of the same origin, induced by H-RAS expression. Indeed, OIS was shown to engage DDR by driving prematurely terminated DNA replication forks and double-strand breaks (Bartkova et al., 2006). Disabling the ataxia telangiectasia mutated (ATM), a kinase sensor of DNA double-strand breaks, contributed to bypass of OIS and an increase in tumour size and invasiveness in a mouse model.

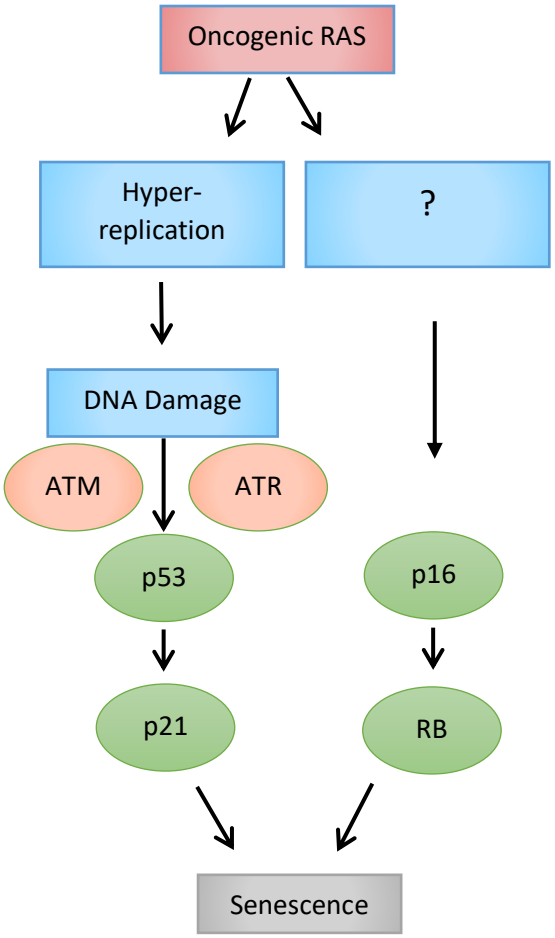

Figure 1.2: Model of Oncogene-Induced Senescence.

The established theory of oncogene-induced senescence posits that OIS induction is driven by hyper-proliferation following oncogene overexpression. This results in the accrual of DNA damage, which elicits a DNA damage response (DDR) to transduce signals via key effector pathways (here the p53/p21 and the p16/RB networks) and to execute senescence. Adapted from Nardella, 2011 (Nardella et al., 2011).

Conversely, DDR can be activated in the absence of DNA damage as shown in E1A+Ras-transformed rodent fibroblasts (Pospelova et al., 2009). Here, based on the comet assay, induction of senescence by p21 or p16 caused DDR activation without detectable DNA breaks. Furthermore, $HRAS^{G12V}$-expressing mammary epithelial cells senesced without the participation of DDR and inhibition of DDR gene products did not affect $NRAS^{Q61K}$-induced senescence in normal human melanocytes. These observations raise the possibility that instead of DNA lesions per se, other forms of damage are sensed by the DDR machinery or DDR itself may be dispensable in the process of OIS (Pankotai et al., 2009). In the light of this, the exact trigger of OIS-induced DDR activation has not been elucidated. If it is an actual elevation in DNA damage levels, the precise structure and genomic locations of DNA lesions as well as the extent of DNA damage generated remain unknown.

Although it is evident that DDR is a fundamental upstream signalling pathway in triggering and maintaining senescence in response to DNA damage in several settings, it is not known whether there are large-scale alterations in DNA pre-senescence and to what extent DNA damage acts as a sensor in OIS. And if there is no involvement of DNA damage, what is the sensor in OIS? Therefore, it appears that the role of DDR in mediating OIS is less straightforward in some experimental models and that pathways that lead to OIS are determined by several biological parameters, ranging from cell types, species, the nature of oncogenic insults and the microenvironment. One of the key challenges is to identify upstream signalling pathways that link oncogenic stimuli to downstream signalling events.

As investigation continues into the OIS cascade and the unknown nature of DNA damage, it is likely that new sensors of OIS and novel signalling pathways might be discovered. Insights into the type of DNA damage will also entail important consequences on how the dynamics of the tumour-suppressive state in OIS are viewed *in vitro* and *in vivo*.

1.2.4 Oncogene-induced Senescence *In Vivo*: the Anti- and Pro-Cancer Modulator

To date, it remains clear and unequivocal that OIS serves as a major barrier to the early stages of tumourigenesis. Multiple lines of evidence obtained from mouse models of cancer strongly advocate for the tumour-suppressive role of OIS. Conditional activation of oncogenic $KRAS^{V12}$ in lung and pancreas tissues resulted in neoplastic lesions, most of which were in the premalignant stage accompanied by senescence markers (Collado et al., 2005). Some adenocarcinomas were also induced, but they were negative for senescence markers. Another work in the same year reported an *in vivo* induction of OIS after NRAS overexpression in a Suv39h1-dependent, H3K9me-mediated response, halting mouse lymphoid cells from progressing into full-blown lymphomagenesis (Braig et al., 2005). An *in vivo* OIS response in premalignant neoplasia was also observed in the mouse prostate following inactivation of the tumour suppressor PTEN, but not in an advanced stage of prostate cancer where combined loss of PTEN and Trp53 was required (Chen et al., 2005).

Essentially, one of the strongest findings of OIS acting to counteract tumour progression emerged from *in vitro and in vivo* experiments in human melanocytic naevi (moles) (Michaloglou et al., 2005). These naevi are benign lesions remaining in the growth-arrested state with a low tendency to transform into malignancy and harbour mutations in *BRAF*, a downstream kinase effector of Ras and the most prevalent mutated proto-oncogene in melanoma. $BRAF^{V600E}$-expressing melanocytes contain several OIS markers, including proliferative arrest, p16 induction and increased SA-β-gal activity, in the absence of telomere shortening. The course of melanomagenesis thus often involves silencing or reversing BRAF-induced senescence. Together with the clear evidence for OIS induction in the cutaneous melanocytes of mice carrying endogenous $Braf^{V600E}$ (Dankort et al., 2009), the biological relevance and significance of OIS i*n vivo* has been confirmed. As one of the best-characterised examples of OIS *in vivo*, melanocytic naevi can persist in a stable proliferative arrest for decades before melanomagenesis occurs. It is thus interesting to understand how genomically stable the tumour suppressor state is before the escape of senescence takes place and cells progress to malignant melanoma.

In addition to being identified a fail-safe, tumour-protective mechanism, senescence also plays active roles in normal embryonic development, tissue homeostasis, wound healing, pathological processes and, putatively, ageing (Muñoz-Espín and Serrano 2014).

Paradoxically, the past decade has begun to witness the diverse and contradictory impacts of OIS on carcinogenesis. Beneath a simple, stable state of replicative cessation lies a hidden layer of metabolically active environments, internal and external of the senescent cells, capable of influencing, altering or even reversing the tumour-suppressive effects of OIS in a spatiotemporal manner. Coming into light are the previously unappreciated non-cell autonomous activities of OIS *in vivo* in promoting tumourigenesis by means of secreted factors of the SASP phenotype in the extracellular compartment (Pérez-Mancera, Young, and Narita 2014). The SASP encompasses immune modulators, inflammatory cytokines, chemokines, extracellular, growth factors and metalloproteinases that cannot only signal recruit immune cells, such as neutrophils, macrophages and natural killer (NK) cells, to eliminate cancer cells (Lesina et al., 2016; Iannello et al., 2013), but also provoke tumour-promoting responses under unfavourable physiological conditions. SASP factors released from OIS cells might promote migration of tumour cells or create an immunosuppressive microenvironment, encouraging proliferation, angiogenesis and metastasis, as shown in skin, prostate, liver cancer models (Malaquin et al., 2013; Laberge et al., 2015; Eggert et al., 2016).

Currently available evidence seems to indicate that the dual role of OIS on cancer pathogenesis is dependent on the tissue context, the composition of the SASP and duration of the senescent state. In this regard, an interesting goal is to selectively eliminate non-beneficial senescent cells that may prime their surrounding cells for malignancy while leaving the functionally advantageous senescent cells intact. Indeed, one elegant study established a transgenic mouse model in which p16-positive cells can be targeted for clearance (Baker et al., 2011). Chemical ablation of p16-expressing senescent cells attenuated age-related phenotypes, increased longevity and improved tissue rejuvenation in late life. A subsequent report also showed that selective elimination of senescent cells significantly reduced spontaneous tumour formation (Baker et al., 2016).

Hence, OIS can be conceptually viewed as *in vivo* antagonistic pleiotropy in action: it has an anti-tumourigenic function in the early phase of oncogenesis but switches to a deleterious, pro-tumourigenic event over time with advanced age. However, the questions of when and why precisely the twisted turn of senescence takes place are still unresolved. Unravelling how senescent cells interact with their microenvironment through short- and long-term secretion of SASP factors is key to understanding the complexity of senescent phenotypes, as well as to the current exploration of senolytic agents for selective clearance of disease-prone senescent cells.

1.2.5 Paracrine Senescence:

It is becoming increasingly appreciated that the definition of cellular senescence extends beyond the singular state of permanent cell cycle arrest, capturing multidimensional aspects of the effects of senescent cells on their surrounding cells with far-reaching biological significance. Logically, the ability of senescent cells to alter their microenvironment must, to a large extent, depend on paracrine signalling, which allows cell-to-cell communication by locally secreted molecules. Following the reports that OIS cells can act on themselves in an autocrine fashion to self-amplify the SASP programme, whose components include the inflammatory molecules IL-6 and IL-8, by continuously activating NF-κB and C/EBPβ (Acosta et al., 2008; Kuilman et al., 2008), paracrine transmission of senescence was described in an elegant experimental system in which OIS cells were co-cultured with normal cells (Acosta et al., 2013). The authors showed that OIS cells spread the senescence phenotype to their healthy neighbouring cells via the release of several soluble SASP proteins. By using quantitative proteomics and small-molecule inhibitor screens, they identified TGFβ, VEGF and CCL2 as part of the inflammasomes and secretomes that modulate paracrine senescence. It was further shown that IL-1 signalling functions as a key upstream regulator of the proinflammatory signalling and the SASP phenotype was suppressed when the NLRP3 inflammasome, which controls IL-1β, was inhibited.

Additional evidence has also highlighted the mechanistic relationship between oxidative stress, DNA damage and paracrine senescence through IL-1 and TGFβ secretion, showing that normal bystander cells can be induced to senesce as a result of DDR signalling (Hubackova et al., 2012). Also consistent with the non-cell autonomous activity of OIS in the context of tumourigenesis, paracrine senescence was observed in mouse and human models of OIS, presenting a link between the upregulation of SASP components and the induction of paracrine senescence *in vivo* (Acosta et al., 2013). More recently, it has been proposed that the paracrine transmission of senescence may apply to the processes of cellular reprogramming, as shown when SASP factors triggered senescence and favoured reprogramming by activation of Oct4, Sox2, Klf4 and c-Myc (OSKM or Yamanaka factors) in non-senescent cells (Mosteiro et al., 2018). These studies collectively extend our understanding of the complex network of the SASP, which contains many layers of regulation for signal amplification and utilises both autocrine and paracrine mechanisms to effect secondary senescence in the cell neighbourhood both *in vitro* and *in vivo*.

Intriguingly, the basis for controlling the extrinsic properties of senescent cells is just beginning to be elucidated, a concept that is likely to be explained not by a static process but by a dynamic and variable quality of different SASP secretome profiles. Proteomic analysis of OIS fibroblasts suggests a switch in the SASP-associated secretomes over time (Hoare et al., 2016b). The study reported two biochemically distinct and functionally antagonistic secretomes whose dynamics are dictated by the engagement of Notch signalling. High levels of NOTCH1 mark the first peak of the senescence time course by which TGFβ is activated and C/EBPβ inhibited. In this phase, senescence develops from pre-senescence to full-fledged senescence and can then be spread. Here, secondary senescence can alternatively be triggered through cell-to-cell contact (juxtacrine), with NOTCH1 signalling acting as the pathway to mediate juxtacrine senescence. The second phase of the secretome programme is characterised by the reliance on C/EBPβ-dominant expression of proinflammatory cytokines accompanied by low levels of NOTCH1. And thus, a dynamic shift from the TGFβ-driven to the C/EBPβ-driven SASP-mediated senescence could provide an explanation for the dual and pleiotropic effects of senescence on tumour development. Downregulation of NOTCH1 in the later-wave secretome, for example, would favour the immunosuppressive microenvironment and inefficient clearance of tumour-prone senescent cells, increasing the susceptibility of normal bystander cells to pre-neoplastic change (S. Lee and Schmitt 2019). In line with this dynamic concept of secondary senescence control is an *in vivo* liver cancer model in which NOTCH1-driven senescence compromised the recruitment of immune cells to the local sites (Hoare et al., 2016).

Nevertheless, the mechanisms that dictate the induction of senescence through paracrine or juxtacrine signalling and control the shift in the spatiotemporal patterns of NOTCH-mediated secondary senescence remain poorly understood. It is conceivable that the secondary induction of senescence is determined by the dynamically continuous spectrum of senescence-associated secretomes as well as other cell-extrinsic factors that contribute to the varied quality, quantity, functional outcomes of compositional changes in the SASP content. To gain a deeper insight into the molecular basis for the regulation of secondary senescence, emerging technologies for single-cell transcriptomics and genomics offer the potential to help identify and characterise more subtle events taking place during cellular senescence, primary and secondary. Accordingly, studying the heterogeneity of a senescent cell population is one approach to addressing the actual contribution of each wave

of the senescent secretomes, and bears profound implications for the development of new and specific drugs that target unfavourable senescent cells.

1.2.6 Hutchinson-Gilford Progeria Syndrome

Progeroid syndromes represent sporadic, rare, autosomal dominant genetic diseases characterised by clinical features of premature ageing (Sinha, Ghosh, and Raghunath 2014). Hutchinson-Gilford progeria syndrome (HGPS), an early-onset form of progeria, has been extensively studied as a model for the ageing process. It is most commonly caused by a silent mutation (G608G) within the *LMNA* gene, which encodes lamin A, resulting in an aberrantly spliced lamin A isoform that is permanently farnesylated called progerin (Eriksson et al., 2003; De Sandre-Giovannoli et al., 2003). Since lamins play a vital role in the architecture of the nuclear membrane by forming part of the protein-based scaffold underlying the nuclear lamina, accumulation of progerin leads to various structural defects in the nucleus, including nuclear lobulation or blebbing, loss of heterochromatin, increased DNA damage and senescence (Eriksson et al., 2003; Scaffidi and Misteli 2008). Mouse models deficient in *Lmna* and *Zmpste24*, which encodes a metalloprotease essential for the maturation of lamin A, also exhibit nuclear abnormalities and accelerated ageing disorders (Pendás et al., 2002; Sullivan et al., 1999). As the only substrate for ZMPSTE24 in mammals, mature lamin A is absent in *Zmpste24*-knockout mice, while pre-lamin A accumulates in the nuclear envelope, causing direct structural disruption (Bergo et al. 2002). Although several characteristics of progeria such as premature senescence and genomic instability represent some of the hallmarks of the normal ageing process, the understanding of how ageing occurs and what is driving it is far from complete. A study on a mouse system whose cells were half *Zmpste24*-proficient and half *Zmpste24*-deficient demonstrated that these mosaic mice age normally, do not harbour overt abnormalities in the proliferative capacity in cell culture and do not show the increased levels of progeria markers, suggesting cell-extrinsic mechanisms in the pathogenesis of progeria (de la Rosa et al., 2013).

1.2.7 Summary

Originally conceived as a permanent state of cell cycle arrest following replicative exhaustion in culture, cellular senescence embodies a stress response whose phenotypes can be evoked by a number of stimuli that include telomere shortening or dysfunction, oxidative stress and DNA damage, inflammatory cytokines and activated oncogenes. Intrinsic changes that accompany the senescence process are predominantly associated with the engagement of the p53 tumour suppressor network and upregulation of the CDK4/6 inhibitor p21, as well as activation of the p16/RB signalling pathway, but the characteristic description of the senescent state can vary from cell to cell and strongly depends on the biological context.

Importantly, much of the current understanding of senescence *in vivo* comes from a substantial body of evidence for the tumour-suppressive function of senescence. In oncogene-induced senescence in particular, the irreversible growth arrest cell-intrinsically acts as a fail-safe mechanism to curb uncontrolled proliferation that would otherwise chart the course for oncogenesis. OIS is, however, far from being a stable state; it exhibits paradoxically opposing effects on cancer development in cell-autonomous and non-cell autonomous manners. The cell-extrinsic effects of senescence underscore the induction of secondary senescence in the surrounding microenvironment and are mediated through components of the senescence-associated secretomes under complex spatiotemporal dynamics.

Chapter 2: Materials and Methods

2.1 Laboratory Procedures

Substantial elements of the research methodologies that underpin this thesis rely on the content of our *Cell Reports* paper, "Notch Signalling Mediates Secondary Senescence" (Teo et al., 2019), which was a collaborative project between the University of Edinburgh, the University of Glasgow and Brown University. All experimental work, except where otherwise indicated and credited, was performed by me. The computational analyses in the paper were driven by Yee Voan Teo, Brown University.

2.1.1 OIS Cell Culture

I used normal diploid human female lung fibroblasts IMR90 isolated at 16 weeks of gestation for all *in vitro* assays (ATCC® CCL-186). pLNCX2-ER:ras^{G12V}-expressing IMR90 (plasmid obtained from Addgene #67844) were maintained in DMEM (ThermoFisher Scientific with pyruvate) with 10% fetal calf serum (FCS) and 1% penicillin-streptomycin in standard ϕ 10cm dishes in 21% O_2/5% CO_2 levels standard incubators. Cells were split at 80% confluency every 3-4 days. 100nM 4-hydroxytamoxifen (4-OHT)(Sigma) was used to induce senescence over the course of 7 days. Dishes that were not treated with 4-OHT were used as control.

For co-culture experiments, ER:IMR90 cells were co-cultured with IMR90:GFP (pGIPZ-GFP, a kind gift from M. Narita to J.C.A.) or an empty vector fused with mVenus (pLPC-puro-mVenus, a kind gift from M. Narita to J.C.A.) or with a dominant-negative form of MAML1 fused with mVenus (pLPC-puro-dnMAML1-mVenus, a kind gift from M. Narita to J.C.A.) cells at 10:1 ratio.

2.1.2 HGPS Cell Culture

I used progeria fibroblasts extracted from *Zmpste24*-deficient mice, which were provided by Lopez-Otin. Cells were cultured under 3% oxygen concentration at 37°C in DMEM (ThermoFisher Scientific) supplemented with 10% fetal bovine serum (FBS), 1% Penicillin Streptomycin, 1% non-essential amino acid, 1% antibiotic-antimycotic and 1% sodium pyruvate. For single-cell RNA sequencing preparation, cells were harvested at passage 6, counted using the Coulter counter and resuspended at a concentration of 500 cells/ml.

2.1.3 Animal Models for *In Vivo* Experiments

Animal welfare guidelines and management have been comprehensively provided by Lu et al., 2015. All animal experiments were performed on healthy, treatment-naive animals according to regulations within the UK and protocols ethically approved by the Animal Welfare and Ethical Review Body (AWERB) and the Home Office (UK). *In vivo* mouse experiments and *ex vivo* techniques were carried out by members of the Bird lab, the University of Glasgow, where the AhCre+/WT *Mdm2*fl/fl and AhCreWT/WT *Mdm2*fl/fl mice (colony N4 C57/Bl6J background) were crossed. Male littermates were housed together, and when used in experiments were all > 20 g body weight and of 10-16 weeks age. Using the protocol provided by Bird et al., 2018, mice were injected intraperitoneally one time with β-Naphthoflavone (βNF, Sigma UK) at 20mg/kg and genotyped as described in Bird et al., 2018.

2.1.4 Hepatocyte Isolation

Following a protocol provided in Lu et al., 2015, primary hepatocytes were isolated *ex vivo* using an adapted version of the retrograde perfusion technique. Next, hepatocyte purification was performed by pelleting through a 40% (v:v) Percoll gradient separation before FACS sorting.

2.1.5 OIS *In Vitro* Immunohistochemistry

$2x10^4$ cells were plated on gelatin-treated coverslips and allowed to attach to the surface overnight. Cells were fixed in 4% paraformaldehyde (PFA) in 1xPBS for 15 minutes, washed three times, and thereafter treated with 0.2% TritonX/PBS for permeabilisation for 5 minutes at room temperature (RT). Anti- C/EBPB clone E299 (Abcam) was used as the primary antibody at 1:500 dilution together with 0.5% goat serum with the incubation time of 45 minutes at RT. Blocking was performed by washing the coverslips in PBS-T (0.1% Tween in 1xPBS) three times for 30 minutes. Incubation with the secondary antibody Alexa Fluor® 488 goat anti-rabbit (1:500 dilution) was subsequently performed at RT for 45 minutes in darkness at RT. 4'-6-diamidine-2-phenyl indole (DAPI) was also used in 1:1000 (1xPBS) to stain the cells in order to visualise the DNA. After secondary incubation, the cells underwent additional washes with PBS-T for another 30 minutes before being dried and mounted with Vectashield antifade mounting medium.

HGPS *in vitro* immunohistochemistry followed the same procedure, but different primary antibodies were used: anti-lamin B1 [Ab16048, Abcam] and anti-γH2AX Phospho (Ser139) [2F3, BioLegend]).

2.1.6 *In Vivo* Immunohistochemistry

For tissue collection, mouse liver sections were harvested and underwent partial storage in paraffin. They were next fixed in 10% formalin (in PBS) for 18 hours before being embedded. Every immunohistochemistry run followed the protocol in Bird et al., 2018. Three μm thick paraffin sections were double-stained for p53/CDKN1A and CDKN1A and CEBPB using the CDKN1A clone HUGO291H (a gift from Serrano lab, CNIO in Madrid), and either C/EBPB clone 1H7 (Abcam) or p53 clone 1C12 (Cell Signaling). Signal visualisation was achieved by TSA-Cy3 (Perkin Elmer, NEL744B001KT, 1:50) and TSA-FITC (Perkin Elmer, NEL741B001KT, 1:50). Images acquisition was performed on a Zeiss 710 Upright Confocal Z6008 microscope. Stained slides were scanned using the Opera Phoenix High Content screening system (Perkin Elmer) scanner and analysed using the Columbus software.

2.1.7 Transwell Assay

ER:Ras^{G12V}-expressing cells were co-cultured with IMR90:GFP cells. The co-cultured cells were seeded in the lower chamber of a transwell system (density $5x10^3$ cells/well) (Corning, Tewksbury, MA). Another pure population of IMR90:GFP cells were placed in the upper chamber of the transwell system. All cells were cultured in 4-OHT for 7 days. All experiments were performed in triplicate.

2.1.8 Flow Cytometry

Cells were washed with Dulbecco's Phosphate Buffered Saline (D-PBS) before being trypsinized by 0.25% trypsin/Versene solution at 37°C until cell dissociation was achieved. Cell suspensions were washed with D-PBS, centrifuged and resuspended in D-PBS/2% FCS/0.5mM EDTA. Cells were incubated with a combination of fluorochrome-conjugated antibodies as follows: anti-Notch1-PE (R&D systems, FAB5317P) and anti-JAGGED1-APC (FAB1726A). Cell counting and sorting of YFP-positive and YFP-negative populations were performed on a BD FACScan flow cytometer (FACSAria II) (BD Biosciences, San Jose, CA) using the BD CellQuest PRO software (BD Biosciences, San Jose, CA). Dead cells were excluded by DAPI staining. Flow data were analysed with FlowJo v10 (Tree Star, Ashland, OR). Flow cytometry was performed with three independent replicates.

2.1.9 RNA Extraction

Total RNA was extracted from three to four independent experiments using the instruction from the RNeasy Mini Kit (QIAGEN). The extracted RNA was quantified by a Nanodrop and RNA quality determined by all RNA that passed with a RIN of 9 or greater via Bioanalyser profiling (Agilent). Ribosome depletion was performed prior to bulk RNA sequencing.

2.1.10 qPCR

Enzymatic digestion of total RNA and cDNA generation were performed according to the Tetro cDNA synthesis kit. qPCR was performed on a Roche LightCycler 480 (Roche) with the Sybr Green method (ThermoFisher). The LightCycler 480 software (Roche) was used to monitor and analyse fluorescent signals generated during PCR amplification. Primer sequences are shown in Table S1.

2.1.11 EdU Incorporation

To measure cellular proliferation, OIS and co-cultured cells were maintained on gelatin-treated 20 mm x 20 mm cover glasses in 6-well plates at a seeding density of $5x10^4$ and incubated with 10mM EdU-treated media for 4 hours. Cells on the cover glasses were washed with PBS and fixed using 4% paraformaldehyde for 15 minutes and rinsed three times with PBS. EdU incorporation into DNA was detected using the Click-iT™ EdU Alexa Fluor™ 555 imaging kit (Invitrogen/Molecular Probes, Eugene, OR). Cover glasses were mounted onto glass slides using the VECTASHIELD® Mounting Medium with DAPI and sealed with fingernail polish. Progeria cells underwent the same treatment and steps as described above.

2.1.12 Proliferative Assay

To measure the proliferative capacity of progeria cells, cells were serially passaged in a 6-well plate at a seeding density of $2x10^4$ cells per well every 3 days until they stopped expanding. The counting of the total number of cells was determined by the Coulter counter at the end of each passage. Population doubling time (PDT), population doublings (PD) and cumulative population doublings were calculated according to formulas PDT = $\ln2*T/\ln(N_T/N_0)$, PD = T/PDT, and cumulative PD = the sum of PD, respectively, where T = culture time, N_T = cell number at the end of a passage, N_0 = cell number at the beginning of a passage. PDT refers to the time taken for the cell population in culture to increase twofold in the middle of the exponential phase of growth. Cell proliferation rates of progeria cells were

compared to those of normal fibroblasts from young mice, using PDL and passage number as the parameters. Each sample was seeded in triplicates for each passage.

2.1.13 SA-Beta Gal staining

$2x10^4$ cells from each experimental condition were seeded in 3 wells of a 6-well plate. To perform the SA-β-galactosidase (SA-β-Gal) assay, cells were washed with 1xPBS and fixed in 0.5% glutaraldehyde for 12 minutes at room temperature (RT). The fixed cells were washed twice with 1xPBS/$MgCl_2$ (pH 6.0) and stained with a mixed solution of 1 mg/ml X-Gal, 100mM $K_3Fe(CN)_6$ and 100 mM $K_4Fe(CN)_6$. Cells were incubated at 37°C overnight in darkness and washed twice with 1xPBS. To acquire a quantifiable result, images of stained cells were captured by a camera connected to an inverted microscope. Cells containing blue stain were counted as senescent, evaluated by two independent observers. At least 200 cells in different fields of vision were counted.

2.1.14 Confocal Microscopy

A BriteMac confocal microscope was used to visualize cells and capture fluorescent images at 40x. The triple band excitation DAPI-FITC-TRITC filter was used to detect fluorescent signals from DAPI, YFP-mVenus and EdU Alexa Fluor® 555, respectively. Images were analysed using Image J, an open-source image processing software.

As for progeria experiments, a Nikon's A1R point scanning confocal laser-scanning microscope was used for capturing immunofluorescent images at 60x for the optimised image quality. The triple band excitation DAPI-FITC-TRITC filter was used to detect fluorescent signals from DAPI, Alexa Fluor® 488 and Alexa Fluor® 555, respectively. The laser power was set at 5.00 and the detector sensitivity fixed at 105 for every fluorescence channel. The pinhole was set at 1.2AU and the images acquired were 2048 x 2048 in pixel.

2.2 Experimental Data Analysis

2.2.1 Microscopic Image Analysis

For OIS and co-culture experiments, the captured images were analysed using Image J, an open-source image processing software. Percentages of SAHF, YFP and EdU-positive cells were calculated by assessing 1600-2000 cells (triplicate counts) in each experimental condition.

Images obtained from progeria experiments were also analysed by Image J, but with additional Macro scripts (Image J Macro). DAPI-stained nuclei were categorised as bleb-positive or -negative, based on the characteristic nuclear lobulation observed in progeria cells. The nuclear peripheral lamin B1 fluorescent intensity was quantified semi-automatically using another Image J Macro developed by the advanced imaging resource team at IGMM (Institute of Genetics and Molecular Medicine). Creation of the script is based on the erosion morphological operator working on a binary mask of the segmented nucleus whose area is known. Erosion removes pixels from the edge of an object an in this manner the nuclear mask is eroded away through consecutive loops until the area is 4/5 of the original area. At this point, a ring region of interest (ROI) is added to the image. This process continues until the area is eroded to 3/5 of the original at which point another ring ROI is added to the image until the innermost ring is reached.

To quantify the intensity of lamin B1, the nucleus was first divided into 5 equal areas, represented by 5 concentric rings [Figure 5.5A**]**. Since lamin B1 was fluorescently tagged with Alexa Fluor® 488, the raw fluorescent intensity detected in the FITC filter (green) for every concentric ring of the nucleus was recorded. The lamin B1 intensity in the outermost ring (referred to as ring 1), which indicates the nuclear peripheral lamin B1, was compared between progeria and WT conditions. To quantify the distribution of lamin B1 within the nucleus, the ratio of lamin B1 intensity in ring 1 to that in ring 4 was calculated and histogram generated. The raw measurements of intensity were also converted into log values. Gaussian mixture model, a histogram probabilistic model, was applied on the log values to generate WT- and KO-specific regions. The probability that a particular cell would belong to one or another region was calculated using the weighted sum model.

2.3 Single-cell Technologies

This thesis highlights the use of single-cell technologies to unravel any genetic heterogeneity or rare subpopulations within cell populations by detecting heterogeneous changes that tend to be averaged out in bulk sequencing. The focus of my research studies is on single-cell transcriptomes of senescent and progeria cells, which have been explored by two single-cell techniques: the Smart-Seq2 and the 10X Genomics Chromium protocols.

2.3.1 Smart-Seq2

The Smart-Seq2 method represents one of the most robust and reliable platforms for single-cell RNA expression analysis. It was developed by Picelli and colleagues (Picelli et al., 2014) and is an improved version of the first Smart-Seq (switching mechanism at 5′ end of RNA template sequencing) (Ramsköld et al., 2012). At the end of the Smart-Seq2 workflow, full-length cDNAs are generated from amplified mRNA transcripts, allowing good read coverage across the transcriptome with the ability to detect rarer transcripts or isoforms without using specialist equipment. This technique, however, has a difficulty in incorporating unique molecular identifiers (UMIs) and unique cellular barcodes, and the number of cells that can be processed is restricted to those seeded in 96 or 384 well plates. Such limitations render gene-level quantification and multiplexing of samples difficult, complicate downstream data analysis and introduce technical variation from several manual pipetting steps.

2.3.2 10X Genomics

The 10X Genomics Chromium workflow is based on microfluidic principles or the GemCode technology (10xGenomics). Using an 8-channel microfluidic chip, the 10X system isolates a large number of single cells in nanodroplets using a Gel bead in EMulsion (GEM) approach. The droplet-based encapsulation is achieved by gel beads, each of which is functionalised with oligonucleotides that contain a unique barcode, a UMI, sequencing adapters and primers, and an anchored 30bp oligo-dT. Cell lysis, reverse transcription, cDNA amplification, molecular tagging, and library construction all take place in one process and up

to 10,000 cells can be processed simultaneously in a single Eppendorf tube. Alternative to the Smart-Seq2 protocol, the 10X system allows for automatic and high-throughput single-cell capture, barcoding and profiling and is compatible with FACS sorting, which offers control over cell input and selection. Yet the 10X platform requires specialist equipment and comes at a substantially increased cost compared to the Smart-Seq2 platform.

2.3.3 Single-cell Data Generation

The Smart-Seq2 protocol (Picelli et al., 2014) was used on ER:IMR90 or hepatocytes after they were sorted on the FACSAria II into 96-well plates.

Single-cell data for all co-culture experiments were obtained through the 10X Chromium technique (10xGenomics). Sorted cell suspensions were loaded onto single-use microfluidic chips. Single-cell RNA-seq libraries were prepared using the GemCodeTM technology and Single Cell 3' v2 Library Kit according to manufacturer specifications. The barcoded sequencing libraries were quantified by quantitative PCR (KAPA) and loaded on an Illumina sequencing platform. Sample demultiplexing, barcode processing and single-cell 3'gene counting were carried out by the 10X's CellRanger pipeline.

Single-cell data from progeria experiments were also generated using the Chromium Single Cell 30 Chip Kit v2.

2.4 Bioinformatics Analysis

The bioinformatics workflow was established by Yee Voan Teo, Brown University, the other co-first author of the paper, who helped drive the computational analysis to fruition.

2.4.1 Sequencing Reads Processing Alignment and Quantification of Smart-Seq2 RNA-seq Data

Smart-Seq2-generated paired-end reads were quality trimmed using Trim galore (http://www.bioinformatics.babraham.ac.uk/projects/trim_galore/) and aligned to the human reference genome, hg19, neomycin sequence from pLNCX2-ER-ras_neo, ERCC spike-in sequences and RasV12 using HISAT v2.0.1beta (Kim et al., 2015). Cells with less than 200,000 hg19 aligned reads, and a ratio of ERCC RNA spike-in control aligned reads to total aligned reads greater than 0.5 were omitted. hg19 aligned reads were randomly downsampled to 200,000 reads. Genes were quantified using HTSeq-0.6.1 (Anders et al., 2015). Cells with more than 80,000 total gene counts and at least 500 genes with at least one count were used for downstream analysis. 224 IMR90 cells (100 Growing cells, 41 Day 2 cells, 42 Day 4 cells and 41 senescent cells) passed this second filtering step and used for downstream analyses.

2.4.2 Sequencing Reads Processing, Alignment, Quantification and Analysis of 10x Chromium RNA-seq Data

Cell Ranger 2.0.1 (10x Genomics) was used to align the GFP and ER:Ras^{G12V} co-culture 10x Chromium RNA-seq reads to hg19, TurboGFP, puromycin sequence from pGIPZ and neomycin sequence from pLNCX2-ER-ras_neo, and to generate gene-cell matrices. The growing and senescence dataset were aggregated using “cellranger aggr.” The data were subsequently processed using Seurat 2.3.0 with cells with less than 15% mitochondrial reads and at least 2500 number of genes being retained (Butler et al., 2018). Seurat 2.3.0 with the default parameters (unless otherwise stated) was used to generate the t-SNE plots (resolution:0.4; dimensions used: 1:15) and three clusters were identified using sparcl 1.0.3 (https://cran.r-project.org/web/packages/sparcl/index.html). SCDE v1.99.1 was used to

identify differentially expressed genes between OIS cluster and secondary senescent cluster (Kharchenko et al., 2014). The DE genes (p-values < 0.05) [Table S2] were used as the defined gene sets for GSEA Preranked analysis of NIS and RIS log2FC ranked genes. GFP+ cells were identified as cells with > 0.3 normalized expression of GFP or puromycin and Ras+ cells were identified as cells with non-zero expression of neomycin or one or more reads supporting the G > T mutation at Chr11:534288 as identified by FreeBayes v0.9.20-8-gfef284a (Garrison and Marth, 2012). Integration analysis between Smart-seq2 time-point data and 10x data were performed using the canonical correlation analysis in Seurat 2.3.0, in which the union of the top 50 highest dispersion genes and the first two dimensions were used.

Cell Ranger 2.0.1 (10x Genomics) was used to align the 10x Chromium RNA-seq reads from mVenus:dnMAML1 or mVenus:EV co-cultured with ER:Ras^{G12V} cells to hg19, mVenus sequence, puromycin sequence from pLPC-puro and neomycin sequence from pLNCX2-ER-ras_neo to generate gene-cell matrices. mVenus cells were identified as cells with more than zero normalized expression of mVenus or puromycin and Ras+ cells were identified as cells with non-zero expression of neomycin or one or more reads supporting the G > T mutation at Chr11:534288 as identified by FreeBayes v0.9.20-8-gfef284a (Garrison and Marth, 2012). The data were subsequently processed using Seurat 2.3.0 with cells with less than 10% mitochondrial reads and at least 2500 genes being retained. Seurat 2.3.0 with the default parameters (unless otherwise stated) was used to generate the tSNE plots (resolution:0.6; dimensions used: 1:7). The cells were projected to the 10x Chromium GFP and ER:Ras^{G12V} co-culture dataset using scmap-cluster v1.4.1.

Cell Ranger 2.0.1 (10x Genomics) was used to align the 10x Chromium RNA-seq reads from progeria cells with the mouse reference genome (mm10). Reads were filtered based on library size, number of expressed genes and mitochondrial proportion by the *scater* package in Bioconductor in R. Cells with library size of less than 20,000, number of expressed genes fewer than 4000 and mitochondrial proportion more than 0.06, were filtered out. 502 WT cells and 201 progeria cells passed these filtering steps. Downstream analyses were performed on the 703 cells.

2.4.3 Sequencing Reads Processing, Alignment and Quantification of *In Vivo* Data

Smart-Seq2 generated paired-end reads were quality trimmed using Trim galore (http://www.bioinformatics.babraham.ac.uk/projects/trim_galore/) and aligned to the mouse reference genome mm10 and ERCC spike-in sequences using HISAT v2.0.1beta (Kim et al., 2015). The mm10 aligned reads were randomly downsampled to 50,000 reads. Cells with less than 50,000 reads, less than 20,000 gene count, less than 500 genes with at least one read detected and with the log-transformed number of expressed genes and library size of 3 median absolute deviation below the median value were removed (Lun et al., 2016). 39 single cells from the induced hepatocytes and 19 cells from the uninduced hepatocytes passed these filters. 22 primary senescent cells were identified from the induced hepatocytes as cells with no reads mapping over exon 5 and 6 (chr10:117695953-117696049, chr10:117696381-117696439, chr10:117701565-117701614 and chr10:117702202-117702335) of *Mdm2* gene before the downsampling. 17 cells were classified as secondary hepatocytes as judged by their gene expression profiles. Differential genes expression between *Mdm2*+ cells and *Mdm2*- cells was identified using SCDE v1.99 and log2FC ranked gene list from SCDE was used in GSEA pre-ranked analysis. Genes with more than zero log-transformed normalized count (McCarthy et al., 2017) were labelled red, and otherwise white in the binary heatmap. Pathway enrichment was identified using WebGestalt (Wang et al., 2017) with genes that have a z-score of greater than 2 in *Mdm2*+ cells /*Mdm2*- comparison.

2.4.4 Differential Gene Expression Analysis and Temporal Ordering of Cells

We used raw counts from HTSeq-0.6.1 (Anders et al., 2015) as an input to single-cell differential expression (SCDE v1.99.1) (Kharchenko et al., 2014) for differential gene expression analysis between growing and senescence. Cut-off for significantly differentially expressed (DE) was set at 0.05. The expression magnitude (fragments per million) was obtained from SCDE and converted to FPKM as an input for Monocle2 (Qiu et al., 2017) Monocle2 was used to order the transitions of senescent cells of different time points at a pseudo-temporal resolution, and single-cell data were reduced to a 2-dimensional space by using the DDRTree algorithm implemented in Monocle2 (Qiu et al., 2017). Specifically, DE

genes between senescence and growing conditions that were identified in SCDE were used to define the trajectory. A consensus clustering approach, SC3, was also applied to the raw count of single cells and used to cluster senescent cells (Kiselev et al., 2017).

For progeria cells, the consensus clustering tool SC3 was used on the raw count of single cells to create 5 clusters of cells. Diffusion maps for single-cell data were created using *destiny*, an open-source R/Bioconductor package. Differentially expressed genes were identified by Discrete Distributional Differential Expression (D3E) (Hemberg Group).

2.4.5 Detection of Ras^{V12} Construct in Smart-Seq2 Dataset

We counted reads with a G > T mutation at Chr11:534288 using samtools v1.2 mpileup and bcftools v1.2 (Li, 2011). Cells with more than 1 read supporting over G > T mutation or at least 9 reads mapping to the neomycin sequence are considered as Ras^{V12} positive cells.

2.4.6 Paracrine-induced Senescence and RIS Microarray Data Analysis

Log2 RMA signal intensity of RIS IMR90 cells and IMR90 co-cultured in transwells with RIS cells were obtained from GEO GSE41318. Differentially expressed genes were identified using limma (Ritchie et al., 2015) and an adjusted p-value of 0.05 was used as the cut-off for significant genes.

2.4.7 Notch and Ras-induced Senescence Data and GSEA Analysis

We used NIS and RIS RNA-seq data with accession number GSE72404. Reads were aligned to as described above. Differential gene expression analysis between NIS and RIS was performed using DESeq2 (Love et al., 2014). The log2 fold change for each gene was used to rank the list of genes in GSEA Preranked analysis(Subramanian et al., 2005). Differentially

expressed (DE) genes between senescence top and bottom were identified using SCDE with a p-value cutoff of 0.05. The DE genes defined the gene set in GSEA Preranked analysis.

2.4.8 Sequencing Reads Alignment and Quantification of Transwell Bulk RNA-Sequencing Data

Reads were aligned to the human reference genome hg19 using HISAT v2.0.1beta (Kim et al., 2015) and those that mapped to annotated genes were quantified using HTSeq-0.6.1 (Anders et al., 2015). Differential gene expression was determined using DESeq2 v1.22.1 (Love et al., 2014). Over-representation analysis was performed using WebGestalt (Wang et al., 2017) and GSEA pre-ranked analysis was performed using the ranking of genes based on the log2FC between GFP contact and GFP no contact.

2.5 Statistical Analysis

All t-tests and one-way ANOVA for the *in vitro* data were performed in R. TukeyHSD was used as the post hoc test for one-way ANOVA. For the *in vitro* data, each experiment and measurement were obtained from three independent experiments unless otherwise specified in the figure legends. Barplots are represented as means with SEM. Statistical significance was set at $p < 0.05$. t-test for the *in vivo* data was performed in R and the two-way ANOVA followed by Tukey's test for the *in vivo* data was performed using GraphPad Prism. All animal data were obtained from three biological replicates. Details of all statistical analysis can be found in associated figure legends. For qPCR analysis, Delta delta Ct method was used for quantification with error bars resulting from the delta Ct expression of three to four biological replicates. A two-sided t-test was used to calculate p-values.

Chapter 3: Single-Cell Transcriptomics of Oncogene-Induced Senescence Systems Part I: OIS Cells Showed Two Facultative Transcriptional Endpoints.

3.1 Introduction

Cellular senescence is a stress response that irreversibly inhibits the cell cycle, suppresses tumourigenesis, promotes wound healing and is strongly associated with ageing (Campisi 2013; van Deursen 2014). Aberrant activation of particular oncogenes or tumour suppressors results in what is called oncogene-induced senescence (OIS), which is widely recognised as an *in vivo* anti-cancer mechanism yet confers a pre-cancerous state (Di Micco et al., 2006; Serrano et al., 1997; Braig et al., 2005; Xue et al., 2007).

Human cells undergoing OIS are characterised by a unique pattern of heterochromatin displayed as punctate DNA foci, known as senescence-associated heterochromatic foci (SAHFs) (Narita et al., 2003; Chandra and Kirschner 2016). OIS cells are also distinguished from normal or quiescent cells by one prominent feature, the senescence-associated secretory phenotype (SASP), whose components include interleukins, chemokines and extracellular matrix proteases that affect the surrounding cells and modify the microenvironment (Acosta et al., 2008; Coppé et al., 2008; Kuilman et al., 2008). These factors play a critical role in tumourigenesis through modulation of the extracellular matrix, and recruitment of immune cells to eliminate unwanted senescent cells, but under an inflammatory microenvironment, SASP instead contributes to cancer initiation, cellular reprogramming and ageing (Mosteiro et al., 2018; de la Rosa et al., 2013; Soria-Valles et al., 2019; Osorio et al., 2012).

Remarkably, SASP can serve to induce secondary senescence in neighbouring cells in a paracrine fashion (Acosta et al., 2013). Paracrine secondary senescence is believed to augment immune surveillance and provide a failsafe mechanism that minimises the risk of retaining damaged cells (Acosta et al., 2013; Nelson et al., 2012; Kuilman et al., 2008). Recent evidence has suggested that ectopic activation of Notch signalling is interpreted in an intermediate stage during primary senescence induction, accompanied by a distinct secretome

(Hoare et al., 2016a). The details of Notch's involvement in secondary OIS mediation are yet to be described.

Here, single-cell RNA sequencing (scRNA-seq) was carried out to investigate the heterogeneity within OIS populations. I used H-RasG12V-induced senescent IMR90 (ER:IMR90) fibroblasts (Young et al., 2009) as the experimental model. The design of the H-RasG12V construct is based on its fusion to a mutant form of the estrogen receptor (ER) ligand binding domain. 4-hydroxy-tamoxifen (4-OHT) is used as a conditional activator of RAS, which drives the ER:IMR90 fibroblasts into cell cycle arrest within 7 days with clear and observable morphological and biochemical phenotypes and 5-10-fold higher levels of the Ras oncoprotein compared to normal physiological conditions, making this system a robust and effective platform to study senescence (Takaoka et al., 2004). The single-cell experiments showed two distinct transcriptional signatures at the end of the primary OIS process, with activation of Notch characterising one transcriptional endpoint uniformly consisting of secondary senescent cells *in vivo* and *in vitro*.

3.2 OIS Cells Bifurcated into Two Sub-Populations

I performed a scRNA-seq time course experiment to investigate the dynamic changes, trajectory and cell-to-cell heterogeneity of H-RasG12V-induced senescent IMR90 (ER:IMR90) fibroblasts (Young et al., 2009) before and after 2, 4, and 7 days, using the Smart-Seq2 protocol (Picelli et al., 2014)[Figure 3.1]. As part of the research collaboration, the downstream computational techniques for scRNA-seq data analysis were performed by Yee Voan Teo, with my constant engagement along the research journey.

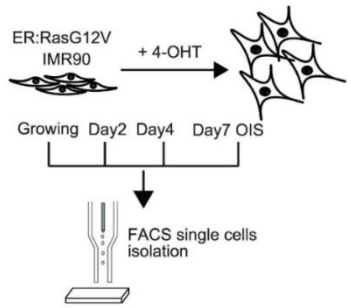

Figure 3.1: Schematic Representation of the Time-Course Experiment. **(ER:IMR90) fibroblasts were induced to become senescent** before and after 2, 4 and 7 days using FACS single cell isolation for the Smart-Seq2 protocol.

Stringent filtering criteria were applied to the scRNA-seq data. These quality control (QC) steps included total mapped reads, ratio of ERCC RNA spike-in control aligned reads to total aligned reads, and total gene counts [Figures 3.2A-3.2C; Table S2]. The cells that passed QC were normalised by downsampling to 200,000 aligned reads for downstream analysis. These filtering steps led to a final cell count of 100/288 for day 0, 41/96 for day 2, 42/96 for day 4, and 41/288 for day 7 [Figure 3.2D]. Another critical QC procedure conducted was to select for senescent cells with reads mapped to the G >T mutation site of RAS gene [Figure 3.3].

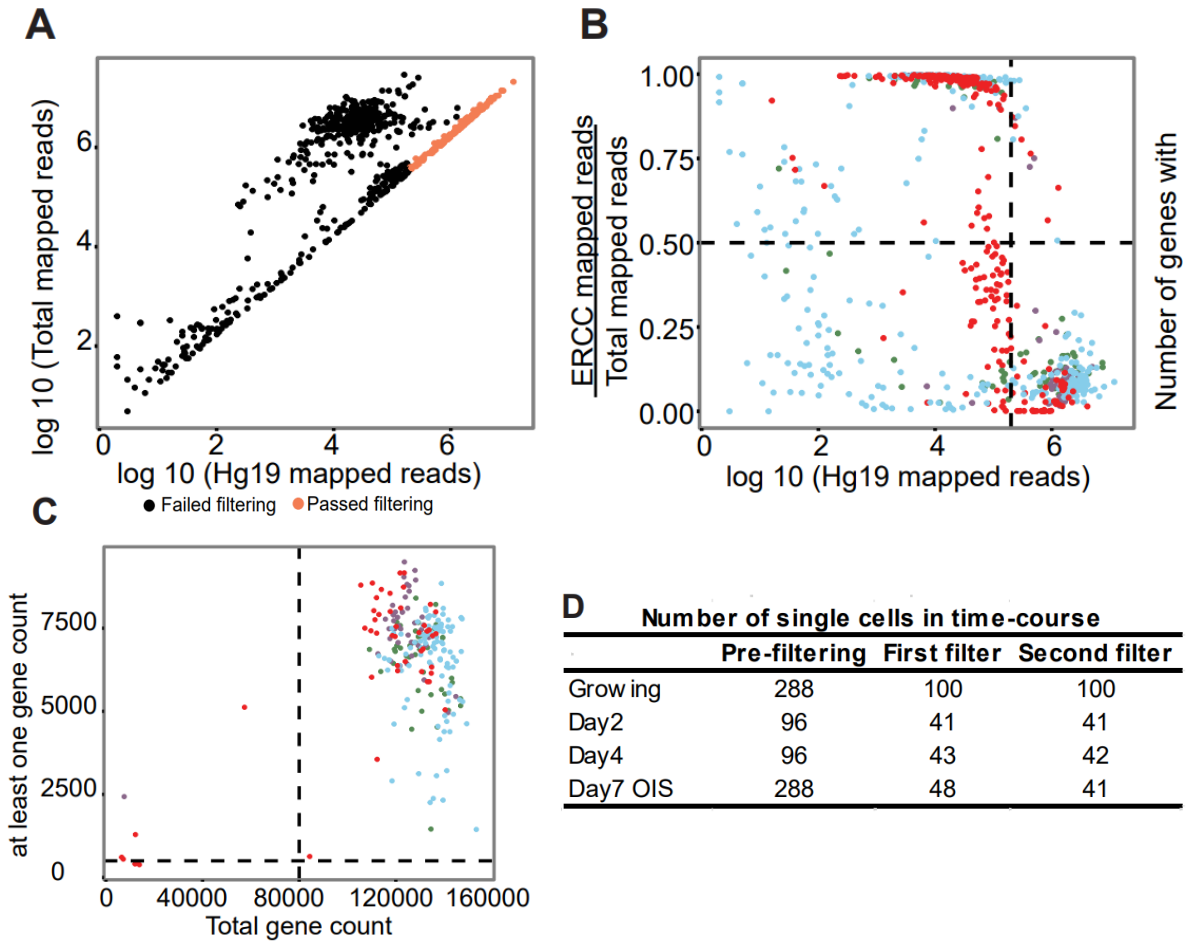

D

Number of single cells in time-course

	Pre-filtering	First filter	Second filter
Grow ing	288	100	100
Day2	96	41	41
Day4	96	43	42
Day7 OIS	288	48	41

Figure 3.2: Filtering Criteria.

(A, B) Filtering according to total mapped reads. Cells with less than 200,000 human aligned reads and with a ratio of ERCC RNA spike-in control aligned reads to total aligned reads that is greater than 0.5 were removed.

(C) The second filtering step was performed to retain cells that have greater than 80,000 total gene counts and at least 500 genes with at least one count. Cell were normalised by downsampling to 200,000 aligned reads for downstream analysis.

(**D**) The number of cells that passed the filtering step in **(A)** and **(B)**.

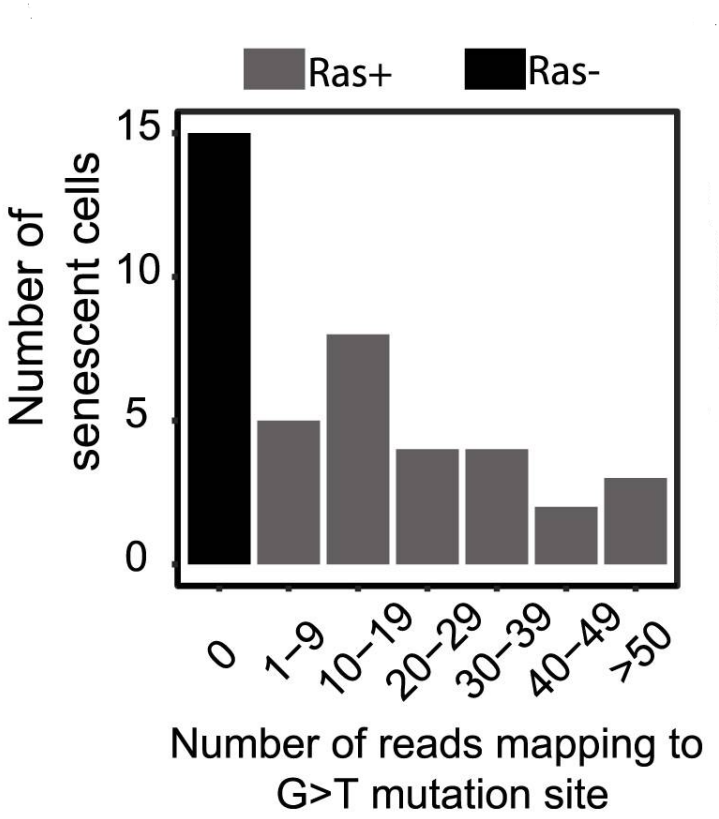

Figure 3.3: Number of senescent cells with reads mapping to the G > T mutation site of RAS gene.

Ras+ cells were identified as cells with non-zero expression of neomycin or one or more reads supporting the G > T mutation at Chr11:534288 as identified by FreeBayes v0.9.20-8-gfef284a

Since OIS induction takes 7 days of culture in 4-OHT, I confirmed a senescence phenotype at day 7 by profiling bromodeoxyuridine (BrdU) incorporation, counting of cells with senescence associated heterochromatic foci (SAHF) and the senescence-associated beta-galactosidase (SA-Beta Gal) assay [Figures 3.4A-C]. At the end of senescence induction, 37/390 cells [9%] incorporated BrdU, 265/390 cells [68%] were SAHF-positive, and 428/523 cells [82%] were stained positive for SA-Beta Gal.

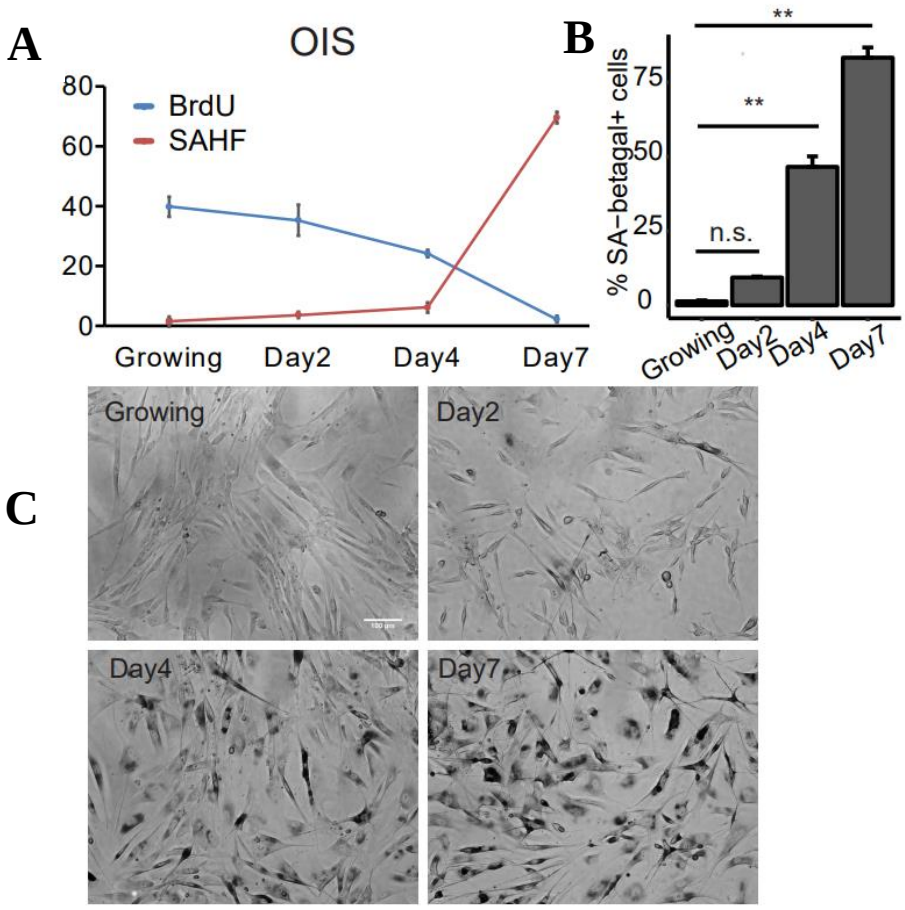

Figure 3.4: Confirmation of Senescence Markers.

(A) BrdU incorporation profiling and proportion of SAHF-positive cells. Cells cultured on coverslips were incubated for 6 h with BrdU (10 µM) and fixed following the kit instructions. The presence of SAHF was detected by DAPI staining.

(B) Percentages of SA-Beta galactosidase-positive cells. Cells were scored as SA-Beta -positive cells based on the presence of galactosidase staining.

(C) SA-Beta galactosidase staining in ER:Ras fibroblasts. SA-Beta gal staining was performed as previously described (Kirschner et al., 2015).

Days indicated time of tamoxifen treatment. Error bars are SEM, n=3 for each time point. $F[3,8] = 234.8$, $p<0.001$; **$p<0.001$ using one-way ANOVA with Tukey's test. Scale bar 100µm.

Next, to assess time-dependent changes in the transcriptome, pseudo-temporal ordering of cells, or pseudotime, was employed to reveal a trajectory of single-cell data based on differential gene expression between growing and senescence [adjusted $p < 0.05$; Table S3; Figure 3.5] (Kharchenko et., 2014).

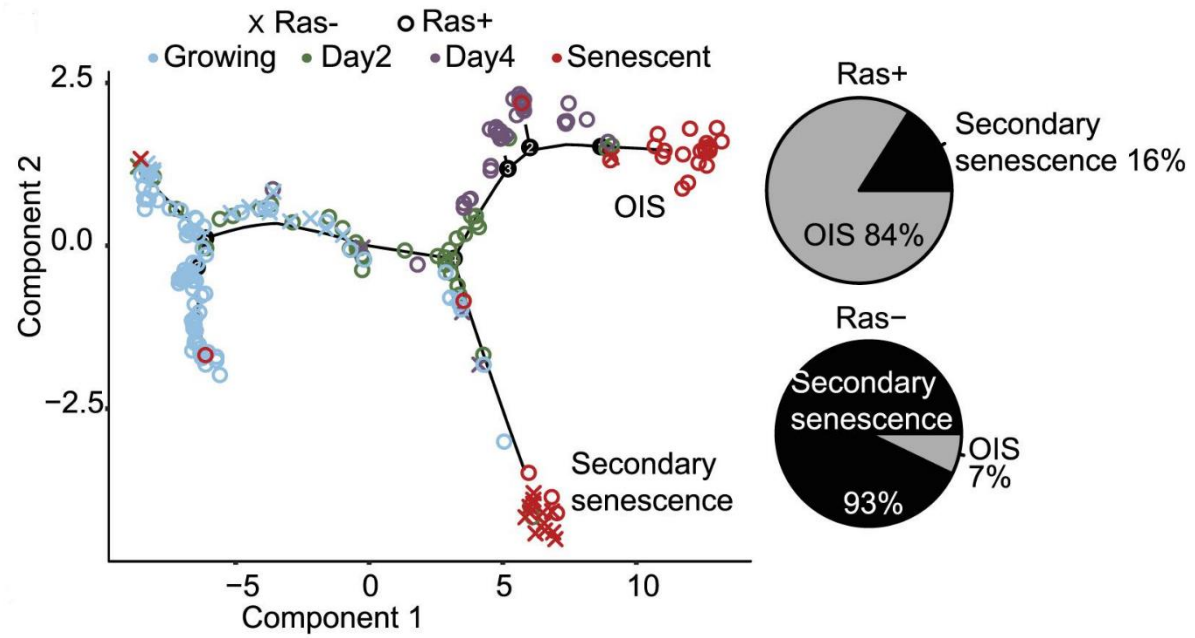

Figure 3.5: Pseudo-Temporal Trajectory of scRNA-seq Data.

Monocle2 plot for the time-course experiment shows the presence or absence of the mutated RAS gene as indicated. Pie charts for the percentage of Ras+/Ras− cells in the top and bottom clusters. Monocle2 was used to order the transitions of senescent cells of different time points at a pseudo-temporal resolution, and single-cell data were reduced to a 2-dimensional space by using the DDRTree algorithm implemented in Monocle2 (Qiu et al., 2017). The figure shows a continuous progression from growing to senescence, with days 2 and 4 cells as intermediates and two distinct senescent populations.

The Monocle2 method, which utilises the principle component analysis (PCA) and dimensionality reduction (Qiu et al., 2017), was applied to plot the pseudo-temporal trajectory of single-cell OIS data. The Monocle2 plot revealed a continuous progression of cells from growing to senescence, featuring intermediate stages at days 2 and 4 and ultimately bifurcating into two distinct senescent sub-populations at day 7 [Figure 3.5]. The result suggests two facultative, alternative endpoints for OIS cells.

3.3 Senescence Top and Bottom Populations Were Separated by the Activation of Ras

To determine whether the split into two senescence populations was a result of RasV12 activation [Figure 3.3], RasV12 expression was overlaid onto the Monocle2 plot [Figures 3.3 and 3.4; Figures 3.6A-B; ta]. The combined datasets showed a progression of RasV12-expressing cells [Figure 3.5; Ras+, round symbols] into two terminal senescence clusters with a 21:4 skew toward the endpoint designated OIS. On the other hand, fibroblasts without detectable RasV12 expression had a consistent progression to the endpoint tentatively designated secondary senescence, implied as the obligate endpoint [cross symbols, Ras−; Figure 3.5; Fisher's exact-test, 1.64×10^{-6}]. The undetectability of RasV12 in the secondary sub-cluster suggests that senescence induction in this cluster was a secondary event.

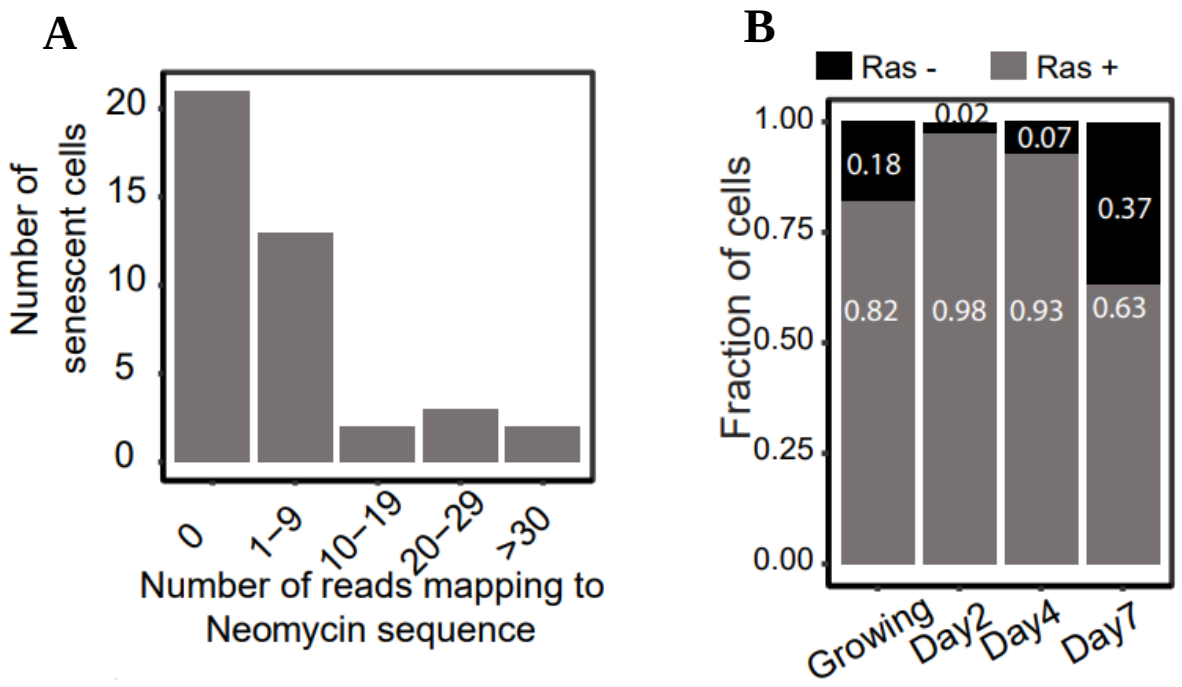

Figure 3.6: Determination of RasV12 Activation and Overlay of RasV12 Expression onto Monocle2.

(A) Number of reads aligning to the neomycin sequence from the pLNCX2-ER-ras_neo construct in senescent single cells in the time-course experiment. Ras+ cells were identified as cells with non-zero expression of neomycin.

(B) Fraction of cells that are RasV12+ in each condition in the time-course experiment.

To further investigate the differences between the top and bottom senescence populations, Ingenuity Pathway Analysis (IPA, QIAGEN) was used [Figure 3.7A]. IPA identified HRAS as one of the top predicted upstream regulators for the senescence top population ($p = 3.1 \times 10^{-34}$) [Figure 3.7A]. Despite this difference, both populations still categorically exhibit upregulation of key senescence genes such as cyclin-dependent kinase 1a (*CDKN1A*) and cyclin-dependent kinase inhibitor 2b (*CDKN2B*) and SASP factors interleukin 8 (*IL8*), interleukin 6 (*IL6*), and interleukin 1B (*IL1B*) [$p < 0.05$ for all genes; Figure 3.7B], confirming the senescence phenotype.

A OIS/Growing in time-course scRNA-seq

Upstream Regulator	Predicted ActivationState	Activation z-score	p-value of overlap
HRAS	Activated	2.936	$3.1E^{-34}$

Genes with adjusted p-value<0.05

B

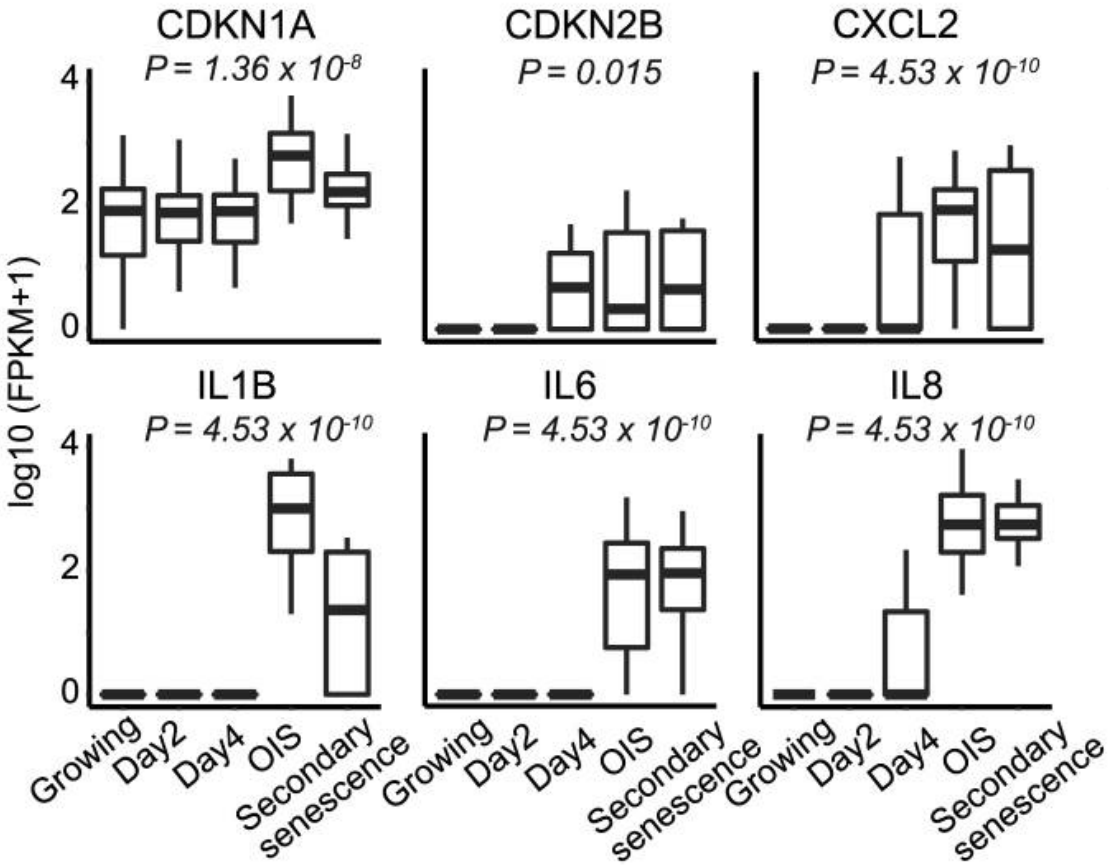

Figure 3.7: Transcriptional Profiles of Top and Bottom (Primary and Secondary) Populations.

(A) IPA analysis of OIS/growing in time-course scRNA-seq. IPA pathway analysis identifies TGFB1 as exclusively activated in the secondary senescence clusters compared to growing or the primary OIS.

(B) Boxplots for the expression of senescence genes in the time course experiment. The top and bottom bounds of the boxplot correspond to the 75th and 25th percentile, respectively. p-values were obtained using differential analysis in SCDE.

A consensus clustering approach, SC3 (Kiselev et al., 2017), was then applied to verify if the two main senescence populations were transcriptomically distinct, using silhouette plot to determine the number of clusters (Rousseeuw 1987) [Figure 3.8A]. SC3 found two senescence clusters with a high degree of overlap with the sub-populations detected by Monocle2 (cluster 1 16/21 or 76% RasV12+ cells, cluster 4 11/15 or 73% RasV12− cells). This consistent finding supports the idea that the bifurcation into two senescence clusters depends upon the absence or presence of RasV12 [Figure 3.8B].

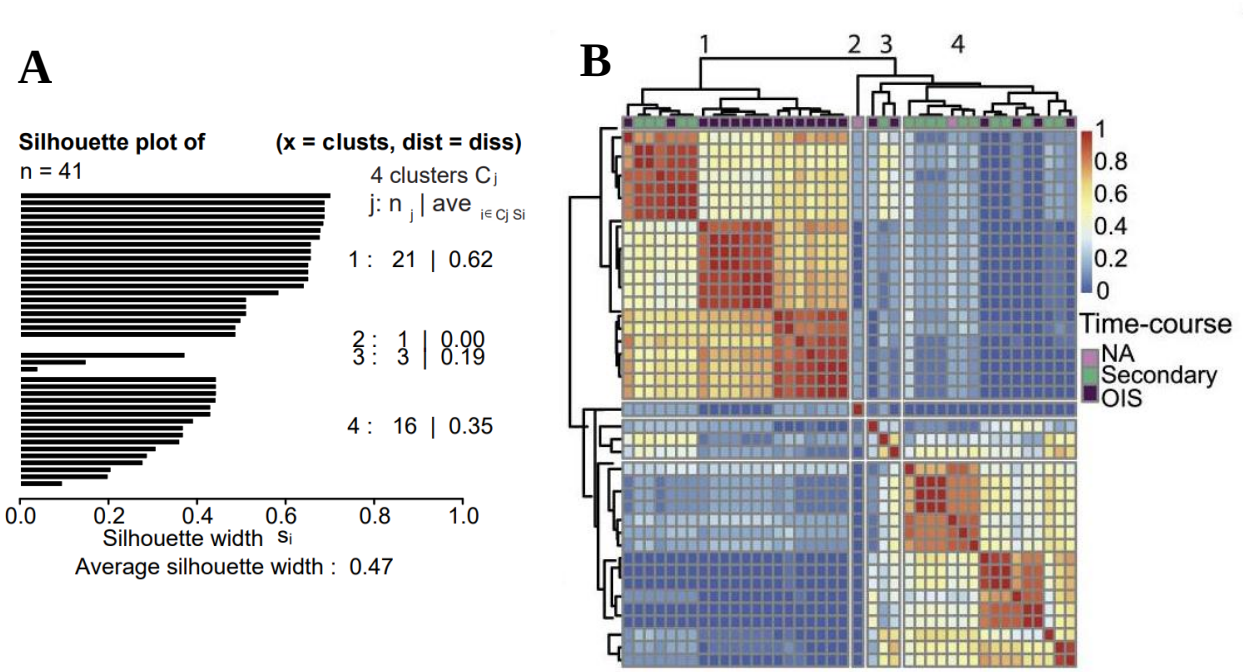

Figure 3.8: Unsupervised Clustering of Senescent Cells.

(A) Silhouette plot to assess the quality of clustering. The average silhouette width was 0.47. Silhouette plot was used to determine the number of clusters.

(B) Unsupervised clustering using SC3 for senescent cells. Cells were annotated as either OIS (top senescence branch, purple), secondary senescence (bottom branch, green), or NA (neither, pink). SC3 detected two senescence clusters largely overlapping with the subpopulations obtained by Monocle2.

3.4 Primary Senescence and Secondary Senescence Were Transcriptomically Distinct

To verify that the two major sub-populations observed represent primary OIS and secondary senescence, I set up a co-culture experiment in which ER:IMR90 were co-cultured with IMR90:GFP fibroblasts in a ratio of 10:1. By treatment with 4-OHT, secondary senescence would be induced in IMR90:GFP-positive cells (Acosta et al., 2013). Using the 10X Genomics Chromium, I obtained scRNA-seq data before and 7 days after RasV12 activation [Figure 3.9A].

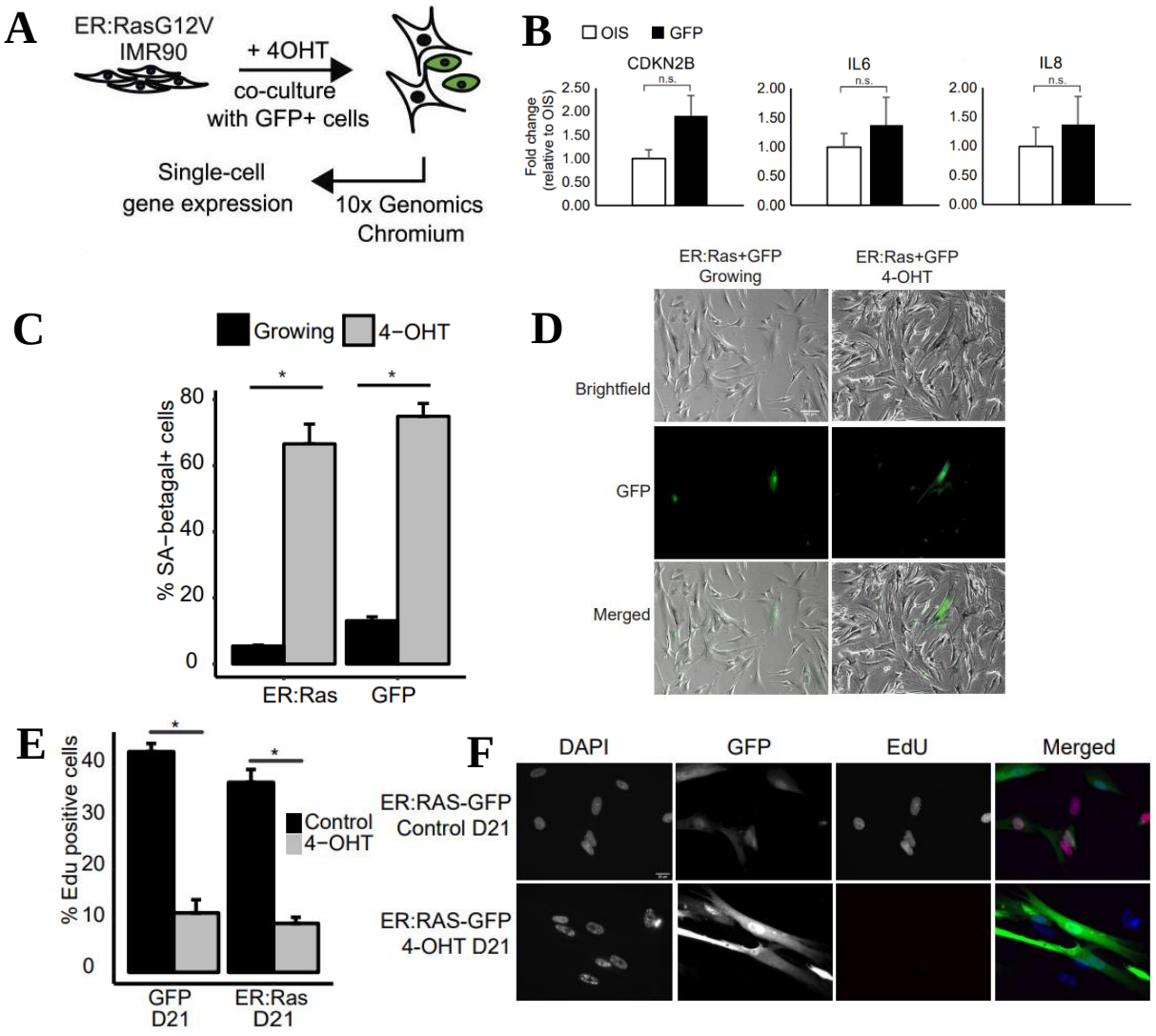

Figure 3.9: Confirmation of Senescence in Co-Cultured Cells.

(A) Schematic representation of the co-culture experiment. ER:IMR90 cells were co-cultured with IMR90:GFP fibroblasts (10:1), where secondary senescence is induced in IMR90:GFP-positive cells. We generated scRNA-Seq data before and 7 days after RasV12 activation by using the 10× Genomics Chromium protocol.

(B) Box plots for gene expression of CDKN2B (n=3), IL6 (n=3), and IL8 (n=3) mRNA measured by qPCR in OIS and GFP cells. Unpaired Student's t-test showed no significant difference in senescent markers expression between OIS and GFP cells. Error bars represent SEM.

(C) SA-Beta galactosidase counts in OIS and GFP cells. (OIS t = 10.199, df = 2.0096, p= 0.009; GFP t = 15.239, df = 2.3673, p= 0.002 using unpaired Student's t-test). Scale bar 100μm.

(D) Representative images from SA-Beta Gal staining in OIS and GFP cells captured by an inverted microscope.

(E) Bar plots showing EdU incorporation in GFP cells co-cultured with ER:Ras cells after 21 days as proportion of all cells scored. Error bars are displayed as SEM; **p<0.001, *p<0.05.

(F) Representative images from EdU incorporation profiling are shown. Scale bar 20μm. (ER:Ras t = -9.899, df = 2.86 68, p=0.0024; GFP t = 10.395, df = 3.3348, p= 0.0012 using unpaired Student's t-test) (n=3 per experiment).

The senescence phenotype was verified on sorted populations by qPCR, as shown by common senescence markers (*CDKN2B, IL6* and *IL8*) [Figure 3.9B; Table S2]. I also performed the SA-Beta Gal assay on both primary and secondary senescent cells and consistently found positive staining in the 4-OHT-treated groups [Figures 3.9C-3.9D]. Furthermore, long-term stable cell cycle arrest was confirmed at 21 days post co-culture by EdU incorporation profiling, with less than 10% of the senescent cell populations, primary and secondary, incorporating EdU [Figures 3.9E-3.9F].

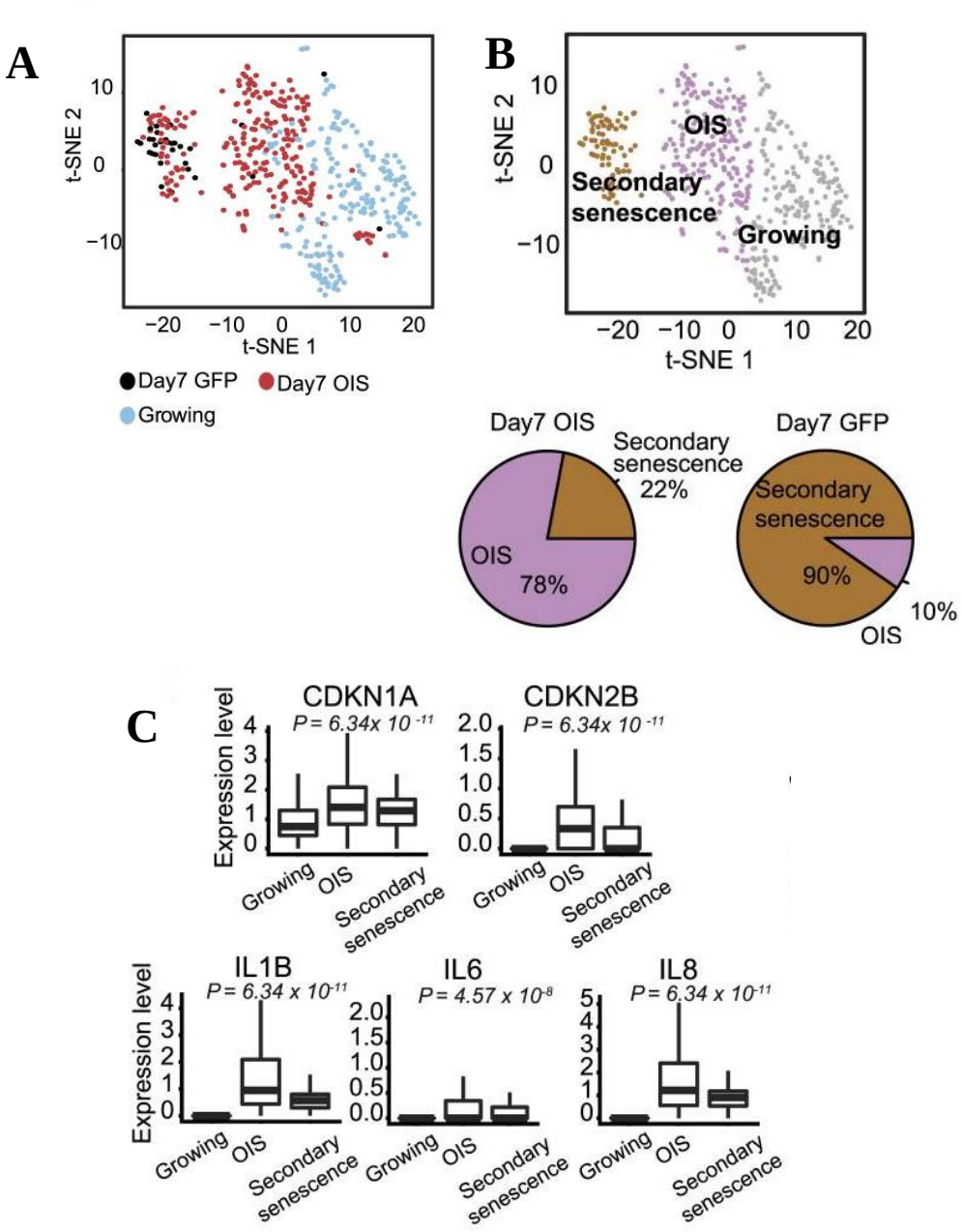

Figure 3.10: 10X Genomics Transcriptional Profiles of Co-cultured Cells.

(A) t-Distributed Stochastic Neighbor Embedding (tSNE) visualization of co-culture scRNA-seq.

(B) tSNE visualization of single cells grouped into 3 clusters. Three distinct clusters, namely growing (blue dots), secondary senescence (GFP positive, black dots) and OIS (RasV12 positive, red dots), were identified with significant enrichment for the OIS and secondary senescence populations.

(C) Boxplots for the expression of senescence genes in the co-culture experiment. The top and bottom bounds of the boxplot correspond to the 75th and 25th percentile, respectively. p-values were obtained using differential analysis in SCDE.

Transcriptome-wide, cells were annotated based on GFP, RasV12 expression, and the G > T mutation of *Ras* gene (Figure 3.10A). Three major clusters were identified using the Seurat and Sparcl packages (Butler et al., 2018; Witten and Tibshirani 2010): the clusters are growing (blue dots), secondary senescence (GFP positive, black dots) and OIS (RasV12 positive, red dots), with significant enrichment for the OIS and secondary senescence populations (chi-square test, $p = 4.1 \times 10^{-14}$; Figure 3.10B). A small fraction of RasV12-expressing cells also existed in the secondary senescence cluster, which reflects the earlier findings of two facultative terminal senescence stages for primary RasV12 senescent cells, with GFP-positive secondary senescent cells being uniformly distributed. In addition, differential gene expression analysis in SCDE confirmed the senescent phenotype by upregulation of genes including *CDKN1A*, *CDKN2B*, and *IL8* in both senescent clusters in comparison with the growing cluster [Figure 3.10C; Table S2].

Next, to integrate the data from two single-cell experiments, the transcriptomes of the time-course and the co-culture experiments were overlaid. Strikingly, a significant portion of cells labelled as OIS and secondary senescence (GFP and part of RasV12) clustered together [Figure 3.11; chi-square test, $p < 0.05$]. It is surprisingly consistent that such a co-clustering pattern with the same senescence signatures was achieved despite the datasets being independently obtained from two different techniques: the 10X and the Smart-Seq2 protocols.

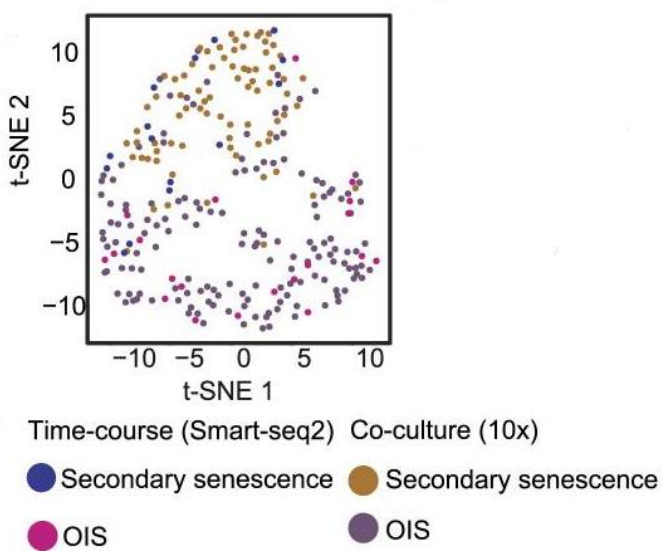

Figure 3.11: Integration Analysis of the Two Senescence Clusters from Time-Course and Co-Culture Experiments.

When overlaying transcriptomes of the time course and the co-culture experiments, a significant number of cells identified as OIS and secondary senescence (GFP and part of RasV12) clustered together.

3.5 Paracrine Senescence Only Partially Explained Secondary Senescence

Strong *in vitro* and *in vivo* evidence has led to the notion that paracrine senescence is the main effector mechanism mediating cell-extrinsic or secondary senescence (Acosta et al., 2013; Kuilman et al., 2008). To test whether the secondary senescence cluster identified here was explained by a paracrine signature, the published bulk RNA-seq data (Acosta et al., 2013) was overlaid our two single-cell datasets. A significant overlap with paracrine senescence genes was found (hypergeometric test: paracrine/OIS and time course secondary senescence/OIS (Ras−/Ras+) $p < 0.001$; paracrine/OIS and 10× secondary senescence/OIS $p < 0.001$, 10× secondary senescence/OIS and time course secondary senescence/OIS (Ras−/Ras+) $p < 0.001$; Figure 3.12; Table S4). However, a great portion of genes shared between the 10X and the Smart-Seq2 single-cell experiments could not be explained, suggesting that additional pathways in secondary senescence were involved.

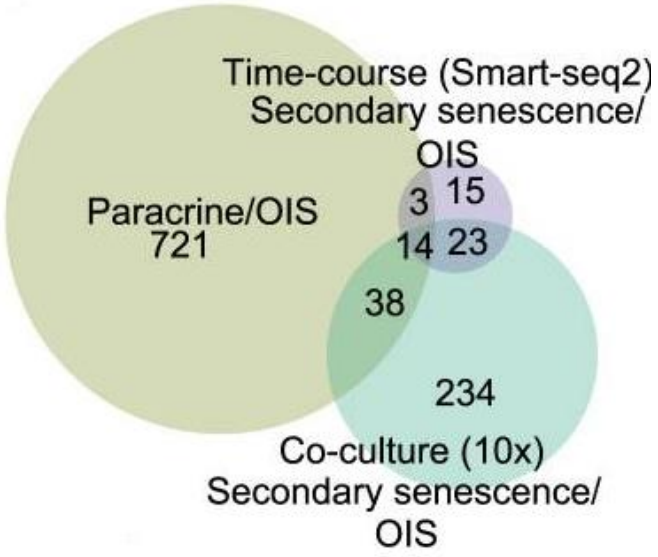

Figure 3.12: Overlap of differentially expressed (DE) genes between paracrine/OIS, time course, and co-culture experiments.

There was a significant overlap with paracrine genes (hypergeometric test: paracrine/OIS and time course secondary senescence/OIS (Ras−/Ras+) $p < 0.001$; paracrine/OIS and 10× secondary senescence/OIS $p < 0.001$, 10× secondary senescence/OIS and time course secondary senescence/OIS (Ras−/Ras+) $p < 0.001$; but a large fraction of genes shared between our two single cell experiments remained unexplained.

3.6 Notch Signatures Characterised the Transcriptome of Secondary and a Subset of Primary Senescent Cells

Since paracrine senescence signatures only partially explain the secondary senescence clusters, additional differential gene expression analysis was carried out to explore consistent differences between the secondary senescence and the primary OIS clusters. Fibrillar collagens (collagen 1A1, 3A1, and 5A2) emerged as one of the most differentially expressed genes [Figure 3.13A]. A previous study also reported downregulation of fibrillar collagens in senescence (Hoare et al., 2016). In our secondary senescence cluster, however, these collagen genes were not downregulated [Table S3; Figure 3.13A]. Similarly, a failure to downregulate collagens was observed in a specialised primary senescence phenotype, established by ectopic, temporal activation of Notch (Hoare et al., 2016). The same study suggested a model of RasV12-induced senescence whose secretome regulation depends on a choice between CCAAT-enhancer-binding protein beta (CEBPβ) and transforming growth factor beta (TGFβ), with Notch-induced senescence specifically repressing CEBPβ and relying on TGFβ [Figure 3.13B] (Hoare et al., 2016).

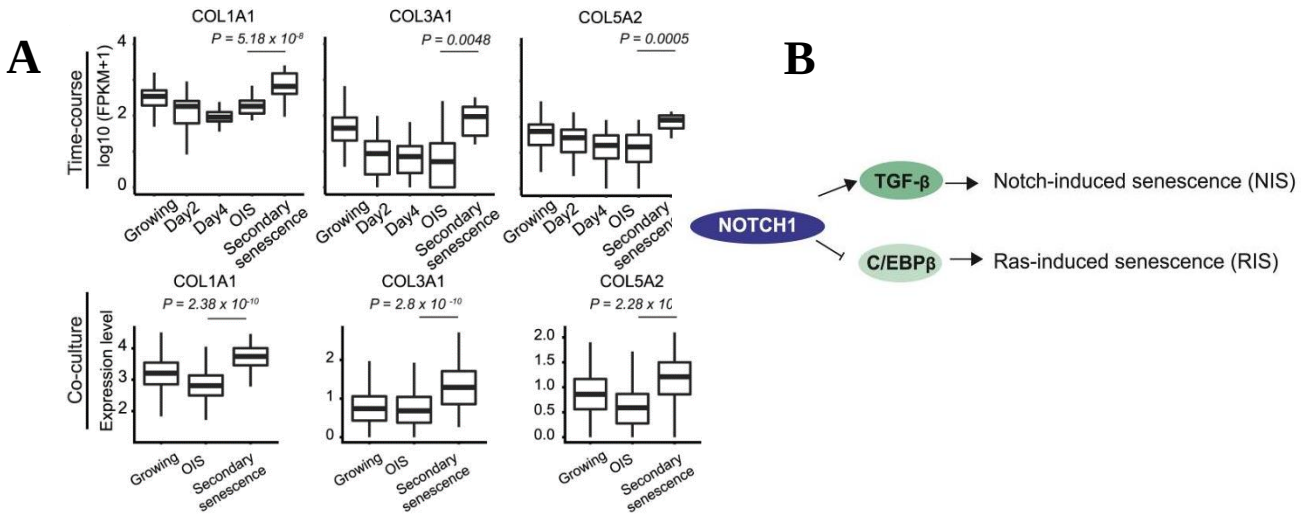

Figure 3.13: Fibrillar Collagen Expression and Secretome Regulation Model of NIS and RIS.

(A) Boxplots for the expression of genes COL1A1, COL3A1, and COL5A2 in the time course and co-culture experiments ($p < 0.05$). The top and bottom bounds of the boxplots correspond to the 75th and 25th percentile, respectively. p-values were obtained using differential analysis in SCDE.

(B) Model suggesting NIS and RIS are regulated by Notch1 through TGFB and CEBPB, respectively.

Here, a variety of analytical methods identified a notch-induced senescence (NIS) signature in the secondary senescence population. First, IPA pathway analysis revealed TGFB1 as one of the most exclusive activator in the secondary senescence clusters compared to growing or the primary OIS [Table 3.1A]. By contrast, the primary OIS clusters specifically contained differentially activated regulators of the CEBPβ transcriptome, RELA and IL1β pathways [Table 3.1B]. Consistently, HRAS was exclusively activated in primary OIS, mirroring the previous RasV12 annotation [Tables 3.1A-B]. In relation to changes in components of the extracellular matrix between the primary and secondary clusters, a previous study also showed that integrin β subunits (β3 or *ITGB3*) were significantly deregulated during OIS and that β3 expression induced senescence by activating TGFβ. (Rapisarda et al., 2017).

Second, candidate genes involved in Notch signaling and TGFB activation were profiled. When TGFβ-induced transcript 1, (*TGFβ1I1*) was plotted with Notch-target connective tissue growth factor (*CTGF*) and *CEBP*β, a significant ($p < 0.05$) upregulation was found in *CTGF* and *TGFβ1I1* genes in the secondary senescence cluster with a simultaneous downregulation of CEBPB, significant on the protein but not mRNA level [Figures 3.14-3.15; $p = 0.016$), resembling the TGFβ and CEBPβ bias in NIS. This bias was confirmed by qPCR [Figure 3.14; TGFβ1 $p = 0.02$, TGFβI $p = 0.05$).

A **Top activated and shared upstream regulator assessed by IPA**

Time-course
(Secondary senescence / OIS)

Upstream Regulator	Activation z-score	p-value of overlap
decitabine	2.058	1.16E-13
TGFB1	1.839	1.64E-12
Brd4	0.788	2.55E-13
TP53	0.653	1.44E-14
ERBB2	0.611	2.01E-13
forskolin	0.488	4.7E-13
D-glucose	0.271	1.45E-12
ERK	-0.193	1E-15
KRAS	-0.805	1E-13
EGF	-0.835	2.57E-16
lipopolysaccharide	-0.97	1.01E-13
HRAS	-3.116	1.09E-17

Co-culture
(Secondary senescence / OIS)

Upstream Regulator	Activation z-score	p-value of overlap
PD98059	4.571	5.34E-29
U0126	3.069	5.91E-29
dexamethasone	2.646	2.65E-33
TGFB1	2.622	1.3E-48
MYCN	-2.054	1.07E-22
Cg	-2.253	2.03E-24
EGF	-2.322	4.52E-22
EGFR	-2.617	3.39E-26
KRAS	-2.989	3.37E-24
PDGF BB	-3.101	4.29E-36
TNF	-3.435	2.34E-29
HRAS	-4.235	8.86E-37

Genes with adjusted p-value<0.05

B **Top upstream regulator assessed by IPA**

Time-course (Secondary senescence/Growing)

Upstream Regulator	Predicted Activation State	Activation z-score	p-value of overlap
TNF	Activated	3.394	2.29E-08
TGFB1	**Activated**	**3.041**	**1.04E-13**
lipopolysaccharide	Activated	2.628	5.76E-15
MAPK1	Activated	2	0.00172
NUPR1	Activated	2	0.0378

Time-course (OIS/Growing)

Upstream Regulator	Predicted Activation State	Activation z-score	p-value of overlap
NUPR1	Activated	6.14	4.81E-17
CDKN2A	Activated	5.171	2.82E-20
IL1B	Activated	5.119	1.4E-18
RELA	Activated	5.09	1.04E-08
TNF	Activated	5.062	1.64E-24
HRAS	**Activated**	**2.936**	**3.1E-34**

Genes with adjusted p-value<0.05

Co-culture (Secondary senescence/Growing)

Upstream Regulator	Predicted Activation State	Activation z-score	p-value of overlap
NUPR1	Activated	3.536	2.04E-09
lipopolysaccharide	Activated	3.075	3.02E-06
TNF	Activated	2.652	1.27E-12
TGFB1	**Activated**	**2.394**	**2.56E-14**
MAPK1	Activated	2.034	0.000543

Co-culture (OIS/Growing)

Upstream Regulator	Predicted Activation State	Activation z-score	p-value of overlap
NUPR1	Activated	6.794	1.81E-27
CDKN2A	Activated	4.315	8.46E-27
RELA	Activated	4.107	2.47E-09
TNF	Activated	4.014	4.78E-27
IL1B	Activated	3.912	7.82E-20
HRAS	**Activated**	**2.441**	**7.23E-18**

Genes with adjusted p-value < 0.05
log2FC > 1 and < -1

Table 3.1: Differentially Expressed Genes in Primary and Secondary Senescence Clusters.

(A) IPA analysis of the two senescence clusters from time-course and co-culture scRNA-seq. Red indicates activated upstream regulator and blue indicates inhibited upstream regulator.

(B) IPA analysis of the two senescence clusters from the time course and co-culture experiments relative to growing.

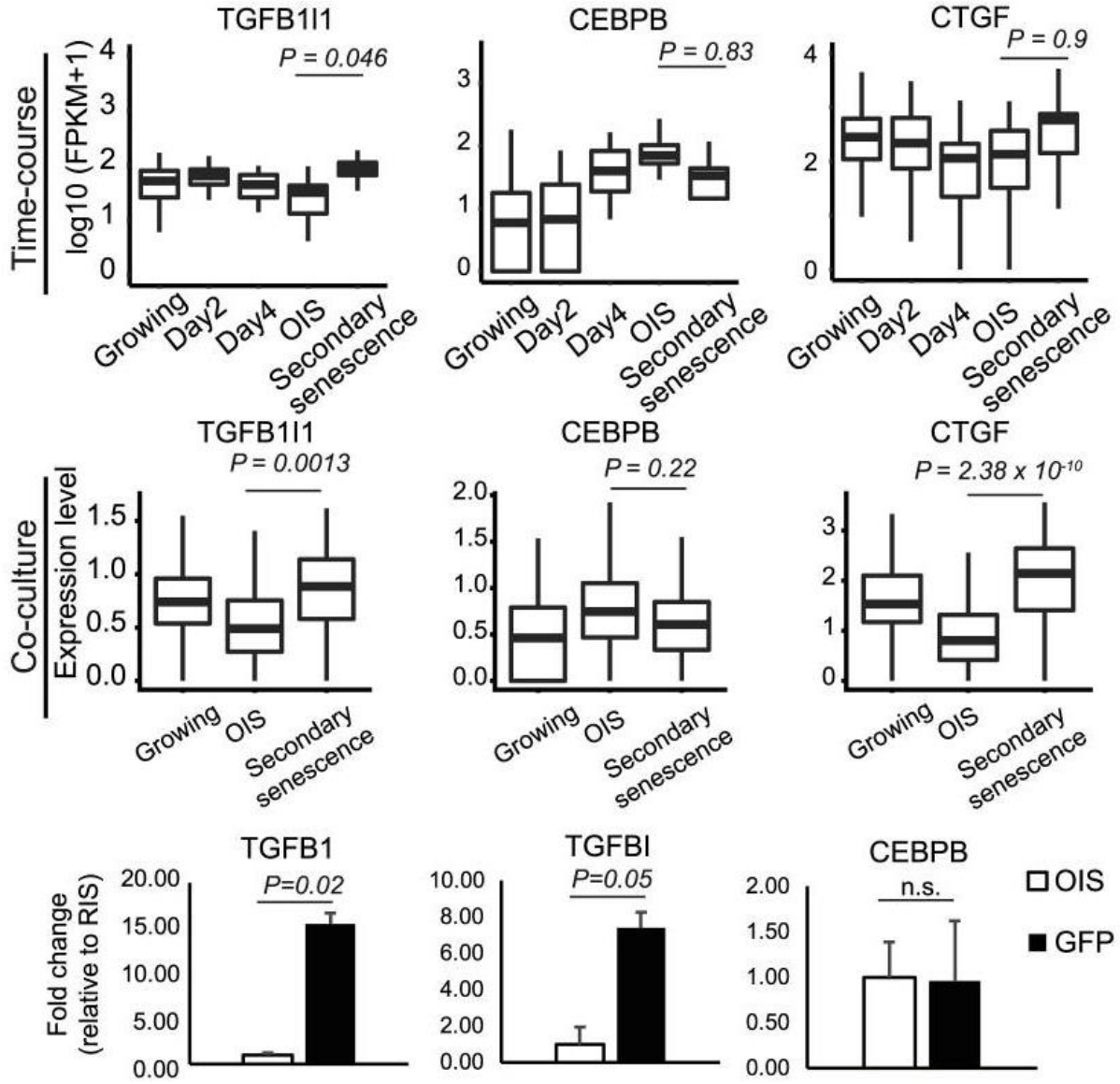

Figure 3.14: Boxplots for the expression of TGFB1I1, CTGF, and CEBPB genes in the time course (top) co-culture experiments (middle), and the relative fold change (bottom) in OIS and GFP.

The top and bottom bounds of the boxplot correspond to the 75th and 25th percentile, respectively. p-values were obtained using differential analysis in SCDE.

Bar graphs denoting expression of TGFB1 (n = 6), TGFBL (n = 6), and CEBPB (n = 3) mRNA as measured by qPCR in OIS and GFP cells (bottom) (TGFB1: t = −3.2317, df = 5.5117, p = 0.02; TGFBI: t = −2.2567, df = 9.8141, p = 0.05; CEBPB: t = 0.068192, df = 3.2294, p = 0.95, unpaired Student's t-test. Error bars represent SEM).

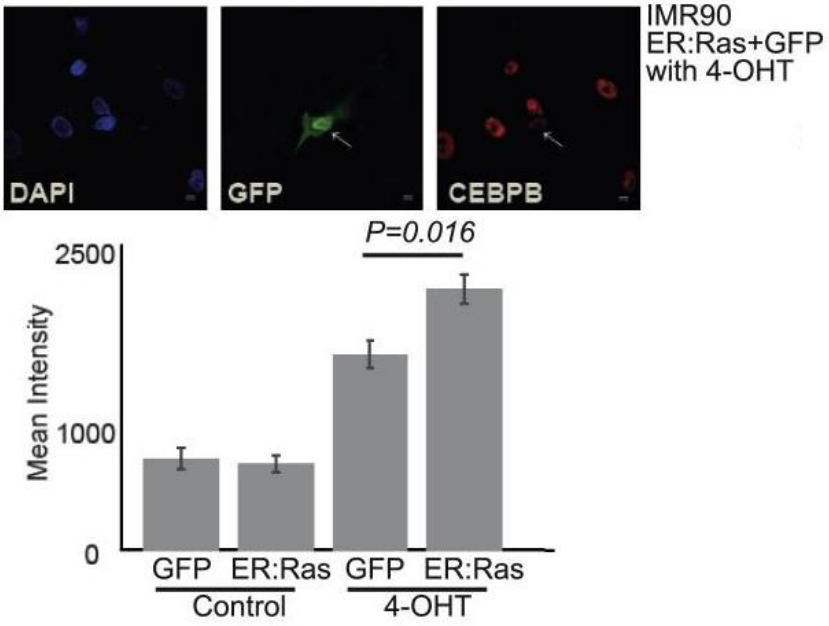

Figure 3.15: Representative image of GFP (secondary senescence) and CEBPB (red) immunofluorescence in the co-culture experiment.

Immunofluroresecence was performed as previously described (Kirschner et al., 2015). Anti- C/EBPB clone E299 (Abcam) was used as 1:500 dilution. Mean intensity for primary (ER:Ras) and secondary senescent cells (GFP) was measured ($p = 0.016$, unpaired Student's t-test). Error bars are displayed as SEM.

Third, an unbiased genome-wide analysis was applied. Gene set enrichment analysis (GSEA) (Subramanian et al., 2005) was used to identify the enrichment of NIS and Ras-induced senescence (RIS) signatures in the primary OIS and secondary senescence transcriptomes, with ranked transcriptome differences between NIS and RIS [Figure 3.16A].

A high enrichment of NIS signatures was found in the secondary senescence transcriptomes from the time-course and co-culture experiments [normalised enrichment score [NES] = 2.61, false discovery rate [FDR] < 0.005 for time course; NES = 2.89, FDR < 0.005 for co-culture experiments; Figure 3.16A]. On the other hand, RIS signatures were enriched in the primary OIS transcriptomes [Fugure 3.16B].

Finally, the extent of NIS in secondary senescence was assessed. A comparison between the most differentially regulated genes (adjusted $p < 0.05$) of RIS and NIS showed that NIS genes are significantly enriched in the secondary senescence clusters in the time course and co-culture experiments, with primary OIS signature being enriched for RIS [Figures 3.16A-D]

A

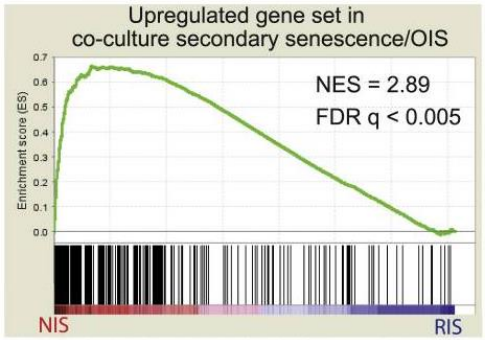

Leading edge genes: NREP, CRYAB, SULF1, LMOD1, MRVI1, ACTA2, MCAM, TNFSF4, CTGF, COL3A1, TGFB2

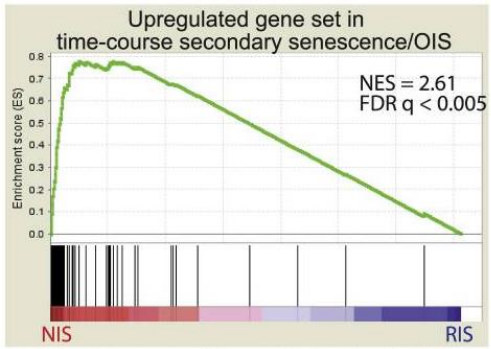

Leading edge genes: COL3A1, CDH11, COL5A2, SPARC, CALD1, VCAN, TPM1, COL4A1, PALLD, COL1A2, COL1A1

B

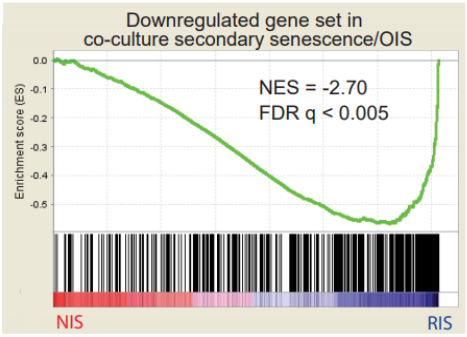

Leading edge genes: STC1, MMP1, SERPINB2, CDCP1, NRG1 SLC16A6, TFPI1, TMEM158, CSF3, IL8, MT2A, HMGA1, IL1B

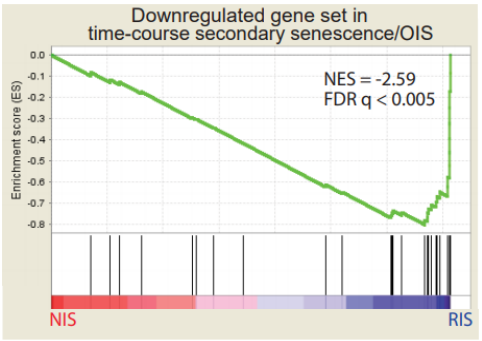

Leading edge genes: MMP3, STC1, MMP1, SERPINB2, SLC16A6, TFP12, IL2B,

C

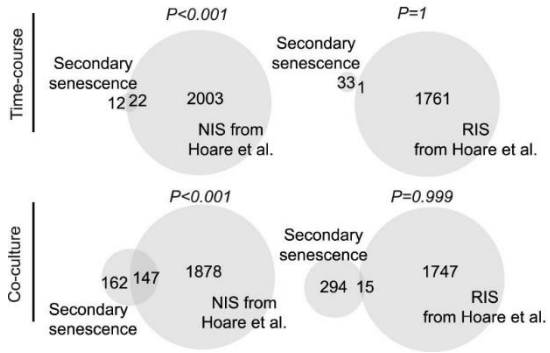

D

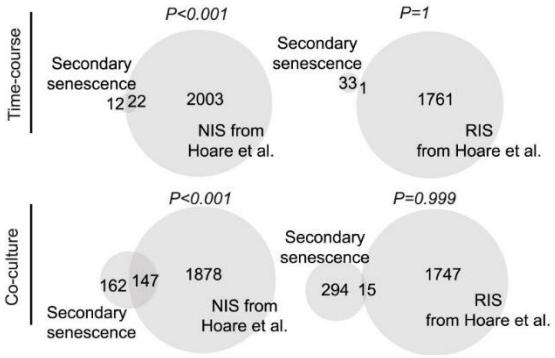

Figure 3.16: Enrichment of NIS Signatures.

NIS and RIS RNA-seq data with accession number GSE72404 were used and their reads aligned. Differential gene expression analysis between NIS and RIS was performed using DESeq2 (Love et al., 2014). The log2 fold change for each gene was used to rank the list of genes in GSEA Preranked analysis (Subramanian et al., 2005). Differentially expressed (DE) genes between senescence top and bottom were identified using SCDE with a p value cutoff of 0.05. The DE genes defined the gene set in GSEA Preranked analysis.

(A) GSEA plots for the enrichment of secondary and primary OIS DE genes (time course and co-culture experiments) in Hoare et al., (2016) NIS and RIS log2FC pre-ranked genes. Normalized enrichment score (NES) and false discovery rate (FDR) are shown.

(B) GSEA was used to assess the enrichment of secondary and primary senescence (OIS) DE genes in Hoare et al.,'s NIS and RIS log2FC pre-ranked genes. NES and FDR are shown.

(C) Venn diagrams overlapping expression signatures from time course (top) and co-culture (bottom) with NIS signature genes. (Secondary senescence: Secondary senescence/OIS upregulated genes; NIS: Hoare et al., (2016) NIS/RIS upregulated genes; RIS: Hoare et al., (2016) RIS/NIS upregulated genes).

(D) Venn diagrams overlapping expression signatures from top panel: time-course and bottom panel: co-culture experiments with NIS signature genes (OIS: OIS/Secondary senescence upregulated genes; NIS: Hoare et al.,'s NIS/RIS upregulated genes; RIS: Hoare et al.,'s RIS/NIS upregulated genes).

3.7 Discussion

The ability to study OIS cells at the single-cell level is a great leap forward in this research field. One important question that needs to be addressed is why some cells can escape from OIS and become cancerous. To answer that question, I first attempted to explore the heterogeneity of OIS cells and determine if all OIS cells are transcriptionally equal. Analysis of OIS heterogeneity provided a compelling rationale for embarking on scRNA-seq studies. In this chapter, I described the findings from single-cell transcriptomics time-course and co-culture experiments after Ras induction and investigated the differences between primary and secondary senescence as a defining source of cellular heterogeneity in OIS.

The two ScRNA-seq technologies employed here, Smart-Seq2 and 10X Genomics, have offered comparisons of the transcriptomes of individual senescent cells and identified rare senescent sub-populations that would otherwise go unnoticed in bulk sequencing experiments. Nevertheless, in the identification of Ras cells by mapping a mutation in the Ras gene, the unmappability of some cells presents a challenge for downstream analyses. This issue could be attributed to dropout events, meaning that the gene expression went undetected as a result of technical limitations during the preparation of cells. An alternative explanation could involve a biological phenomenon, namely the formation of SAHF, which will be discussed in details later on in Chapter 4.

In the first part of the downstream analysis process, lineage tracing (Monocle2) and unsupervised clustering (SC3) separated the Ras induced senescence population into two groups based on single cell transcriptomes and referred to as primary and secondary senescence populations. It was clear that both senescence clusters showed the senescence phenotype, as confirmed by a plethora of senescence assays and markers, but the inability to detect Ras activation in the secondary cluster suggests that senescence was secondarily established. Given that the two single-cell experiments were conducted independently and utilised two different techniques to generate the data, the consistent co-clustering of senescence signatures from the two datasets warrants the conclusion that primary and secondary senescence populations had distinct transcriptomes.

Since paracrine transmission of senescence is as a well-established mediator of secondary senescence (Acosta et al., 2013), the lists of differentially expressed genes found in the secondary senescence transcriptomes were compared with the list of paracrine-induced senescence genes. Interestingly, the overlap between them was small, with a large number of genes not intersecting. Previous work indicates that Notch signalling regulates the senescence secretomes, in turn affecting the functional output of senescence (Hoare et al., 2016a). In agreement with this model, our gene profiling and enrichment analyses identified notch-induced senescence signatures in the transcriptomes of secondary and a subset of primary senescent cells. The results point to the novel role of the Notch pathway in regulating secondary senescence.

Another prominent observation that must be discussed concerns the dynamics of OIS shown in the time-course analysis [Figure 3.5]. While the intermediate stages present over the temporal trajectory of OIS induction reflect dynamic shift and functional transition of OIS, it remained to be elucidated whether the spatio-temporal pattern of senescence control fits in the Notch-regulated 2-state model of SASP in which high Notch activity drives the first phase in a TGFβ-dependent and CEBβ-suppressive manner, while the latter phase is characterised by the pro-inflammatory secretome and derepression of CEBPβ (Hoare and Narita 2017). To understand more about the function of Notch in this regard, the next chapter will focus on the mechanistic link between Notch signalling and establishment of secondary senescence.

3.8 Summary

In summary, two major transcriptional endpoints in primary OIS were identified, with a uniform assignment of secondary senescent cells. Subsequent analyses revealed a pronounced NIS signature in the secondary senescence population and in a subset of primary senescent populations as an alternative endpoint to OIS.

Chapter 4: Single-Cell Transcriptomics of Oncogene-Induced Senescence Systems Part II: NIS is a Secondary Senescence Effector Mechanism during OIS.

4.1 Introduction

Notch signalling is evolutionarily conserved across bilaterian animals and has its origin in cell-fate decisions during wing development in *Drosophila* (Couso et al., 1994). The canonical Notch pathway is executed through a single-pass transmembrane Notch receptor on the signal-receiving cell upon direct binding with its ligand located on the apposing signal-sending cell [Figure 4.1] (Ito et al., 2017). This cell-to-cell, ligand-receptor interaction causes the Notch receptor to undergo a conformational change and triggers a proteolytic cleavage of the Notch extracellular domain by the ADAM/TACE metalloproteinase family. The resulting intermediate transmembrane form of the receptor is subsequently subjected to a second cleavage by the γ-secretase complex, which releases the Notch intracellular domain (NICD) from the inner membrane, allowing it to translocate to the nucleus to bind to the DNA-binding protein RBPJ, mastermind-like 1(MAML1) and other transcriptional activators. The formation of this transcriptional complex displaces co-repressors and activates target gene expression. Notch-mediated cell-to-cell interactions are highly context-dependent but essential for the development of multicellular organisms with implications in diseases such as cancer.

Recent lines of evidence have favoured the role of Notch in the modulation of senescence and mediation of secondary senescence (Hoare et al., 2016; Parry et al., 2018). The transition from growing cells to Ras-induced senescence (RIS) cells was accompanied by a progressive increase in the expression of the Notch receptor, with the level of downstream Notch signalling depending on the activity of the growth factor-rich, TGFβ secretome or the CEBPβ-rich, pro-inflammatory SASP secretome (Hoare et al., 2016a). It was shown that Notch relies on TGFβ signalling during the early phase of RIS, transcriptionally suppressing CEBPβ. Notch activity was later downregulated at full RIS, with CEBPβ being de-repressed and pro-inflammatory SASP promoted. Ectopic expression of the Notch1 intracellular domain (N1ICD) in the context of RIS led to an upregulation of the Notch1 ligand JAG1 in adjacent cells and was found to laterally induce senescence, presenting the evidence for *in vitro* non-autonomous transmission of Notch-induced senescence (NIS) (Hoare et al., 2016a). However, the effects of

primary OIS cells (without ectopic activation of Notch) on secondary naïve cells that are not under oncogenic stress had not been described before. This chapter focuses on *in vitro* and *in vivo* experiments that have established Notch-mediated juxtacrine senescence as an essential mechanism of secondary senescence in OIS.

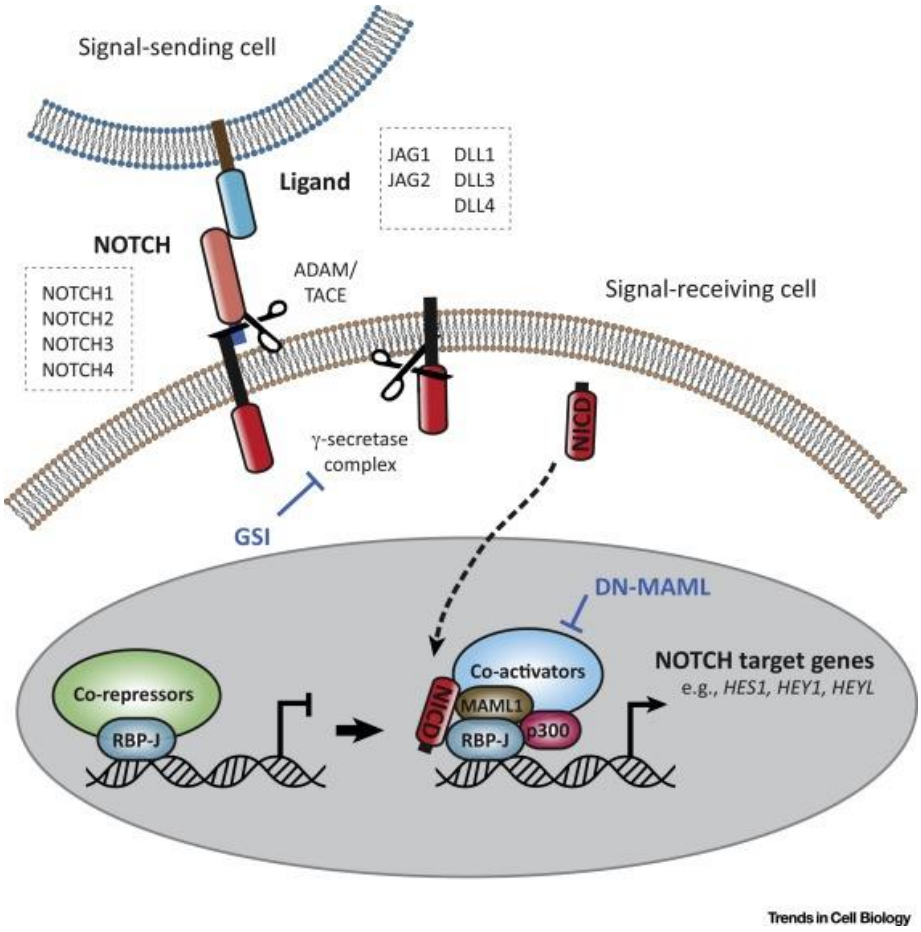

Figure 4.1: The Canonical Notch Signalling Pathway [Taken from Ito, Hoare, and Narita 2017; licence number granted: 4658430825772].
Notch signalling is achieved by an interaction between a 'signal-sending' cell and a 'signal-receiving' cell through ligand–receptor binding in a cell–cell contact-dependent manner. Humans have five DSL family ligands, Jagged (JAG) 1 and 2, and Delta-like (DLL) 1, 3 and 4, and four single-pass transmembrane-protein receptors (NOTCH 1, 2, 3, and 4). The Notch receptor undergoes a series of proteolytic cleavage steps when bound to its ligand: the receptor ectodomain is then cleaved by metalloproteases of the ADAM/TACE family, followed by a second cleavage step by the γ-secretase complex, releasing the Notch intracellular domain (NICD). The NICD can then enter the nucleus to bind to the DNA-binding protein RBP-J on chromatin. This binding displaces co-repressors from the complex and recruiting transcriptional co-activators, such as MAML1, p300, and others, and allows the formation of active transcription complexes on Notch target genes, such as the HES and HEY family of transcription factors. Inhibition of Notch signalling is possible by pharmacological or genetic intervention at each critical point in the pathway. γ-secretase inhibitors (GSIs) or expression of the dominant-negative form of MAML1 (DN-MAML) are examples.

4.2 Notch Perturbation Compromised Secondary Senescence

To test if Notch signalling acts as an effector mechanism in secondary senescence, I set up co-culture systems between primary OIS cells and secondary Notch-incompetent cells. IMR90 fibroblasts with compromised Notch signalling were generated by introducing a dominant-negative form of mastermind-like protein 1 fused to mVenus (mVenus:dnMAML1) or empty vector (mVenus:EV) control and co-cultured with ER:Ras IMR90 cells in the presence of tamoxifen [Figure 4.2A].

Many pieces of evidence point to a causal involvement of Notch signalling in secondary senescence. First, EdU labelling was performed between mVenus:dnMAML1 and mVenus:EV cells at days 0 and 7 [Figure 3B]. At day 7, mVenus:dnMAML1 had significantly more EdU incorporation compared to mVenus:EV cells ($p = 0.01$), with day 7 mVenus:dnMAML1 cells showing similarly high levels of EdU incorporation as growing mVenus:dnMAML1 and growing mVenus negative ER:Ras conditions ($p = 0.997$ and $p = 0.08$), suggesting that the secondary senescence was not induced as a result of Notch inhibition (Figure 3B). As expected, ER:Ras cells showed low levels of EdU incorporation at day 7 tamoxifen ($p = 0.01$ for ER:Ras/mVenus:dnMAML1 co-culture and $p = 0.0005$ for ER:Ras/mVenus:EV co-culture; Figure 4.2B). Also, day 7 co-cultured mVenus:dnMAML1 cells exhibited lower expression of extracellular matrix gene COL3A1 ($p = 0.02$) and Notch target CTGF [$p = 0.056$; Figure 4.2C] as measured by qPCR, compared to mVenus:EV, confirming Notch signalling impairment.

Second, mVenus (YFP) signal was scored between mVenus:dnMAML1 and mVenus:EV cells at day 0 (growing) and day 7 co-culture with ER:Ras. The number of day 7 mVenus:dnMAML1 cells was significantly more than that of mVenus:EV cells ($p = 0.01$), suggesting that primary OIS cells have reduced secondary senescence effect on neighbouring cells when Notch signalling was perturbed [Figure 4.2D]. No significant difference in mVenus-positive cells was observed in growing mVenus:EV compared to mVenus:dnMAML1 cells ($p = 0.38$), showing that the dnMAML1 itself does not affect cell numbers [Figure 4.2D].

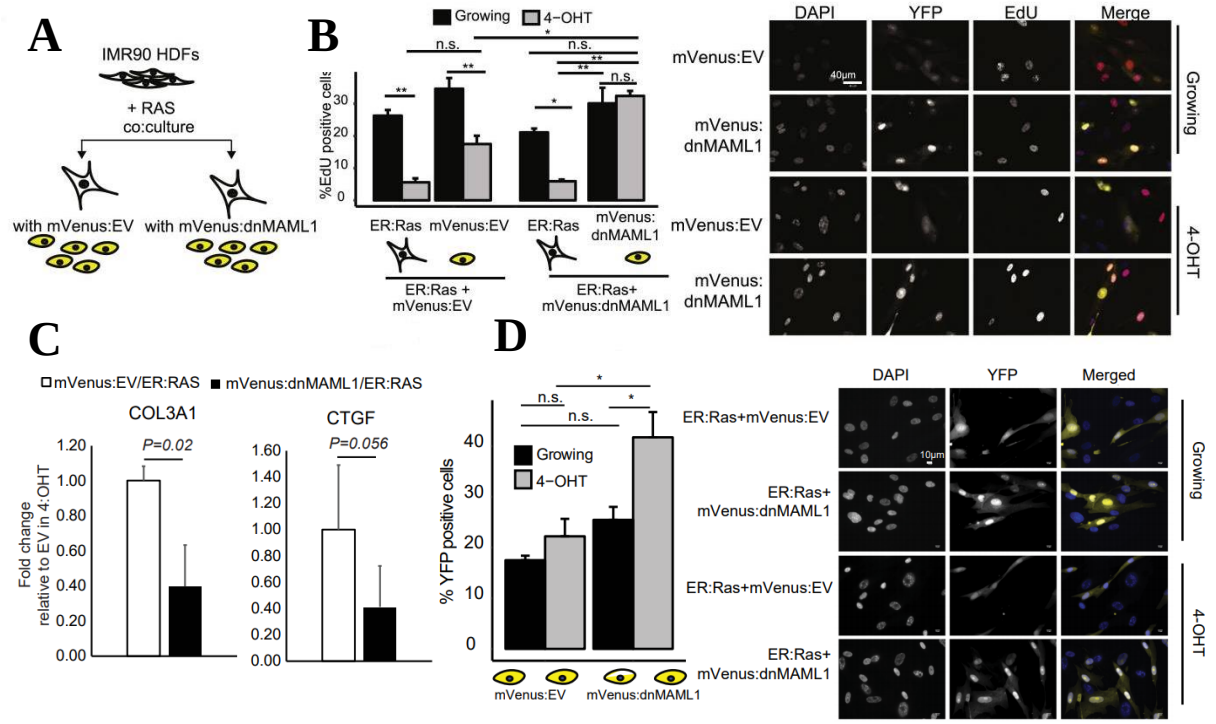

Figure 4.2: Notch Perturbation in Co-Culture Systems as Shown by Immunofluorescence.

(A) Schematic representation of co-cultures with perturbed Notch signalling. We generated IMR90 fibroblasts with compromised Notch signalling by introducing a dominant-negative form of mastermind-like protein 1 fused to mVenus (mVenus:dnMAML1) or empty vector (mVenus:EV) control and co-cultured with ER:Ras IMR90 cells in the presence of tamoxifen.

(B) Bar plot for EdU incorporation in growing (black) or senescent (gray) EV or dnMAML1 cells co-cultured with ER:Ras as proportion of all cells scored. Error bars are displayed as SEM; $F[7,16] = 20.63$, $p < 0.001$, one-way ANOVA with Tukey's test. ($n = 3$ per condition). Representative images are shown.

(C) Bar plot showing the expression of CTGF ($n=6$) and COL3A1 ($n=3$) genes in EV or dnMAML1 cells compared to ER:Ras senescent cells by qPCR. (COL3A1: $t=5.3405$, $df=2.4861$, $p=0.02$; CTGF: $t=2.2104$, $df=8.4894$, $p=0.056$ using unpaired Student's t- test). Error bars represent SEM.

(D) Bar plot denoting the proportion of growing (black) or senescent (grey) mVenus cells with dnMAML1 or EV as proportion of all cells scored. Error bars are displayed as SEM; $F[3,8] = 10.05$, $p<0.05$ using one-way ANOVA with Tukey's test ($n=3$ for each condition). Representative images of mVenus cells and cells stained with DAPI are shown on the right. Scale bar 10μm.

4.3 SAHF Formation Was Absent in Secondary Senescence

Third, SAHF formation in primary OIS and secondary senescence was investigated. Primary OIS cells displayed SAHF as expected [$p = 4.437 \times 10^{-6}$; Figure 4.3A]. Secondary senescent cells (mVenus:EV) did not show significant SAHF formation when compared to OIS [p = 0.32; Figure 4.3A]. Interestingly and consistently, in primary OIS cells, SAHF-negative cells exhibited a failure to downregulate COL1A2 and higher levels of Jag1, compared to SAHF-positive cells, suggesting that SAHF-positive cells were primary senescent cells while SAHF-negative cells were secondary senescent cells.

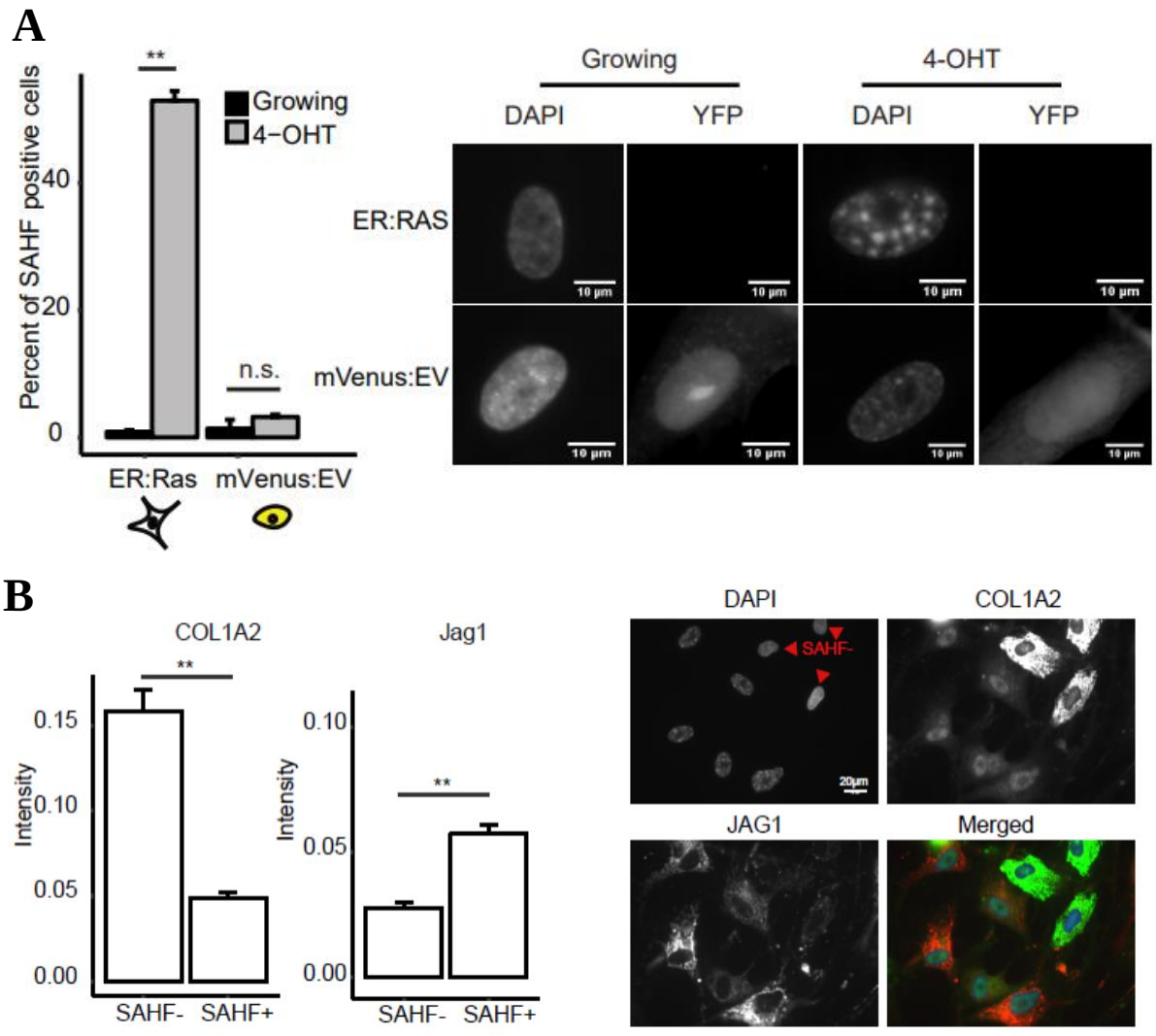

Figure 4.3: SAHF Formation and Immunofluorescence of Fibrillar Collagens in Co-Culture Systems.

(A) SAHF counts in OIS and secondary senescent (unpaired Student's t-test, ER:Ras t=-34.05, df=2.12, ** p<0.01; mVenus:EV t=-1.23, df=2.28, p=0.32; n=3 for each condition). Representative images are shown on the right.

(B) Bar plot showing the expression of COL1A2 and Jag1 genes in primary OIS cells by immunofluorescence (unpaired Student's t-test; ** p<0.01). Error bars represent SEM. Representative images are shown on the right.

4.4 Notch Perturbation Compromised Transcriptional Signatures of NIS

To establish transcriptional differences between secondary senescence with and without Notch signalling, scRNA-seq data were obtained from IMR90 mVenus:EV and mVenus:dnMAML1 co-cultures with ER:Ras IMR90 at day 7 tamoxifen using the 10X protocol. To integrate this dataset with our previous secondary senescence transcriptomes [Figure 3.10A], the mVenus:EV and mVenus:dnMAML1 were projected by Scmap (Kiselev et al., 2018). Scmap clearly matched all primary senescent cells containing RasV12 to the OIS population [Figure 4.4A) and identified significantly more secondary senescence cells in mVenus:EV compared to mVenus:dnMaml1 [Figure 4.4A; 37% versus 24%, chi-square test, p = 0.00062], confirming a role of Notch in secondary senescence.

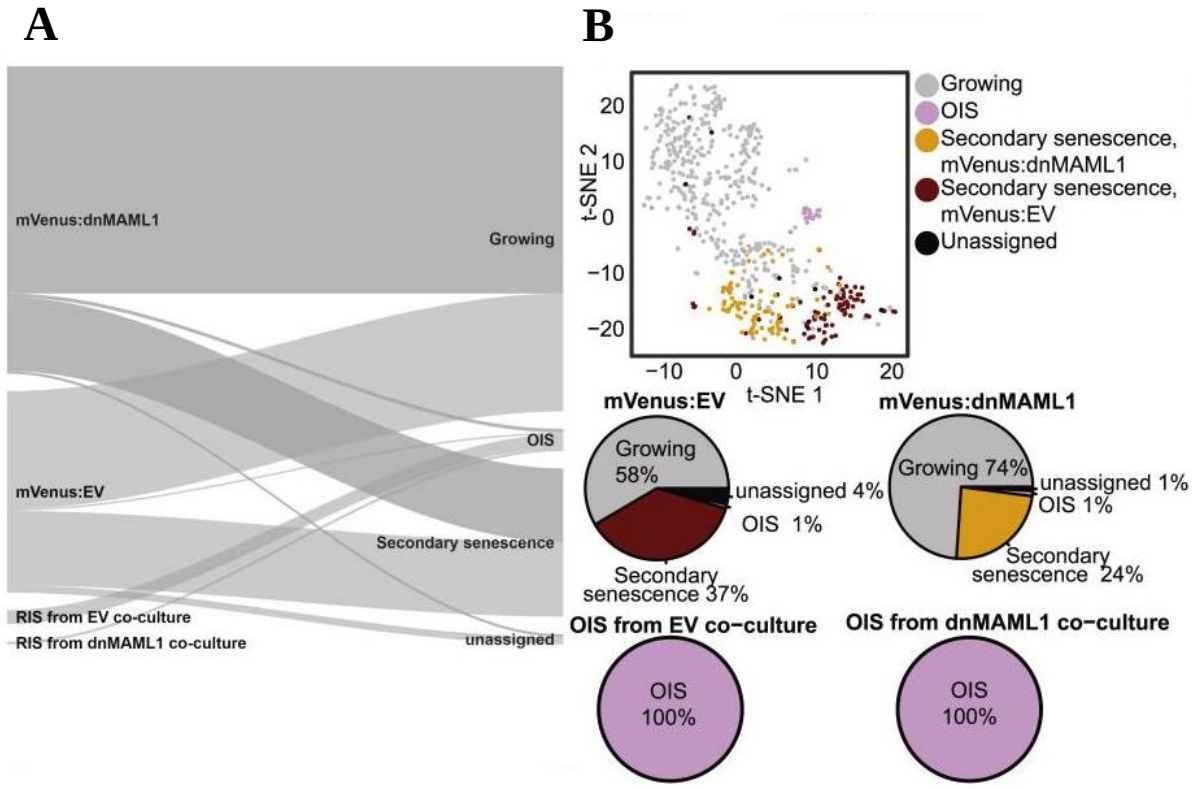

Figure 4.4: Integrated Analysis of Co-Culture Data.

This 10X dataset were combined with the previous secondary senescence transcriptomes. We then projected the mVenus:EV and mVenus:dnMAML1 using Scmap (Kiselev et al., 2018).

(A) Scmap cluster projection of the dnMAML1 and EV 10× scRNA-seq dataset to the GFP co-culture 10× scRNA-seq dataset (see 3.10A). Scmap clearly matches all primary senescent cells containing RasV12 to the OIS population and identifies significantly more secondary senescence cells in mVenus:EV compared to mVenus:dnMaml1.

(B) tSNE plot of single cells coloured by the projection toward the GFP co-culture 10X dataset (see Figure 3.10A). Pie charts show percentage of cells.

To explore transcriptomic differences between secondary senescence, all cells were plotted by Seurat, which separated mVenus:EV and mVenus:dnMAML1 into distinct secondary senescence clusters [Figure 4.4B].

Differences in the activation of Notch pathway between mVenus:EV and mVenus:dnMaml1 were confirmed by GSEA analysis [Figure 4.5A; NES = −1.35] and on the gene level for fibrillar collagens [Figure 4.5B; $p < 0.05$]. GSEA analyses also showed that Notch signalling weakened the cytokine response in senescence as mVenus:EV and mVenus:dnMaml1 had a differential regulation of SASP factors (Figure 4.5C; NES = 1.1) and the interferon-gamma response [Figure 4.5E; NES = 1.48]. Importantly, mVenus:dnMaml1 showed an upregulation of E2F targets, whose downregulation is one of the hallmarks of

senescence, compared to mVenus:EV [Figure 4.5D; p = not significant (n.s.)] (Narita et al., 2003), which explains why the strong phenotype differences were observed between the two conditions [see Figure 4.2B].

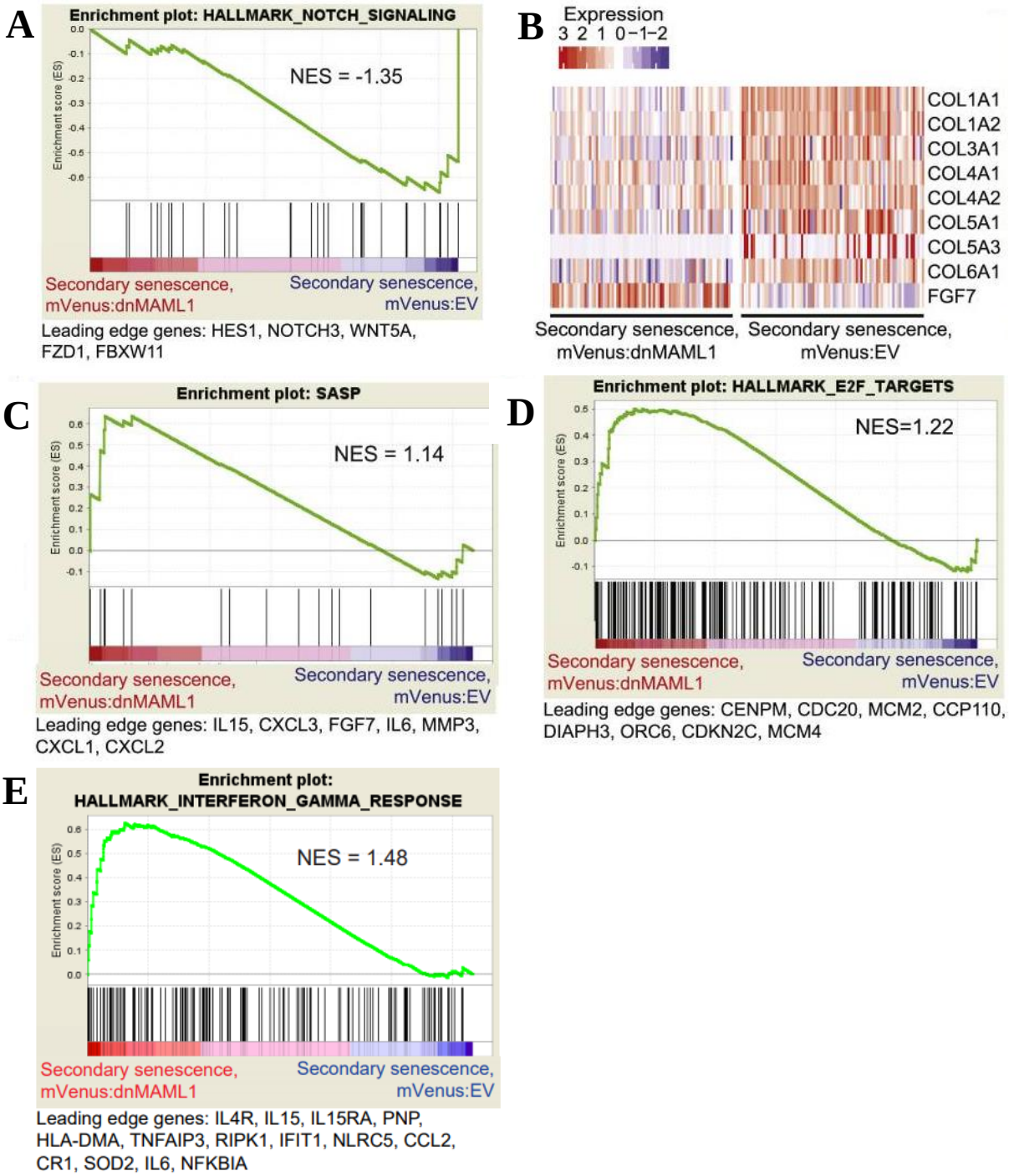

Figure 4.5: Enrichment of Notch in Secondary Senescence mVenus:Ev.

The differences in the activation of Notch pathway between mVenus:EV and mVenus:dnMaml1 were confirmed by GSEA analysis.

(A) GSEA pre-ranked test for enrichment of Notch signaling in mVenus:EV identified as secondary senescence by scmap.

(B) Heatmap of single-cell data comparing mVenus:EV and mVenus:dnMAML1 for collagens and SASP genes. Red, upregulated and blue, downregulated.

(C) GSEA pre-ranked test for enrichment of SASP genes in mVenus:dnMAML1 identified as secondary senescence by scmap.

(D) GSEA pre-ranked test for enrichment of E2F targets in mVenus:dnMAML1 identified as secondary senescence by scmap.

(E) GSEA pre-ranked test for enrichment of interferon gamma response in mVenus:dnMAML1 identified as secondary senescence by scmap.

4.5 Notch Acts in a Juxtacrine Manner to Induce Secondary Senescence

It is well established that Notch induces senescence in a juxtacrine manner through cell-to-cell contact. To verify the effect of cell-to-cell contact on the secondary senescence transcriptome, transwell experiments were set up. ER:Ras cells were co-cultured with GFP cells (GFP contact; Figure 4.6A) and GFP cells on their own in the transwell of the same well (GFP no contact). In this setting, GFP no contact cells shared media with ER:Ras cells, where cytokines could be transferred without cell-to-cell contact. Bulk RNA-seq of GFP contact and no contact cells were performed 7 days after tamoxifen induction and confirmed enhanced expression of previously observed marker genes for NIS secondary senescence in GFP contact cells [Figure 4.6B].

In addition, enrichment of Notch (NES = 1.59, FDR q = 0.019) and TGFB (NES = 1.87, FDR q = 0.0016) signalling [Figures 4.6C and 4.6D] was confirmed in GFP contact cells, as judged by GSEA. Equally, GSEA confirmed repression of E2F target genes in GFP contact compared to GFP no contact fibroblasts [Figure 4.6E] except for E2F7, whose upregulation is known in senescence [Figure 4.6B] (Aksoy et al., 2012). GSEA analysis suggests that the global differences between GFP contact and no contact cells bore a close resemblance to the differences between mVenus:EV and mVenus:dnMaml1 secondary senescence [Figure 4.6F]. Pathway analysis also indicated significant upregulation of previously described senescence

pathways, such as “Senescence and Autophagy in Cancer” and “Matrix Metalloproteases” in GFP contact compared to GFP no contact cells [Figure 4.6G].

A

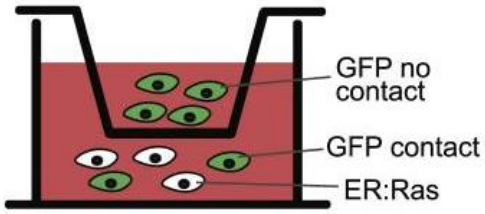

B

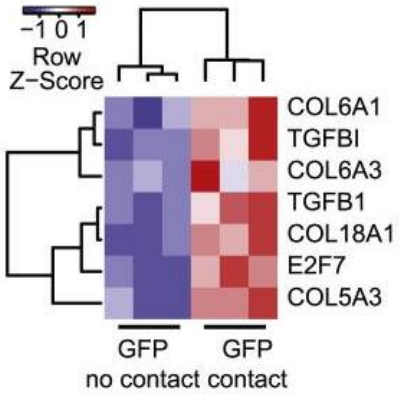

C

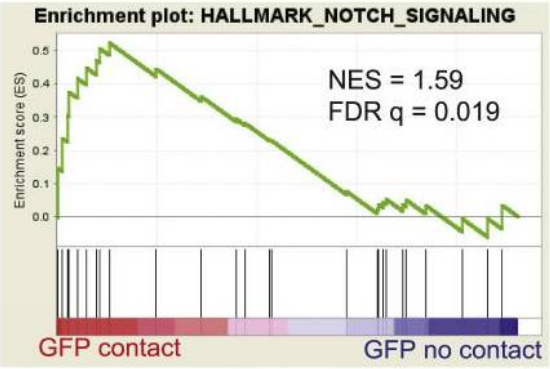

Leading edge genes: PSENEN, HES1, CCND1, DTX4, NOTCH3, WNT5A, DTX2, SAP30, FZD1

D

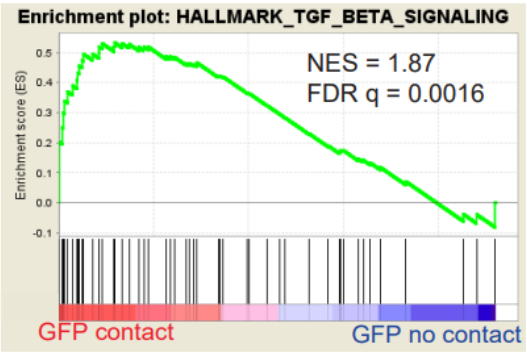

Leading edge genes: BMP2, SLC20A1, PMEPA1, WWTR1, THBS1, SKIL, SMAD7, TGFB1, NOG

E

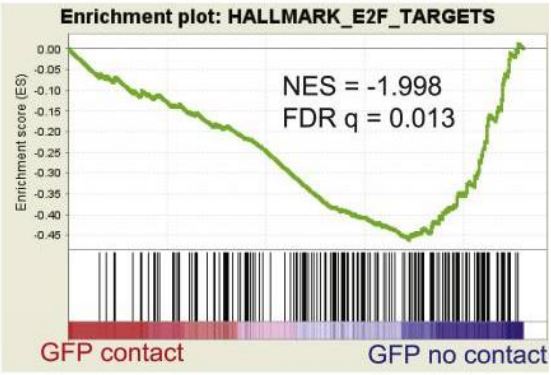

Leading edge genes: E2F8, SPC25, WDR90, SHMT1, CDKN3, PSMC3IP, EZH2

F

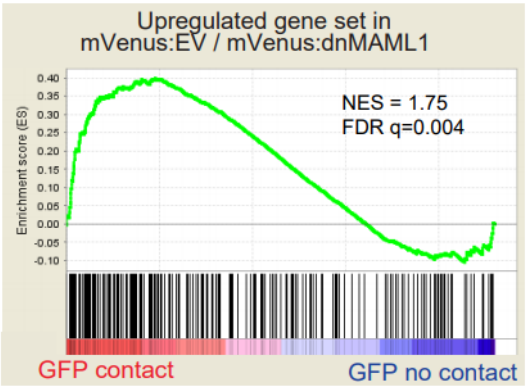

Leading edge genes: COL5A3, CHN1, KCNG1, LRRN3, OLFM2, NNMT, ADAM19, DSP, HES1

G

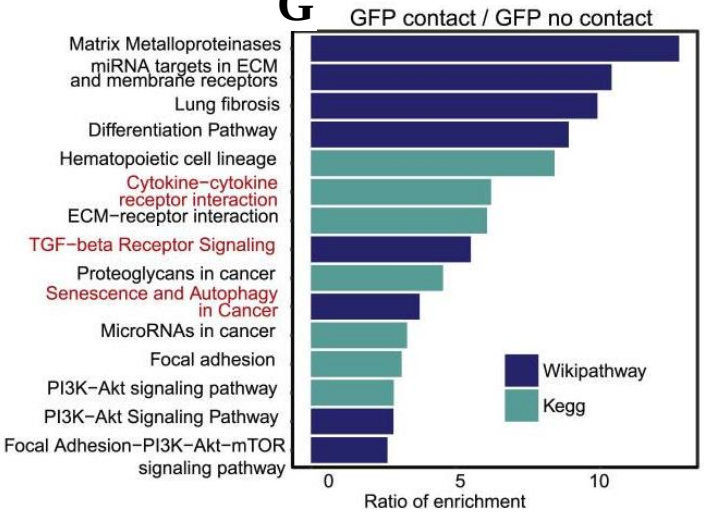

Figure 4.6: Transwell Experiments.

To verify the effect of cell-to-cell contact on the secondary senescence transcriptome, transwell experiments were set up.

(A) Schematic representation of transwell co-culture assay of OIS and GFP cells. ER:Ras cells wer co-cultured with GFP cells and GFP cells on their own in the transwell of the same well (GFP no contact). In this setting, GFP no contact cells shared media with ER:Ras cells, where cytokines can be transferred but no cell-to-cell contact is possible.

(B) Heatmap of significantly differentially expressed genes ($p < 0.05$) between GFP contact and GFP no contact cells. We performed bulk RNA-seq of GFP contact and no contact cells 7 days after tamoxifen induction and confirmed enhanced expression of previously observed marker genes for NIS secondary senescence in GFP contact cells.

(C) GSEA pre-ranked analysis for enrichment of Notch signalling in GFP contact cells compared to GFP no contact cells.

(D) GSEA pre-ranked test for enrichment of TGF-beta signalling in GFP contact compared to GFP no contact cells. mVenus:dnMAML1 identified as secondary senescence by scmap.

(E) GSEA pre-ranked analysis for enrichment of E2F targets in GFP no contact compared to GFP contact cells. Leading edge genes are indicated.

(F) GSEA pre-ranked test for enrichment of mVenus:EV signature genes in GFP contact/GFP no contact upregulated gene set.

(G) Pathway analysis for DE genes between GFP contact/GFP no contact ($p < 0.05$).

Overall, GSEA analysis confirmed the enrichment of Notch in the GFP contact cells compared to the GFP no contact.

4.6 Transition to Secondary Senescence Was Notch-Dependent

OIS induction is a multi-step process with an early proliferative phase at days 1–3, followed by a phenotype transition phase at days 3–5, and established senescence from day 7 after RasV12 expression (Young et al., 2009). To compare the impact of the different phases of primary OIS onto secondary senescence, mVenus:EV or mVenus:dnMAML1 cells were co-cultured repeatedly with ER:Ras cells at days 3–6 or at days 7–10 after RasV12 induction [Figure 4.7A].

As expected, ER:Ras cells showed low levels of EdU incorporation in mVenus:dnMAML1 (day 7, $p = 0.01$) or mVenus:EV co-culture (day 7, $p < 0.001$) [Figures 4.7B-4.7C] as a result of primary OIS. Co-culturing mVenus:EV with ER:Ras cells in the phenotype transition phase (days 3–5 after RasV12 induction) caused a significant decrease in EdU incorporation when compared to uninduced co-cultures ($p < 0.001$; Figure 4.7B), suggesting that secondary senescence induction requires transition-phase primary OIS cells. The transition-phase effect also required Notch because it could not be induced in mVenus:dnMAML1 cells ($p = 0.12$; Figure 4.7C).

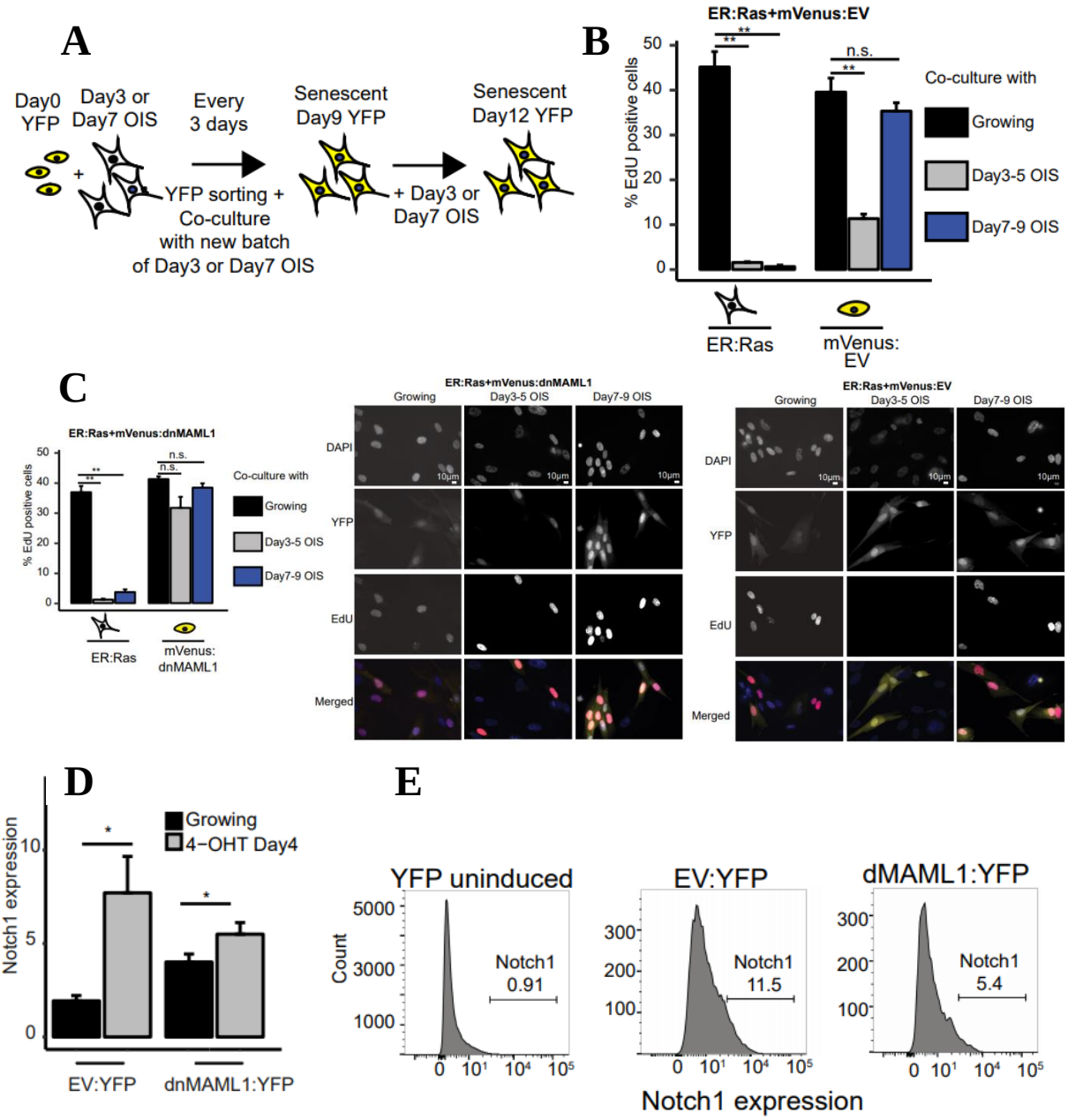
A
Day0 YFP
Day3 or Day7 OIS
Every 3 days
Senescent Day9 YFP
Senescent Day12 YFP
YFP sorting + Co-culture with new batch of Day3 or Day7 OIS
+ Day3 or Day7 OIS
B
ER:Ras+mVenus:EV
% EdU positive cells
Co-culture with
Growing
Day3-5 OIS
Day7-9 OIS
ER:Ras
mVenus: EV
C
ER:Ras+mVenus:dnMAML1
ER:Ras+mVenus:EV
Growing
Day3-5 OIS
Day7-9 OIS
DAPI
YFP
EdU
Merged
mVenus: dnMAML1
D
Notch1 expression
Growing
4-OHT Day4
EV:YFP
dnMAML1:YFP
E
YFP uninduced
EV:YFP
dMAML1:YFP
Count
Notch1 0.91
Notch1 11.5
Notch1 5.4
Notch1 expression

Figure 4.7: Dynamic Co-cultured Experiments.

(A) Schematic representation of co- culturing mVenus cells with Day 3 or Day 7 OIS cells. To compare the impact of the different phases of primary OIS onto secondary senescence, we co-cultured mVenus:EV or mVenus:dnMAML1 cells repeatedly with ER:Ras cells at days 3–6 or at days 7–10 after RasV12 induction.

(B) Bar plot showing EdU incorporation in OIS or mVenus:EV cells in growing (black), co- culture with Day 3 OIS (grey) or Day 7 OIS cells (blue). Error bars are displayed as SEM; $F[5,18] = 144.4$, $p<0.001$ using one-way ANOVA with Tukey's test (n=3 for each except for Day 3 OIS (n=6)). Representative images are shown below the bar plot. Scale bar 10μm.

(C) Bar plot showing EdU incorporation in OIS or mVenus:dnMAML1 cells in growing (black), coculture with Day 3 OIS (grey) or Day 7 OIS cells (blue). Error bars are displayed as SEM. $F[5,24] = 58$, $p<0.001$ using one-way ANOVA with Tukey's test (n=3 for all conditions except for Day3 OIS (n=6)). $^{**}p<0.001$, $^{*}p<0.05$. Representative images are shown on the right of the bar plot. Scale bar 10μm.

(D) Barplot showing the upregulation of NOTCH1 on the cell surface of mVenus:EV and mVenus:dnMAML1 cells 4 days after co-culture with ER:Ras compared to nonco-cultured, growing mVenus:EV (mVenus:EV $t = -3.27$, $df = 2.01$, p-value = 0.041; mVenus:dnMAML1 $t = -3.29$, $df = 3.03$, p-value = 0.023 using one-sided t- test). Error bars represent SEM. Representative FACs plots showing NOTCH1 staining of YFP uninduced fibroblasts and YFP:EV and YFP:dnMaml1 at 4 days of co-culture.

In contrast, the co-culture between mVenus:EV cells and primary OIS cells in established senescence phase (days 7–10 after RasV12 induction) did not lead to a reduction in EdU incorporation in mVenus:EV cells compared to uninduced co-cultures ($p = 0.59$; Figure 4.7B), mirroring results obtained in mVenus:dnMAML1 co-cultures ($p = 0.99$; Figure 4.7C). From day 4 co-culture, there was a significant upregulation of Notch1 on the cell surface of mVenus:EV ($p = 0.041$ day 4, $p = 0.038$ day 7; data not shown) and mVenus:dnMaml1 ($p = 0.023$ day 4, $p = 0.046$ day 7; data not shown) cells compared to growing, providing a pathway to NIS induction [Figure 4.7D]. Overall, the data identified Notch as a key mediator of secondary senescence.

4.7 *In Vivo* Model of Primary and Secondary Senescence Was Generated in Hepatocytes

To test the involvement of NIS *in vivo*, a model where primary senescence is induced in a subpopulation of hepatocytes following *Mdm2* deletion was generated in the Bird lab, Glasgow (Bird et al., 2018). The activation of this model by hepatocyte-targeted recombination of *Mdm2* (β-napthoflavone [βNF] induction AhCre, Mdm2−) resulted in primary senescence in *Mdm2*− cells. Crucially, *Mdm2*− hepatocytes induced secondary senescence in neighbouring hepatocytes (Bird et al., 2018) [Figure 4.8A]. In this model, the presence of p53 induction through *Mdm2*deletion with medium levels of CDKN1A (non-senescence/primary $p < 0.001$) marks primary senescence induction (Bird et al., 2018) [Figure 4.8B; Figures 4.8C-4.8D]. Physiological levels of P53 and high levels of CDKN1A (CDKN1A expression secondary/primary $p < 0.0001$) marks secondary senescence in *Mdm2*normal (*Mdm2*+) hepatocytes as described (Bird et al., 2018) [Figure 4.8B]. Based on these characteristics, cells can be readily distinguished by immunohistochemistry with 23% of primary and 10% of secondary senescence hepatocytes detected [Figure 4.8C]. We have previously shown that both subpopulations of hepatocytes upregulate senescence markers (gH2AX, Il1A, SA-Beta Gal) and reduce BrdU incorporation (Bird et al., 2018

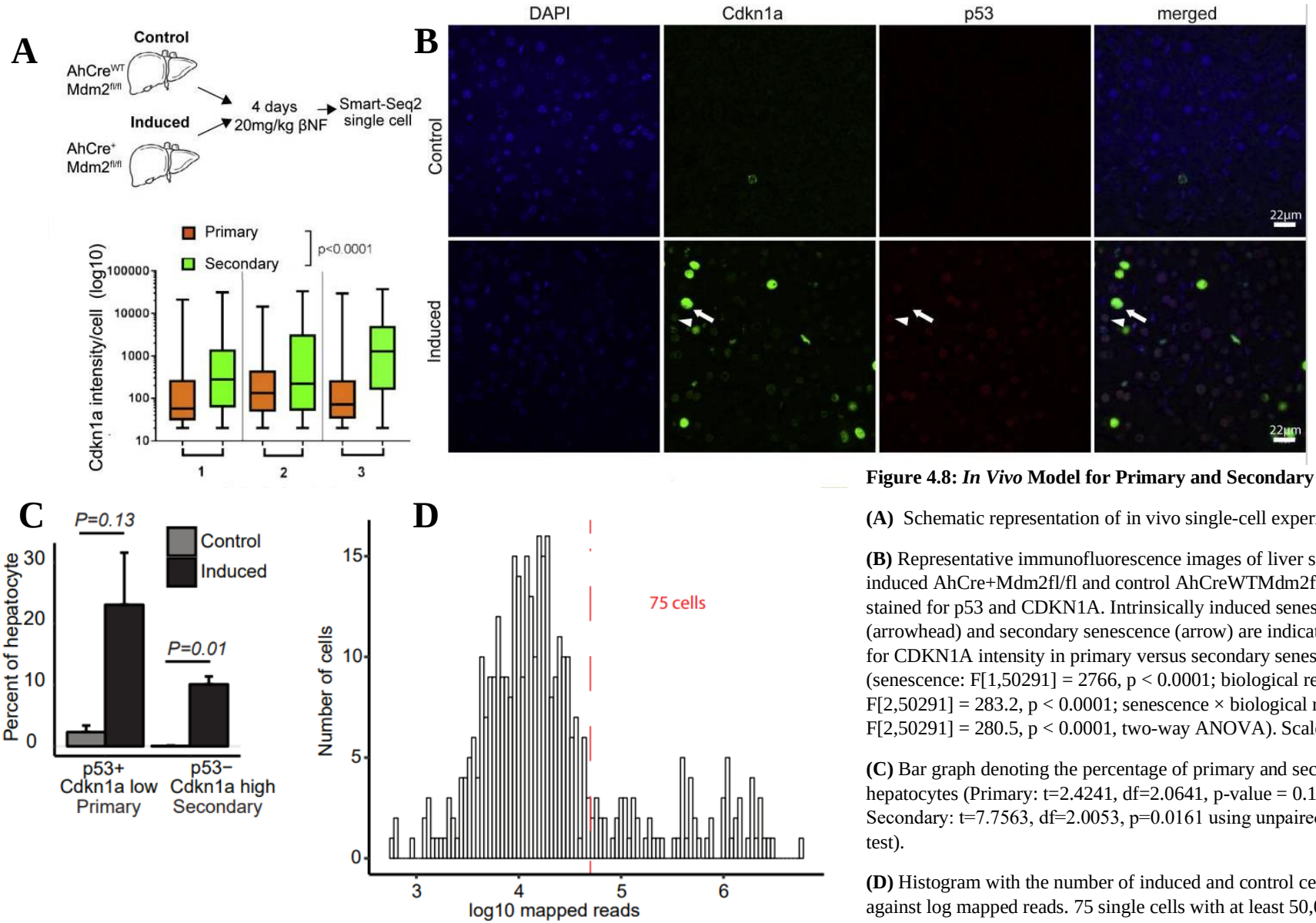

Figure 4.8: *In Vivo* Model for Primary and Secondary Senescence.

(A) Schematic representation of in vivo single-cell experiment.

(B) Representative immunofluorescence images of liver section from induced AhCre+Mdm2fl/fl and control AhCreWTMdm2fl/fl mice stained for p53 and CDKN1A. Intrinsically induced senescence (arrowhead) and secondary senescence (arrow) are indicated. Boxplot for CDKN1A intensity in primary versus secondary senescent cells. (senescence: $F[1,50291] = 2766$, $p < 0.0001$; biological replicates: $F[2,50291] = 283.2$, $p < 0.0001$; senescence × biological replicates: $F[2,50291] = 280.5$, $p < 0.0001$, two-way ANOVA). Scale bar, 22 µm.

(C) Bar graph denoting the percentage of primary and secondary hepatocytes (Primary: $t=2.4241$, $df=2.0641$, p-value = 0.1324; Secondary: $t=7.7563$, $df=2.0053$, $p=0.0161$ using unpaired Student's t-test).

(D) Histogram with the number of induced and control cells is plotted against log mapped reads. 75 single cells with at least 50,000 aligned reads are downsampled to 50,000 reads.

4.8 NIS Signatures Characterised Secondary Senescent Hepatocytes

To investigate if primary and secondary senescence transcriptomes were distinct *in vivo*, scRNA-seq was performed on hepatocytes using the Smart-Seq2 protocol [Figure 4.8A]. 39 single cells from induced *Mdm2*-deleted mouse liver passed the filtering criteria for downstream analysis [Figures 4.9A and 4.9B; Table S2]. *Mdm2*− cells were distinguished from *Mdm2*+ hepatocytes by the absence of mapping reads over exon 5 and 6 of the *Mdm2* gene [Figure 4.9B]. Both senescent populations expressed *Cdkn1a* consistently with the differences in CDKN1A protein levels as shown by immunohistochemistry [Figure 4.8B], with lower (but not significant) *Cdkn1a* expression in *Mdm2*−compared to *Mdm2*+ hepatocytes [Figure 4.9C], enabling primary and secondary senescence to be distinguished.

To verify a senescence phenotype in both *Mdm2*− and *Mdm2*+ hepatocyte populations, pathway analysis was conducted, showing upregulated pathways being enriched in p53 signalling, including CDKN1A, DNA damage response, and cytokine signalling [Figure 4.9D]. To determine if NIS plays a role in secondary senescence *in vivo*, the single-cell data were analysed by using three independent methods. Single-cell differential expression (SCDE) identified differentially expressed genes between *Mdm2*+ and *Mdm2*− cells [Table S3], and genes were ranked between *Mdm2*+/*Mdm2*− cells for downstream analysis. First, pathway analysis demonstrated enrichment in Notch signalling (ratio of enrichment [RE], 7.07), Delta-Notch signalling (RE, 4.63), and TGFB (RE, 4.11) signalling pathways [Figure 4.9E].

Second, GSEA ranked the Notch signalling pathway (NES = 1.07) as one of the top 20 Kegg pathways enriched in Mdm2+/Mdm2− [Figure 4.9F] with leading-edge genes *Maml1* and *Jag2* found specifically in Mdm2+ cells [Fisher's exact-test = 6.93×10^{-7}; Figure 4.9G]. Regardless of Mdm2 status, the majority of cells expressed the same level of housekeeping and hepatocyte-specific genes [Figure 4.9G]

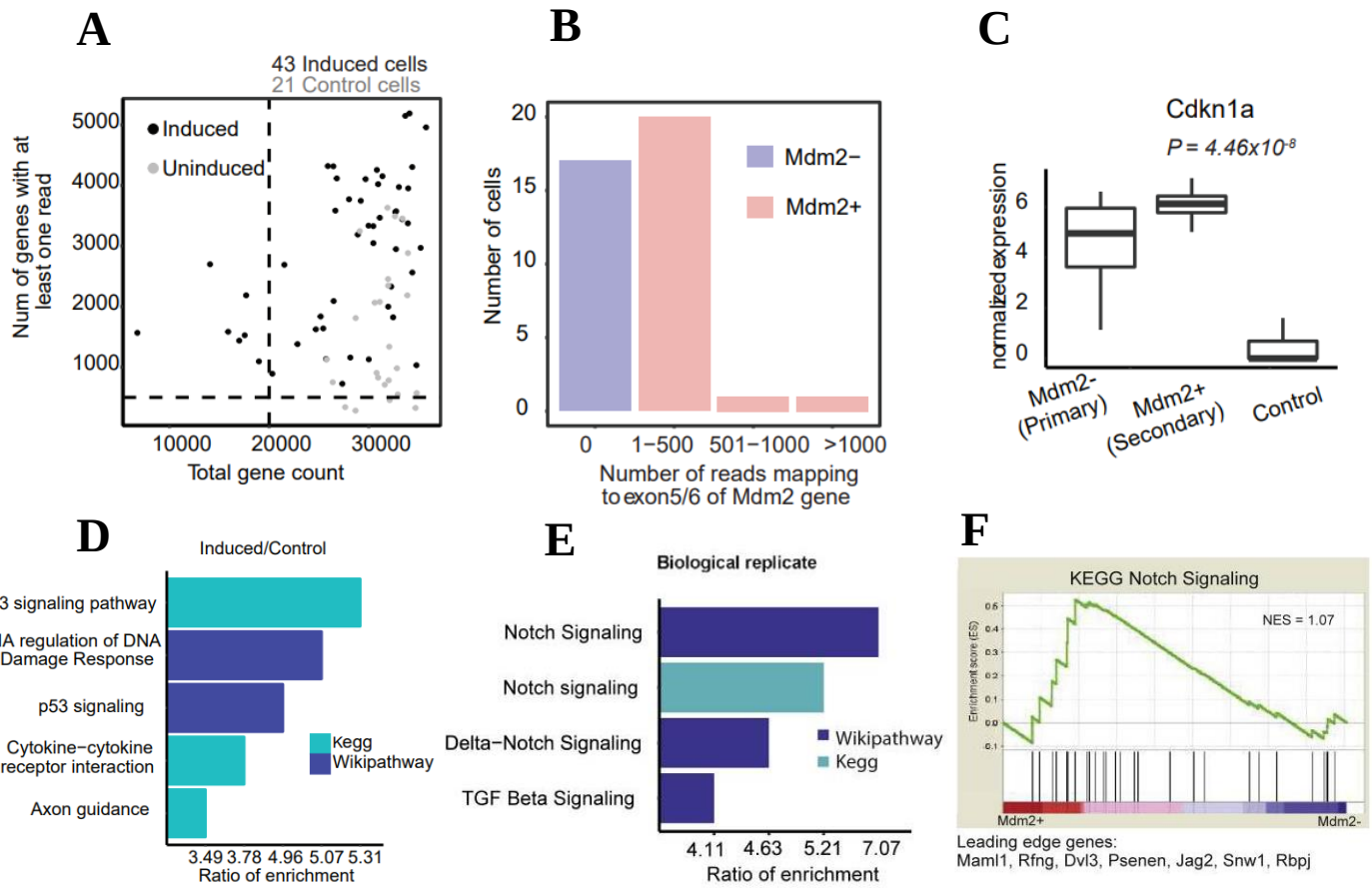
A
43 Induced cells
21 Control cells
Induced
Uninduced
Num of genes with at least one read
Total gene count
B
Mdm2−
Mdm2+
Number of cells
Number of reads mapping to exon5/6 of Mdm2 gene
C
Cdkn1a
P = 4.46x10-8
normalized expression
Mdm2- (Primary)
Mdm2+ (Secondary)
Control
D
Induced/Control
p53 signaling pathway
miRNA regulation of DNA Damage Response
p53 signaling
Cytokine−cytokine receptor interaction
Axon guidance
Kegg
Wikipathway
Ratio of enrichment
E
Biological replicate
Notch Signaling
Notch signaling
Delta−Notch Signaling
TGF Beta Signaling
Wikipathway
Kegg
Ratio of enrichment
F
KEGG Notch Signaling
NES = 1.07
Mdm2+
Mdm2-
Leading edge genes:
Maml1, Rfng, Dvl3, Psenen, Jag2, Snw1, Rbpj

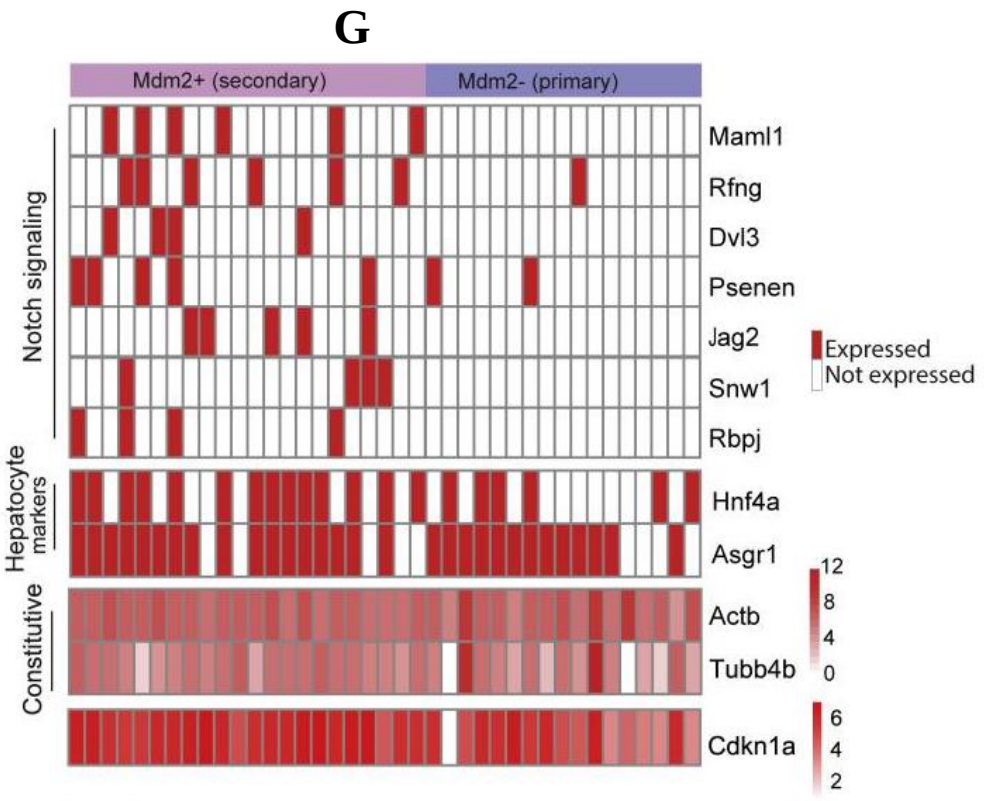
G
Mdm2+ (secondary)
Mdm2- (primary)
Notch signaling
Hepatocyte markers
Constitutive
Maml1
Rfng
Dvl3
Psenen
Jag2
Snw1
Rbpj
Hnf4a
Asgr1
Actb
Tubb4b
Cdkn1a
Expressed
Not expressed

Figure 4.9: Single-Cell *In Vivo* Data Analysis.

ScRNA-seq was performed on hepatocytes using Smart-Seq2. After filtering, we retained 39 single cells from induced *Mdm2*-deleted mouse liver for downstream analysis.

(A) Dot plot with the number of genes with at least one read to total gene count for induced (black) and control (grey) cells. Cells with a total gene count of more than 20,000 and 500 genes detected were retained.

(B) 17 Mdm2- cells were identified as cells with no reads mapping to exon5/6 of Mdm2 gene and 22 Mdm2+ cells contained reads mapping to the exons.

(C) Box plots showing the expression of Cdkn1a in induced cells relative to control (p=4.46x10-18). The top and bottom bounds of the boxplot correspond to the 75 and 25th percentile, respectively. p-values were obtained using differential analysis in SCDE.

(D) Pathway analysis for induced/uninduced hepatocytes. Kegg pathways are shown in turquoise and Wikipathways in blue.

(E) Pathway analysis for Mdm2+ (secondary) genes. GSEA revealed Notch signaling pathway (NES = 1.07) as one of the top 20 Kegg pathways enriched in Mdm2+/Mdm2−.

(F) GSEA for Mdm2+/Mdm2− cells (NES = 1.07). Leading edge genes are indicated.

(G) Heatmap for Notch pathway, hepatocyte markers, and Cdkn1a genes in Mdm2+ and Mdm2− cells. Constitutive genes and Cdkn1a were coloured by their expression relative levels (binary: red expressed, white not expressed).

Third, SCDE analysis confirmed that Notch and TGFB targets *Maml1* (adjusted *Z* score [aZ] = 0.4) and *Rfng* (aZ = 0.39) with effector protein *Smad3* (aZ = 0.26) were specifically upregulated in *Mdm2*+ compared to *Mdm2*−hepatocytes (Figure 4.10A). To assess the proposed TGFB and CEBPB bias between primary and secondary senescence *in vivo*, liver samples from uninduced and induced mice were stained for CDKN1A and CEBPB by immunohistochemistry. Consistent with the previous *in vitro* data, higher CEBPB protein was significantly expressed in primary ($p < 0.0001$; Figure 4.10B] compared to secondary senescent hepatocytes. These lines of evidence from hepatocytes show that NIS signature characterises secondary senescent *in vivo*.

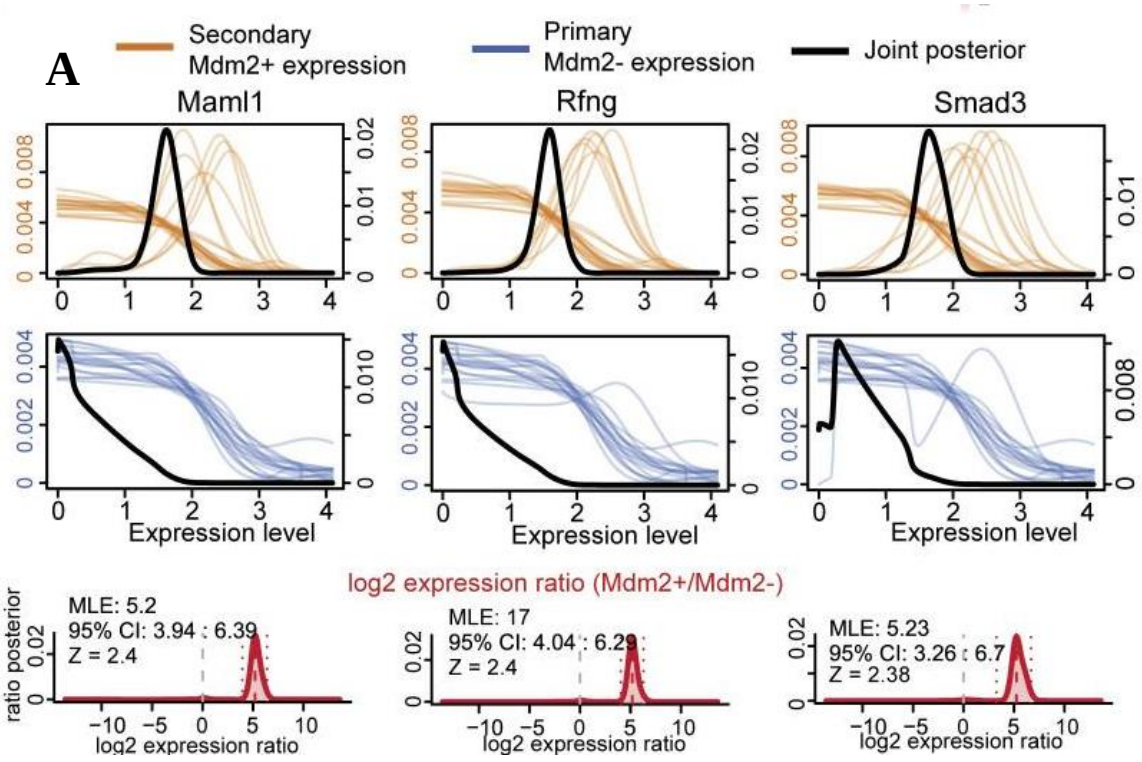
A
Secondary
Mdm2+ expression
Primary
Mdm2- expression
Joint posterior
Maml1
Rfng
Smad3
Expression level
log2 expression ratio (Mdm2+/Mdm2-)
ratio posterior
MLE: 5.2
95% CI: 3.94 : 6.39
Z = 2.4
MLE: 17
95% CI: 4.04 : 6.29
Z = 2.4
MLE: 5.23
95% CI: 3.26 : 6.7
Z = 2.38
log2 expression ratio

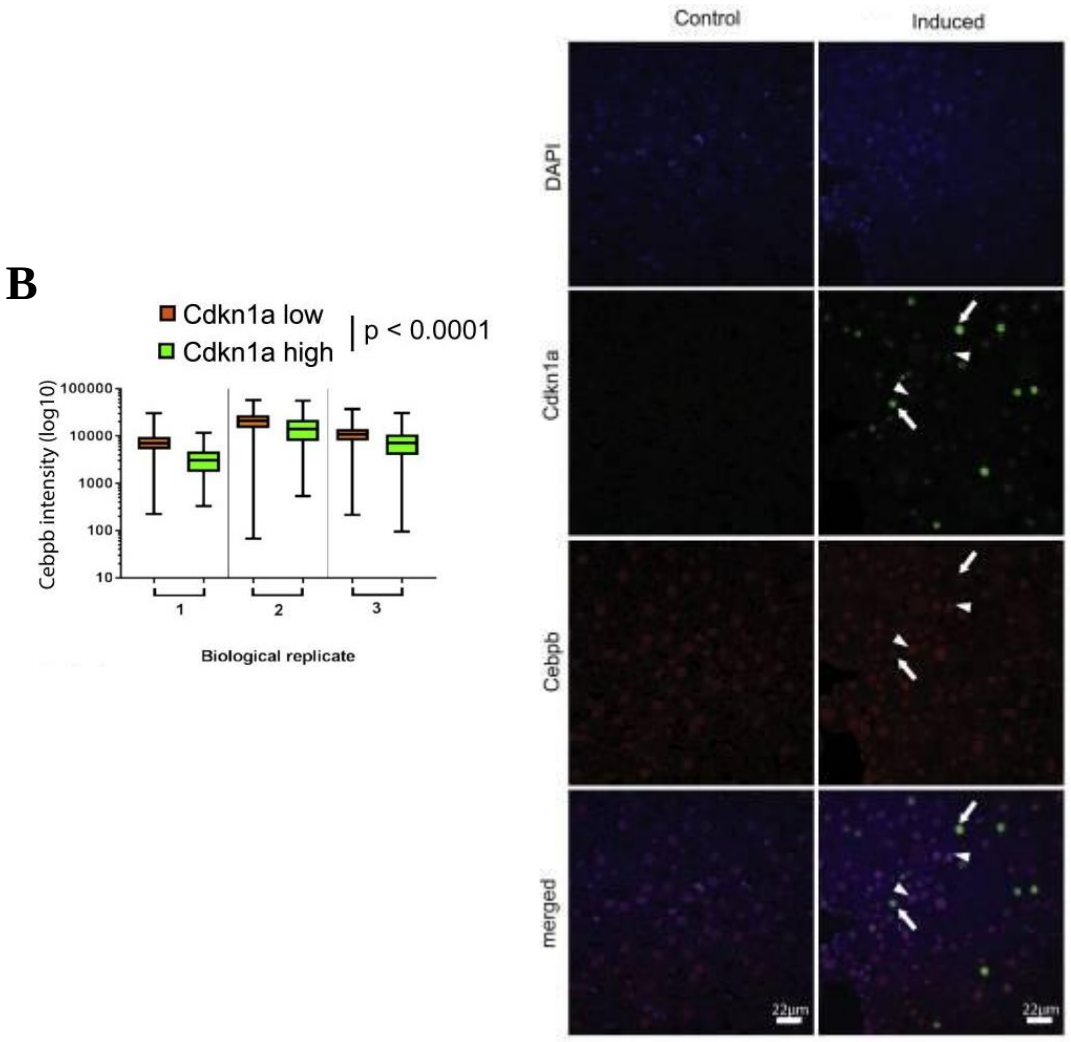
B
Cdkn1a low
Cdkn1a high
p < 0.0001
Cebpb intensity (log10)
Biological replicate
Control
Induced
DAPI
Cdkn1a
Cebpb
merged
22μm

Figure 4.9: *In Vivo* Enrichment in Notch Signatures.

Differentially expressed genes between *Mdm2+* and *Mdm2−* cells were identified using single cell differential expression (SCDE).

(A) SCDE for Maml1, Rfng, and Smad3 in Mdm2+ cells (orange lines) and Mdm2− cells (blue lines). Joint posterior is marked by black line. Fold change of the genes in Mdm2+/Mdm2− is indicated in red, and dotted lines mark the 95% confidence interval. MLE, maximum likelihood estimation; CI, confidence interval; Z, Zscore. SCDE analysis confirmed the specific upregulation of Notch and TGFB targets *Maml1* (adjusted *Z* score [aZ] = 0.4) and *Rfng* (aZ = 0.39) with effector protein *Smad3* (aZ = 0.26) in *Mdm2+* compared to *Mdm2−* hepatocytes.

(B) Representative immunofluorescence images of liver section from induced and control mice. Primary senescent cells (arrowheads) and secondary senescent cells (arrows) are indicated (CDKN1A: $F[1,60145] = 353.3$, $p < 0.0001$; biological replicates: $F[2,60145] = 1044$, $p < 0.0001$; CDKN1A × biological replicates: $F[2,60145] = 8.96$, $p < 0.0001$, two-way ANOVA). Scale bar, 22 μm.

4.9 Discussion

The understanding of tumour heterogeneity has greatly advanced, but it remains why cancer cells exhibit cellular heterogeneity in a pre-cancerous state. Do cells equally respond to the same oncogenic cue or does oncogenic activation lead to a heterogeneous population? Gaining insight into the heterogeneity in a pre-cancerous state will inform distinct propensities for transformation in subpopulations. Similarly, senescence can be induced by various stressors to overwrite the current transcriptional state that cells are in, but to what level does the pre-senescent state of these cells reflect the outcome of a senescence stimulus, particularly an oncogenic insult? These questions highlight the importance of understanding cellular heterogeneity in cellular senescence.

Using single-cell approaches, my research studies have uncovered heterogeneity in primary OIS and secondary senescence transcriptomes following oncogenic activation. The two transcriptional endpoints for primary OIS, namely a Ras-driven and a NIS programme, have been identified from single-cell experiments. The establishment of paracrine senescence via SASP is believed to be the main mechanism for secondary induction of senescence in OIS (Acosta et al., 2013, Kuilman et al., 2008). The results shown in this chapter, as well as in the previous chapter, challenge this canonical view and implicate NIS as a synergistic driver of secondary senescence *in vitro*, in the most studied OIS background (RasV12) and in the liver *in vivo*.

Primary and secondary senescent cells had never been viewed as functionally distinct end stages in OIS. Here, I have provided strong evidence that primary OIS and secondary senescence are functionally different, utilising the system that expressed dominant-negative form of the mastermind-like 1 protein by which Notch-mediated transcriptional activation was inhibited. Relatively little is known about the role of MAML coactivators in OIS apart from its importance as a central regulator in Notch signalling whose deregulation was found in several types of cancer such as human lymphomas (Köchert et al., 2011). The involvement of MAML coactivators in the complex signalling networks of cellular senescence remains to be unveiled.

Overall, the data indicate cells carrying a composite transcriptional signature of paracrine and juxtacrine events as a facultative endpoint for cells with detectable Ras activation (primary). Notch signalling has been found to be the mediator of the secondary senescence endpoint through cell-to-cell contact (juxtacrine), which is consistent with the model of a

transient state towards primary senescence induction (Hoare et al., 2016). These results also highlight a need for primary Ras fibroblasts to be in the transition phase phenotype to mediate secondary senescence by Notch.

Looking beyond the fact that Notch is the main mediator of secondary senescence, I also reported an interesting pattern of SAHF suppression in secondary senescent populations, which is in agreement with an earlier report where impaired Notch signalling partially suppressed SAHF formation in primary senescence (Parry et al., 2018). The co-occurrence between SAHF-negative phenotype and secondary senescence has far-reaching consequences in the field of senescence biology. It offers a possible explanation for a long-standing question in the field since 2003 when SAHF was discovered: what is the difference between SAHF-positive and SAHF-negative senescent cells? A simple answer would be primary OIS cells are SAHF-positive, while secondary senescent cells are SAHF-negative.

It is clear that primary senescence and Notch-mediated juxtacrine senescence possess distinct gene expression profiles and potentially different transformation potentials (Acosta et al., 2013, Hoare et al., 2016). Interestingly, as can be seen from the gene set enrichment analysis of secondary senescence clusters, components of Wnt signalling were also identified as leading genes (Wnt5A and Fzd1). It is well established that overactivation of canonical Wnt signalling promotes cancer while OIS acts to suppress it. Available evidence suggests that the onset of primary OIS requires Wnt suppression and activation of Wnt delays primary OIS (Adams and Enders 2008). Further work is needed to understand why a relative de-repression of Wnt signalling took place during Notch-enriched secondary senescence compared to primary senescence. Some of the findings also indicate a functional diversification; for instance, secondary senescence showed the blunted SASP response and the induction of fibrillar collagens compared to OIS. The transformation potential of these heterogeneous populations, however, is an area that still needs to be explored further.

Finally, given the nascent stage of research on secondary senescence, the biological significance of this juxtacrine mechanism is yet to be revealed. An unpublished result obtained from the scRNA-seq experiment of OIS cells discussed in Chapter 3 appears to provide a clue to the link between the biological meaning of senescence and its mechanism. The Notch ligand JAG1 was upregulated specifically in primary senescence cells [Figures 4.11A-B]. This could deliver an explanation as to why the secondary spread of senescent cells can be contained locally, as opposed to the senescence process expanding endlessly once established. Secondary

senescent cells, which express low levels of the ligand JAG1, will not be able to induce further senescence responses [Figure 4.11C]. Such a local containment might be beneficial for the clearance of unwanted senescent cells by the immune system.

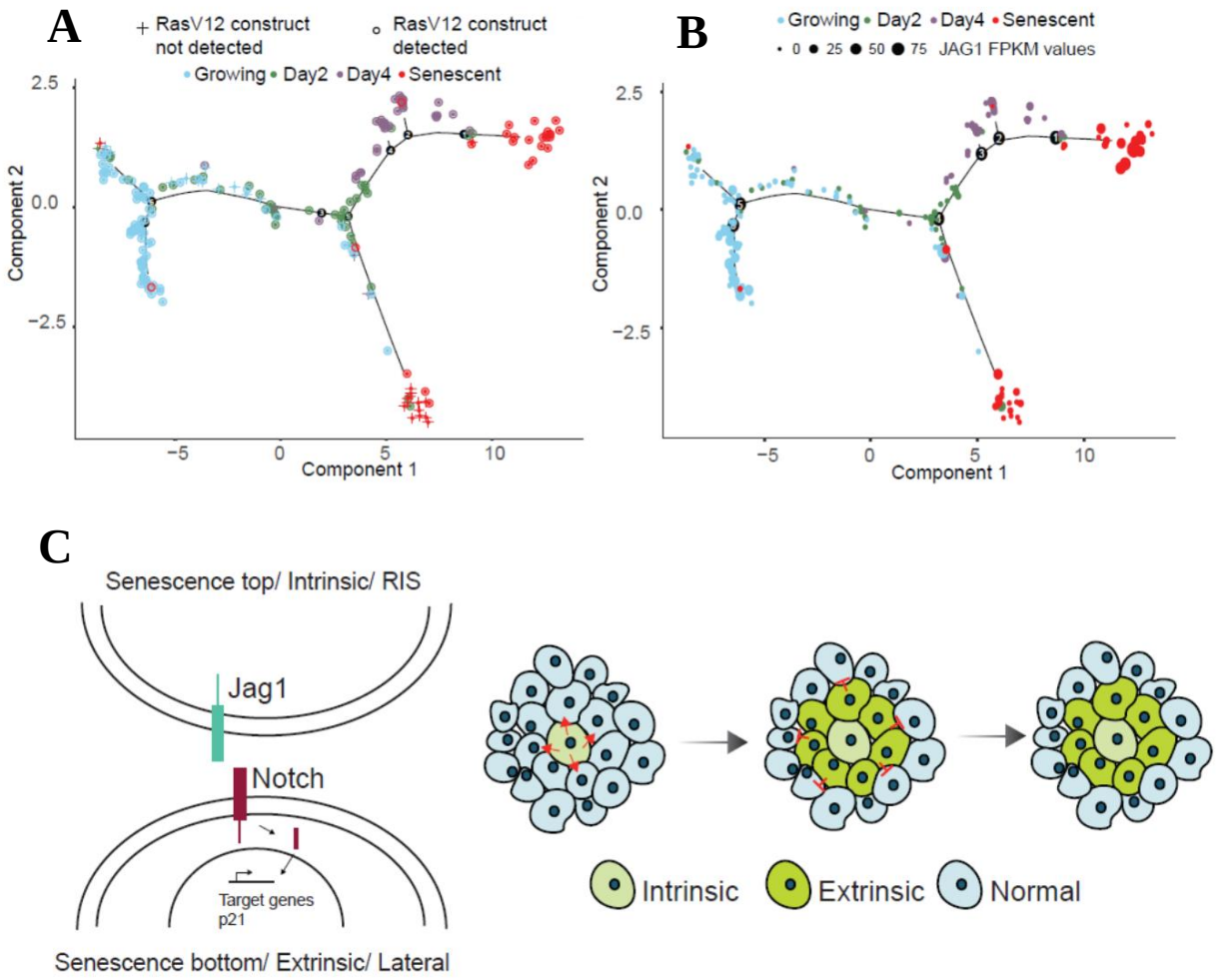

Figure 4.11: Single-cell Time Course Analysis of OIS cells and a Proposed Model for the Role of Secondary NIS.

(A) Monocle2 plot for the time-course experiment shows the presence or absence of the mutated RAS gene as indicated.

(B) Monocle2 plot for the time-course experiment shows the FPKM values of JAG1 expression.

The data indicate cells carrying a composite transcriptional signature of paracrine and juxtacrine events as a facultative endpoint for cells with detectable Ras activation (primary).

(C) Schematic representation of how secondary senescence is locally contained. Since the Notch ligand JAG1 was upregulated specifically in primary senescence cells, this could explain why the secondary spread of senescent cells can be contained locally, as opposed to the senescence process expanding endlessly once established. Secondary senescent cells, which express low levels of the ligand JAG1, will not be able to induce further senescence responses. Such a local containment might be beneficial for the clearance of unwanted senescent cells by the immune system.

4.10 Summary

By establishing a co-culture system in which Notch signalling could be interrupted and from which single-cell data were obtained, it was confirmed that secondary senescence requires Notch signalling in vitro. The in vivo hepatocyte model also recapitulated the induction of secondary senescence that was characterised by Notch-induced senescence signatures. In summary, Notch signalling has been identified as a main effector of secondary senescence.

Chapter 5: Single-Cell Transcriptomics of Hutchinson-Gilford progeria syndrome (HGPS)

5.1 Introduction

Attempts in ageing research have been directed to studies in model organisms from the yeast to the mouse. Hutchinson-Gilford progeria syndrome (HGPS), a group of sporadic, rare, autosomal dominant genetic diseases characterised by clinical features of premature ageing, allows researchers to explore the molecular events that explain accelerated age-related phenotypes (Sinha, Ghosh, and Raghunath 2014). The identification of *LMNA* as the target gene for mutations causing structural abnormalities in the nucleus and characteristics of premature ageing has led to the generation of hypotheses of the mechanism that drives the ageing process.

Several ageing models have revolved around the hypothesis that stem cell exhaustion is responsible for ageing-related dysfunction [Figure 5.1]. A substantial amount of evidence in haematopoietic stem cells shows that a decline in stem cell function and self-renewal capacity causes tissue degeneration and ageing phenotype (Rossi et al. 2007; Oh, Lee, and Wagers 2014). Progressive impairment of stem cell functionality with age may arise because of the exposure to intrinsic/extrinsic stress over a lifetime, but the mechanism behind this is still being unravelled (Pazhanisamy 2009). Alternatively, we could interpret ageing as a result of a 'toxic environment' created from damaged or defected cells, which then toxically impact on neighbouring cells and tissues. Studies that lend support to this model reported that removal of senescent cells from mouse tissues can delay the onset of age-associated disorders in adipose tissue, skeletal muscle and eye, as well as extend their healthy lifespan (Baker et al., 2011). Given that persistent secretion of inflammatory cytokines and other systemic factors during chronic senescence can favour both degenerative and hyperplastic pathologies (Campisi 2013), it is plausible that accumulation of senescent cells might systematically promote an ageing environment and therefore the ensuing loss of cellular function.

This chapter focuses on the second project, which explored single-cell heterogeneity in progeria cells, specifically the proportion of progeria cells that were compromised phenotypically and transcriptionally. Although much research has been conducted on the cellular features of progeria cells, characterising them at the single-cell level is a challenging

task. The first phase of this project addressed the question of how many cells are affected by the progeria condition through cellular phenotyping of progeria nuclei. I began the study by performing immunofluorescence labelling of lamin B1 in *Zmpste24*$^{-/-}$ and wild-type cells. B-type lamins are involved in the regulation of organogenesis as well as the organisation of the nuclear lamina (Dreesen et al., 2013). Lamin B1 co-localises with prelamin A in *Zmpste24*$^{-/-}$ mice (Pendás et al., 2002) and low levels of lamin B1 have been reported in HGPS and senescent fibroblasts (Scaffidi and Misteli 2008; Taimen et al., 2009), but the causal relationship between lamin B1 levels and progeria condition remains to be established. Through the quantification of lamin B1, I hope to understand the extent of cellular heterogeneity in progeria cells.

The second part of the work exploited a state-of-the-art single-cell technology, the 10X Genomics platform, to characterise the transcriptome of individual progeria cells and variation in gene expression within the progeria population. A great amount of computational resources required for analysing the single-cell data were obtained from Jeanette Baran-Gale, who developed the upstream bioinformatics pipeline for scRNA-seq quality control and profiling and guided me through subsequent downstream processing of the data. By combining the morphological profiles with the transcriptional profiles, I hoped to gain insight into the disease state of progeria and improve our understanding of the ageing process.

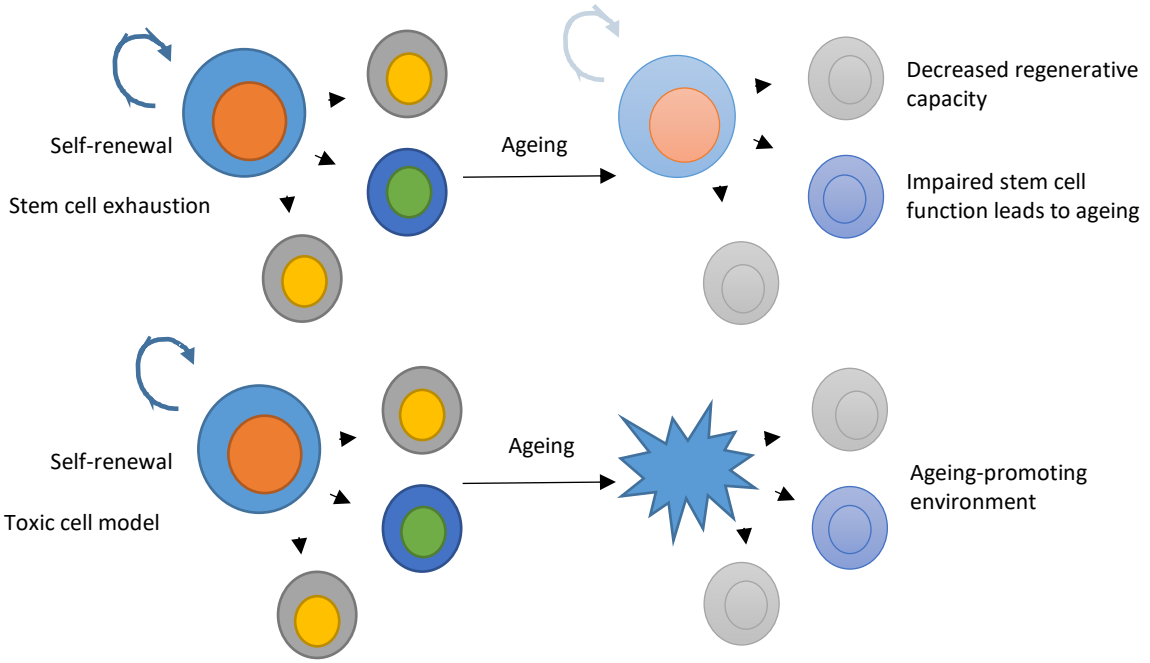

Figure 5.1: Schematic Diagram of the Toxic Ageing Model.

An attractive interpretation of ageing is that cells age as a result of a 'toxic environment' created from damaged or defected cells, which then toxically impact on their healthy and normal neighbouring cells and tissues.

5.2 Progeria Cells Showed Senescent Markers

To understand the heterogeneity of premature ageing, I started to explore cellular phenotypes of progeria cells obtained from *Zmpste24*-deficient (*Zmpste24*$^{-/-}$) mice, commonly used as a model system to study progeroid diseases. I examined whether these knock-out (KO) cells exhibited early signs of senescence. As expected, the KO progeria cells senesced prematurely compared to the control cells as revealed by the senescence-associated β-galactosidase assay [Figure 5.2]. While no observable control cells (0%, n = 200) were stained positively for β-galactosidase activity at passage 6, approximately 48% (n = 200) of KO progeria cells were positive at passage 6 [Figure 5.2]. The results concur with previous findings in *Zmpste24*$^{-/-}$ mice [Varela, 2005].

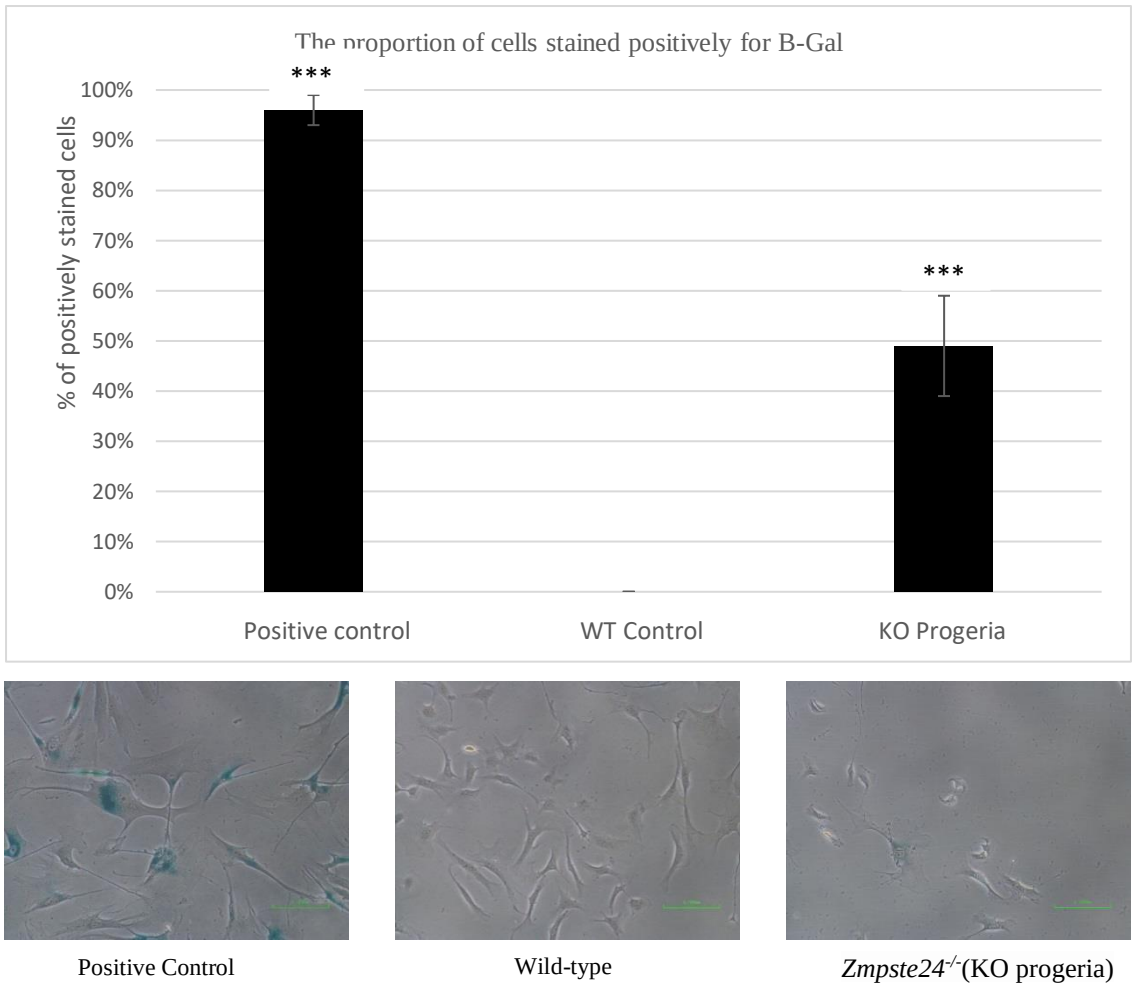

Figure 5.2: SA-Beta Gal Counts for Progeria Cells.

Cells were stained for the presence of SA-β-gal as described in the methodology. The number of SA-β-gal-positive cells was counted for each condition. H-Ras^{V12} cells undergoing full senescence at day 7were used as a positive control. The experimental conditions were normal adult wild-type (WT) fibroblasts at passage 6, and progeria fibroblasts *(Zmpste24$^{-/-}$)* at passage 6. Representative images are shown at the bottom. Error bars are ± SEM, n=300 for each experimental condition, and *** P < 0.001 vs WT control. Scale bar 100μm.

Since cellular senescence refers to the irreversible growth arrest of cells, I measured the proliferative ability of progeria fibroblasts and their WT counterparts. Cells were cultured at low oxygen levels (3%) and passaged successively until they stopped dividing. WT cells exhibited a sustained growth rate throughout the duration of 30 days before reaching a growth plateau after 20-21 population doublings (PDs) [Figure 5.3]. KO progeria cells, on the other hand, showed a marked decrease in their proliferative capacity, entering growth arrest after 8-9 PDs, indicating early senescence. This is in agreement with the previous publication and confirms the characteristics of progeria cells, which include reduced proliferation and the expression of markers for cellular senescence.

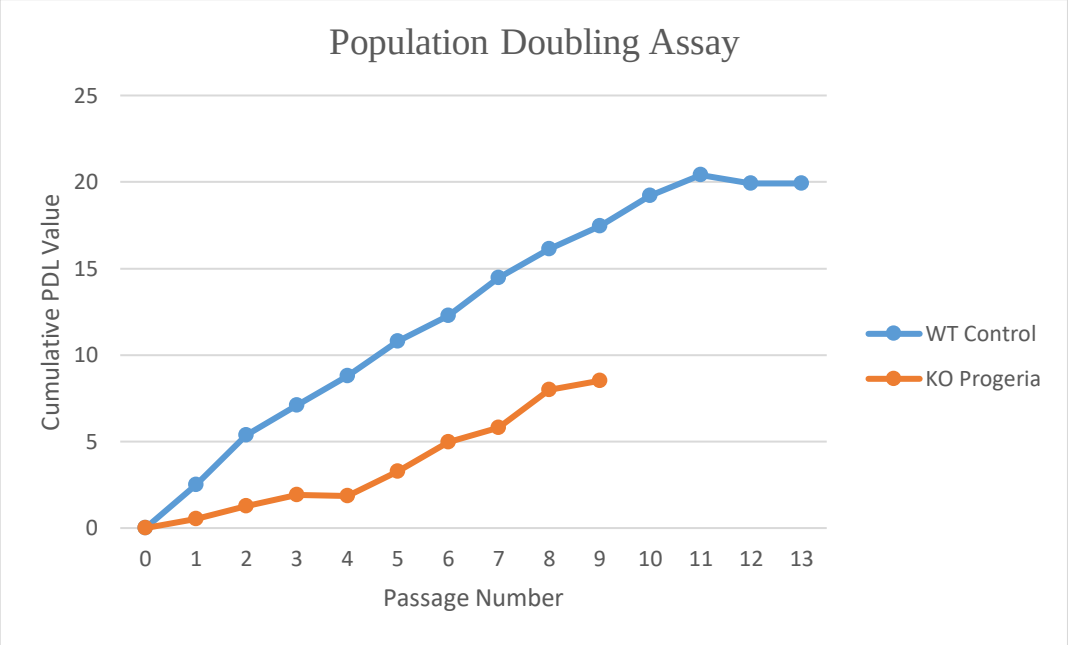

Figure 5.3: Population Doubling Assay of WT and Progeria Cells.

Cell proliferation was estimated by the population doubling assay. Cells were serially passaged in a 6-well plate at a seeding density of $2x10^4$ cells per well every 3 days until they stopped expanding. The counting of the total number of cells was determined by the Coulter counter at the end of each passage (n = 3 for each passage and conducted in one replicate).

As it has been well established that *Zmpste24*$^{-/-}$ nuclei contain blebs, described as nuclear envelop invagination and lobulation [Pendas, 2002], I next explored whether the majority of progeria cells here correspondingly showed structural abnormalities when subject to microscopic scrutiny. Interestingly, immunofluorescence analysis of *Zmpste24*$^{-/-}$ cells revealed only a very small percentage (2%) of progeria cells affected by the blebbing phenotype [Figures 5.4A-B]. Without being invaginated or lobulated, approximately 98% of *Zmpste24*$^{-/-}$ nuclei appeared to have normal nuclear membranes, suggesting that not all progeria cells are phenotypically abnormal.

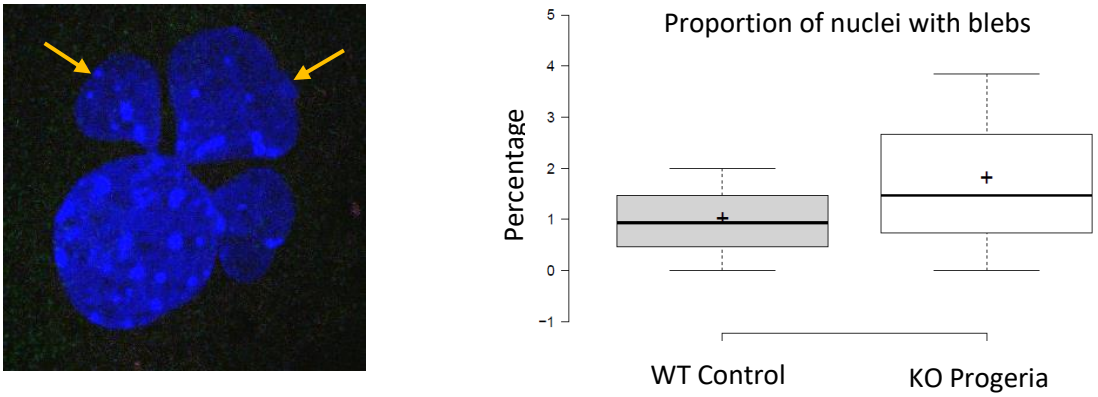

Figure 5.4: Characterisation of Progeria Blebbing.

Representative immunofluorescence image of a grossly abnormal nucleus. Nuclei were visualized with DAPI (blue). Yellow arrows indicate the blebbing feature. Objective magnification, 60x. DAPI-stained nuclei were categorised as bleb-positive or -negative, based on the characteristic nuclear lobulation observed in progeria cells. Percentages of bleb-positive cells are shown (n = 300, p > 0.05).

5.3 Not All Progeria Cells Were Phenotypically Abnormal

The fact that not all progeria cells showed the gross morphology of blebs prompted me to investigate the nuclear lamina in *Zmpste24*$^{-/-}$fibroblasts by carrying out immunostaining of lamin B1, a major structural component of the nuclear envelope. Previous work in *Zmpste24*$^{-/-}$ fibroblasts did not find any difference in lamin B1 when compared with WT fibroblasts (Pendás et al., 2002). Strikingly, I found a redistribution of lamin B1 in *Zmpste24*$^{-/-}$ cells, accompanied by a loss of peripheral lamin B1 [Figures 5.5A-G].

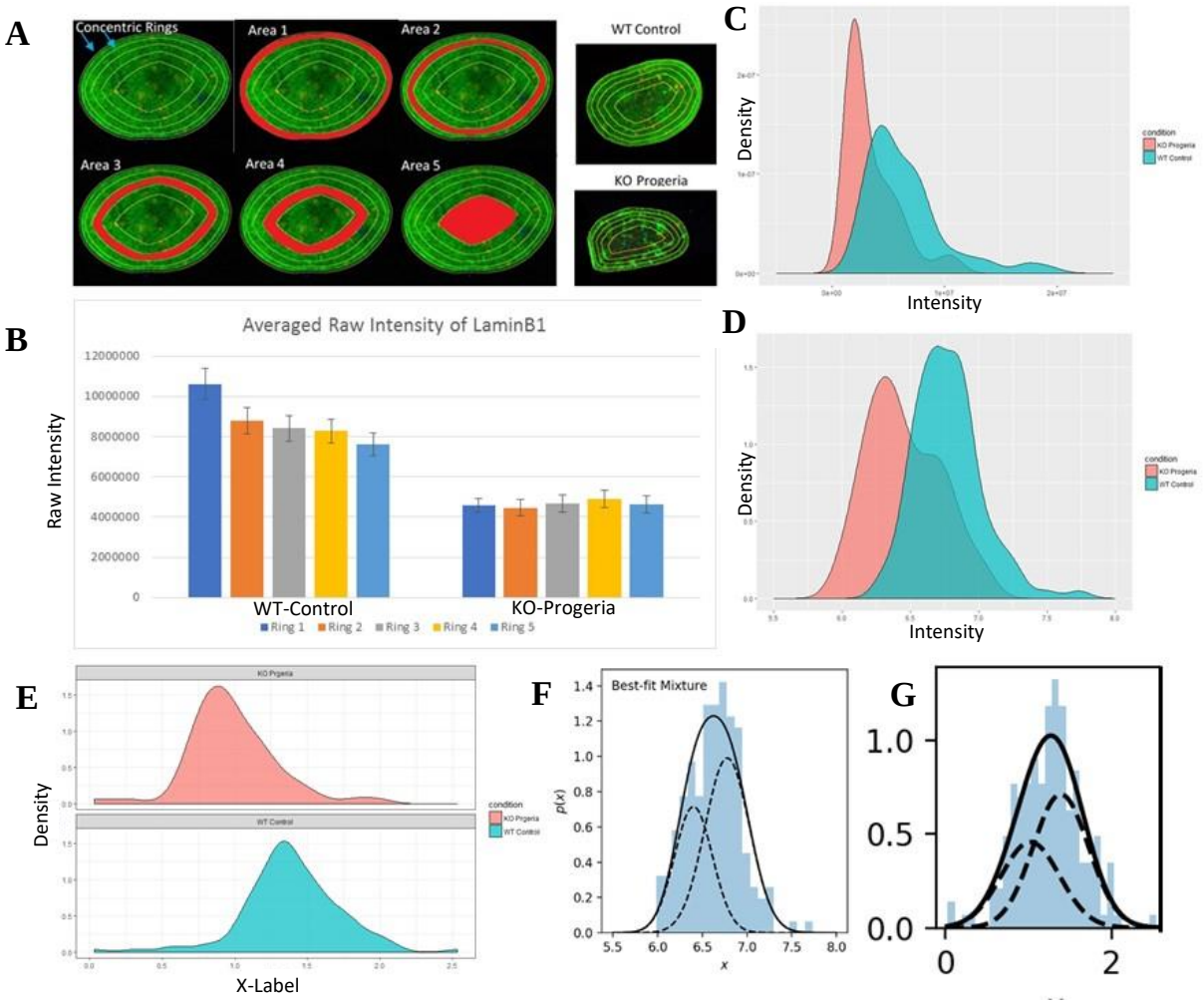

Figure 5.5: Quantifications of LaminB1.

(A) Illustration of a concentric ring Macro. The nuclear peripheral lamin B1 fluorescent intensity was quantified semi-automatically by calculating the intensity of lamin B1 in 5 areas. Creation of the Macro software is based on the erosion morphological operator working on a binary mask of the segmented nucleus whose area is known.

(B) Bar charts of averaged raw intensity of lamin B1 across 5 concentric rings (n = 200; error bars are ± SEM).

(C) Histogram of raw lamin B1 intensity in the WT and progeria conditions (n = 200).

(D) Histogram of the log-transformed raw lamin B1 intensity in the WT and progeria conditions (n = 200).

(E) Separate histogram of ratio of lamin B1 intensity in ring 1 over ring 4 in the WT and progeria conditions (n = 200).

(F) Histogram for Gaussian mixture model test on the log-transformed raw lamin B1 intensity in the WT and progeria conditions. Variance = 0.045 and 0.062 (n = 200).

(G) Histogram for Gaussian mixture model test on the ratio of raw lamin B1 intensity in ring 1 over ring 4 the WT and progeria conditions. Variance = 0.124 and 0.112 (n = 200).

Overall, the histograms show the probability that a cell of a particular phenotype would belong to one or another region. The results suggest that up to 50% of progeria nuclei had normal lamin B1 expression and behaved like WT nuclei did.

To verify such a difference in lamin B1 localisation pattern between WT and progeria nuclei, the lamin B1 fluorescent intensity in both conditions was measured. Using the Macro script to capture lamin B1 signals in 5 concentric rings, I found that the intensity of lamin B1 in progeria cells was significantly lower (P <0.001) than that of control cells across all concentric rings [Figure 5.5B]. To further quantify the proportion of progeria cells that showed a reduction in lamin B1 levels and those that did not, the Gaussian mixture model was adopted to create two regions of lamin B1 intensity, one for WT, another for progeria cells, based on the log values of averaged raw lamin B1 intensity [Figures 5.5F-G]. In this way, the probability that each intensity value would be characterised as WT-like or progeria-like could be calculated using the weighted sum model. I found that 78% of WT cells had normal lamin B1 levels as WT cells would have, whereas 56% of KO cells showed reduced lamin B1 levels as expected from progeria cells [Figure 5.5F]. The remaining percentages (22% WT and 44% progeria) of cells were estimated to belong to each other's opposite conditions. The ratio of lamin B1 intensity in ring 1 to the intensity in ring 4 was also calculated and the Gaussian mixture model applied. Compared with the WT condition, progeria cells showed a shift in the intensity ratio of ring 1 to ring 4 towards 1.0, demonstrating a reduction in lamin B1 distribution in the nuclear lamina [Figure 5.5G]. Similarly, 75% of WT cells and 49% of progeria cells were classified as WT-like, and 25% of WT and 51 progeria as progeria-like. Overall, the results suggest that up to 50% of progeria nuclei had normal lamin B1 expression and behaved like WT nuclei did.

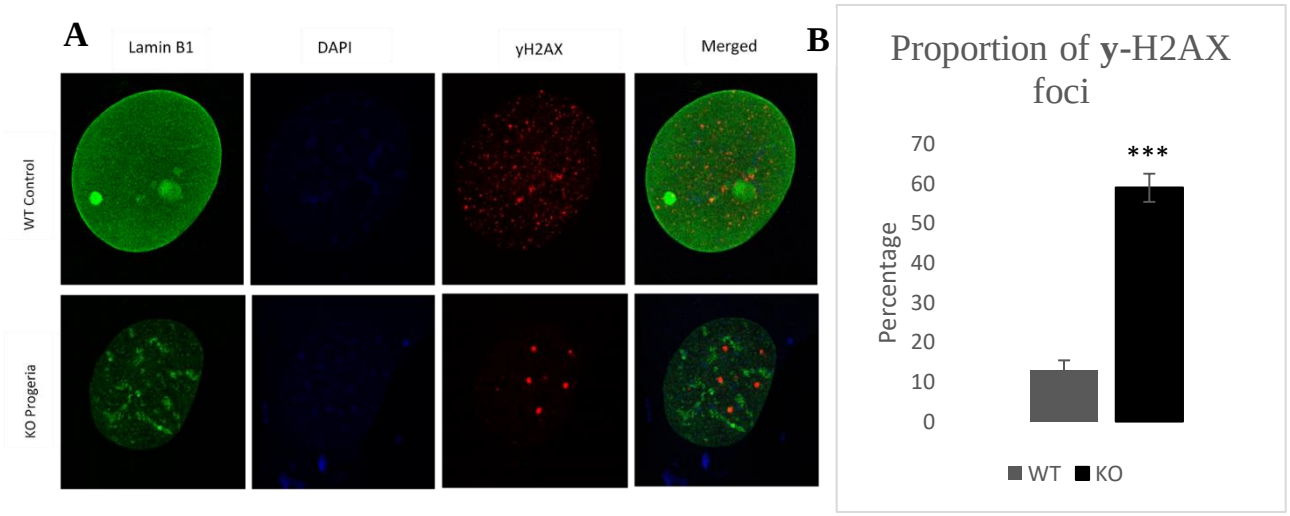

Figure 5.6: Immunofluorescence Staining of LaminB1 and γH2AX.

HGPS cells on coverslips were fixed and visualised using the immunohistochemistry protocol as described in the methodology.

(A) Representative immunofluorescent images of WT and KO (*Zmpste24*$^{-/-}$) fibroblasts at passage 6 with DAPI and anti-γH2AX Phospho (Ser139). Objective magnification, 60x (*n* = 300).

(B) Bar graphs denote the proportion of γH2AX-positive cells, as measured by the presence of at least 3 foci (*n* = 300; *** $p < 0.001$). Error bars represent SEM.

Finally, since progeria cells exhibited increased DNA damage and DNA repair defects (Liu et al., 2005), I analysed immunofluorescent images of γH2AX staining, a common proxy for double-strand break-induced DNA damage [Figure 5.6A]. As expected, only 15% of WT cells were γH2AX-positive compared to 59% in progeria cells [Figure 5.6B]. The quantification of all the morphological features, which reflect a heterogeneous distribution, is summarised in Table 5.1.

Phenotype	%WT	%KO
B-Galactosidase	**0** (n = 300)	**48 ± 3.5** (n = 300)
Blebs	**2 ± 1.1** (n = 300)	**3 ± 1.0** (n = 300)
Loss of Lamin B1 Intensity	**22*** **± 3.5** (n = 200)	**56*** **± 4.3** (n = 200)
Reversal of Lamin B1 Distribution	**25*** **± 3.2** (n = 200)	**51*** **± 2.6** (n = 200)
yH2AX	**15*** **± 5.4** (n = 300)	**59*** **± 10.6** (n = 300)

Table 5.1: Heterogeneity Table of Morphological Features.

The table summaries all the heterogeneous phenotypes, as characterised by different assays.

n indicates the number of sample size.

* mean percentage of cells with a particular phenotype ± SEM.

5.4 More Progeria Cells Entered the G2/M Phase

Next, to investigate single-cell heterogeneity of the transcriptomes of WT and progeria cells, single-cell RNA sequencing was performed using the 10x Chromium technology. Three quality control metrics were calculated for library size, number of expressed genes and percentage of mitochondrial content, leaving 502 WT cells and 201 *Zmpste24*$^{-/-}$ cells that passed the QC filters [Figure 5.7A]. By applying SC3 with $k = 5$ on the dataset, the cells could be stably clustered [Figure 5.7B]. SC3 reported 5 consensus clusters based on the expression of marker genes [Figure 5.7C]. To provide more informative cues about the transcriptome signatures of these cells, *cyclone*, the cell-cycle predictor for single-cell transcriptome data, was applied on the clustering outcome, assigning a cell-cycle stage to each single cell.

To allow better visualisation of single-cell expression data, a non-linear reduction dimension tool was applied on the $\log_2$-transformed expression dataset to create diffusion maps

(*destiny* package) [Figure 5.8]. Individual cells were coloured by condition, the 5 consensus clusters, cell-cycle stages and expression levels of genes of interest.

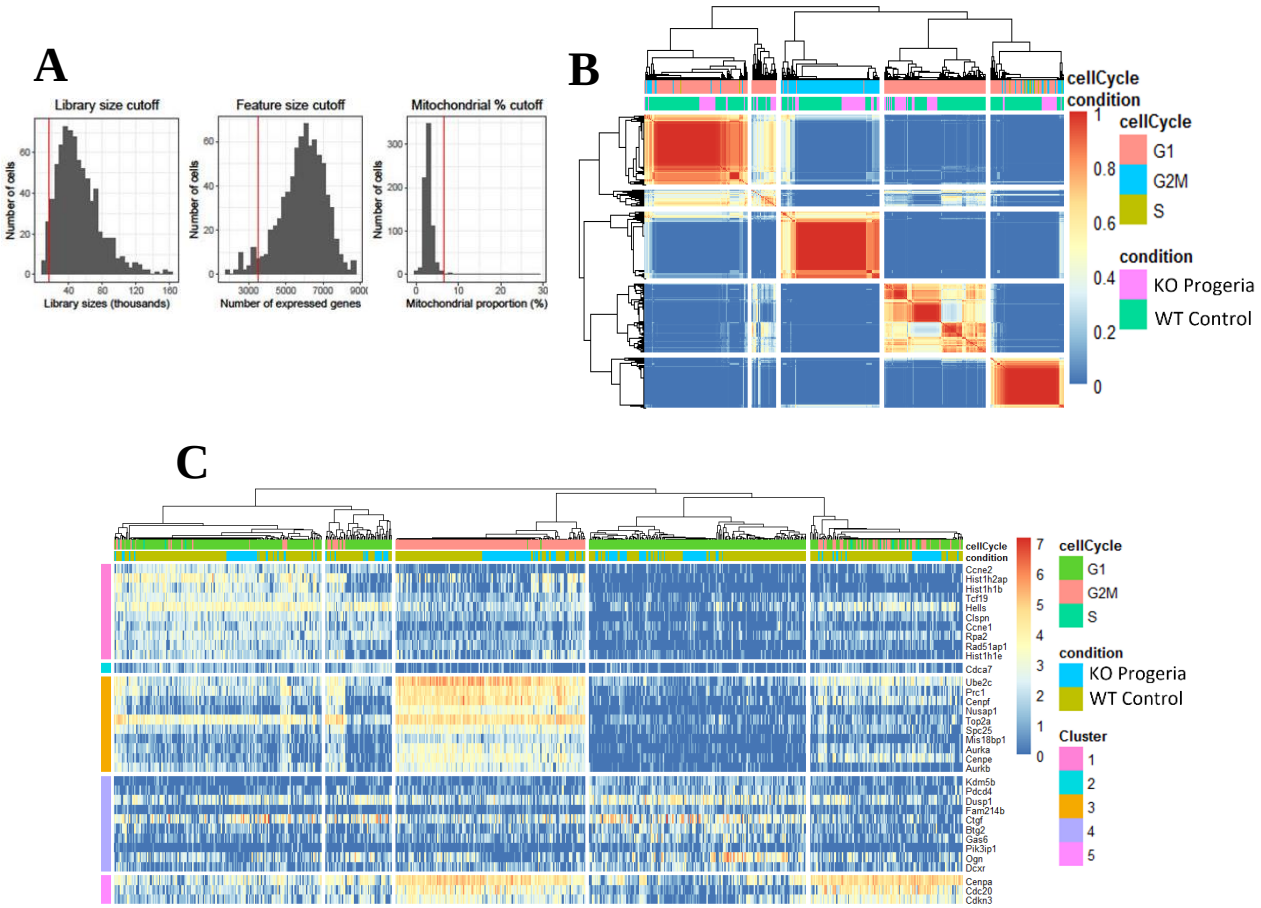

Figure 5.7: Transcriptional Profiles of Progeria Cells.

Single-cell RNA sequencing was performed on WT and progeria cells using the 10x Chromium technology. The figures show transcriptomic profiles in different metrices.

(A) Quality control metrics for library size, number of expressed genes and percentage of mitochondria.

(B) Consensus matrix as generated by SC3 for progeria and WT datasets, indicating how often each pair of cells was assigned to the same cluster by the different parameter combinations (1, always; 0, never), corresponding to k value = 2. Colours at the top indicate reference labels corresponding to conditions and cell cycle stages.

(C) Marker-gene expression matrix of WT and progeria cells. Clusters (separated by white vertical lines) correspond to k = 5. Only the top 10 marker genes are shown for each cluster.

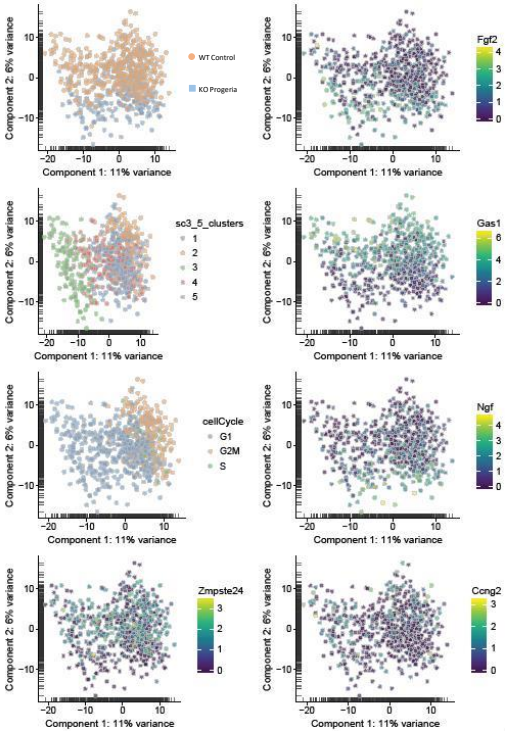

Figure 5.8 Diffusion maps single-cell expression data.

Two-dimensional PCA representation of cells based on levels of all differentially expressed genes.

Points represent individual cells.

Cells belong to two genotypes: WT control and KO progeria.

The number of clusters is 5.

Cells are labelled according to cell cycle stages.

The five diffusion maps show genes of interest (*Zmpste24*, *Fgf2*, *Gas1*, *Ngf*, *Ccng2*).

Regarding the cell-cycle phase, it is clear that 87% of all cells were in G1, 10% in G2/M and the rest in S [Figure 5.9A]. While G1 cells were dominant, SC3 could clearly separate G2/M-specific cluster from other clusters. Interestingly, the proportion of progeria cells in G2/M was almost twice as much that of control cells. An increase in the mitotic population was observed before in progeria smooth muscle cells [Figure 5.9B; Cao et al., 2014]. This led me to explore deeper the genes that were specifically expressed/depressed in the G2/M sub-population.

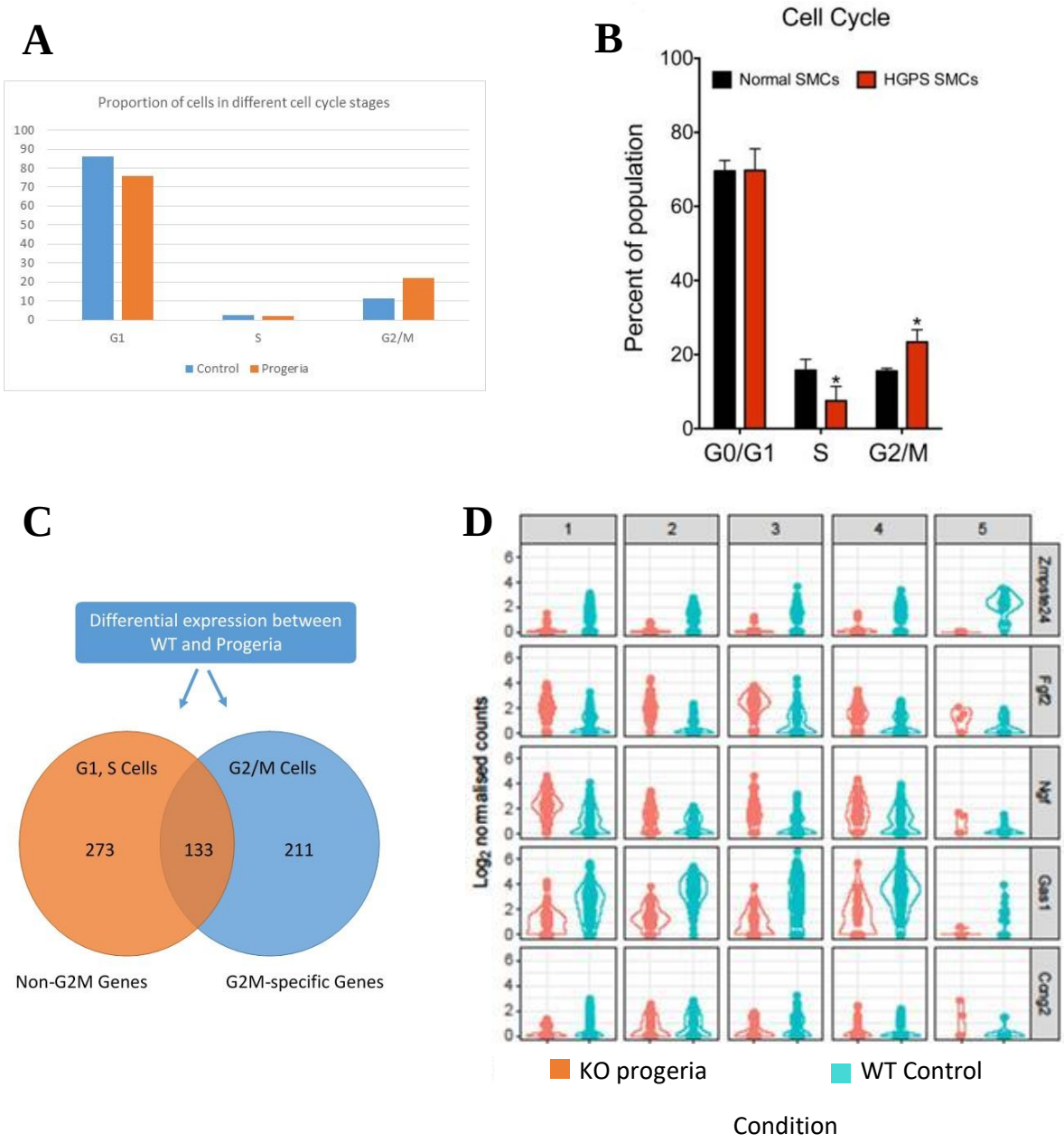

Figure 5.9: Cell Cycle Profiling of Progeria Cells.

(A) Bar charts of the proportion of WT and progeria cells in different cell cycle stages.

(B) Cell cycle analysis of normal and HGPS SMCs at day 14, illustrating the distribution of G0/G1, S, and G2/M phases [Cao, 2014].

(C) Venn diagram showing distribution and overlap of differentially expressed genes as identified by D3E in non-G2M and G2M-specific cells from the WT and progeria conditions.

(D) Violin plots showing $\log_2$ normalised counts of gene expression in WT and progeria cells. Columns indicate clusters, rows indicate genes of interest.

Non-G2/M cells were then excluded and G2/M cells re-clustered to extract the G2/M marker genes the defined the WT and progeria clusters. D3E was also used to produce a list of genes that are differentially expressed between the mitotic population and non-G2/M population. 211 genes were found to be specific to the G2/M cells [Figure 5.9C]. *Zmpste24, Fgf2, Ngf, Gas1 and Ccng2* stood out as the genes of interest, as shown by their expression dimension and $\log_2$expression levels across the 5 clusters [Figures 5.9C-5.8D]. In the G2M-only progeria cells, *Zmpste24* was expectedly downregulated, indicating the disruption of the gene in that causes progeria. *Gas1* (growth arrest-specific 1) was also down-regulated, followed by *Ccng2*. Surprisingly, growth factor genes such as *Fgf2* and *Ngf* were highly expressed in these supposedly non-dividing cells.

Finally, all the marker genes used to perform consensus clustering were re-investigated and analysed by D3E to identify differentially expressed genes between the WT and progeria conditions. These genes were ranked by their *p-value* and fold change in expression. By selecting the top differentially expressed genes, a heatmap of gene expression levels was generated [Figure 5.10] for the WT and KO conditions [Figure 5.10]. With further downstream processing, it would be possible to estimate the proportion of cells in different conditions and clusters that upregulated or downregulated the genes of interest. This estimation will also be applicable for the comparison between G2/M-specific WT and KO subpopulations.

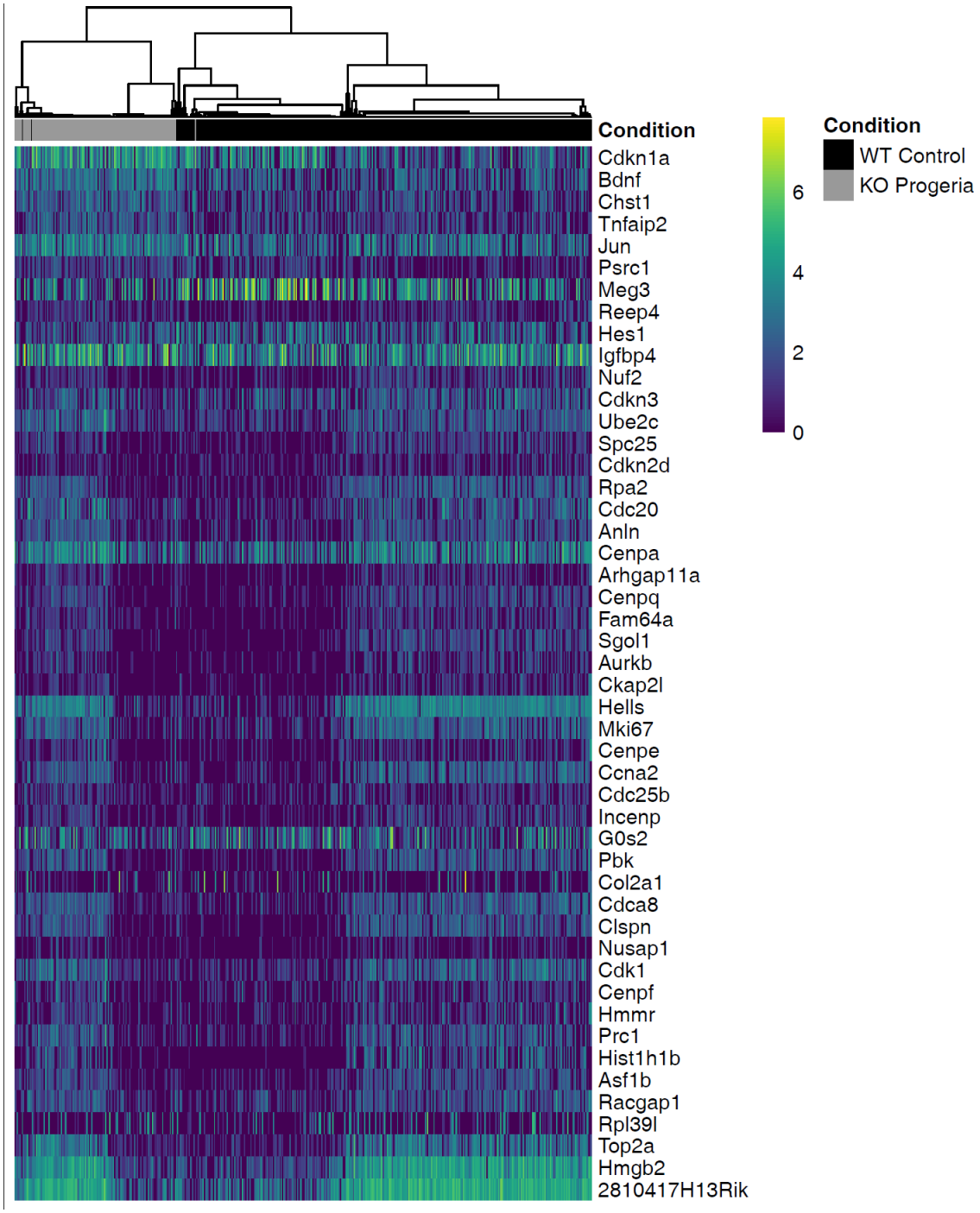

Figure 5.10: Heatmap of Differentially Expressed Genes in WT and Progeria Cells.

Heatmap of expression of genes of interest for WT and progeria cells. The heatmap is based on $\log_2$ normalised counts of differentially expressed genes as identified by D3E. Genes are ranked by order of fold change between the two conditions. The result shows an overview over similarities and dissimilarities between samples, with Cdkn1a being the top differentially expressed gene between the two conditions.

5.5 Discussion

As the only substrate for ZMPSTE24 in mammals, mature lamin A is absent in *Zmpste24*-knockout mice, while pre-lamin A accumulates in the nuclear envelope, causing direct structural disruption (Bergo et al. 2002). Similarly, reduced lamin B1 levels are associated with progeria and senescent fibroblasts (S.-J. Lee et al., 2016; Scaffidi and Misteli 2008). In this study, I examined the levels and distribution of lamin B1 in progeria cells and how many of them were affected by *Zmpste24* deficiency. The results identified the loss of peripheral lamin B1 and its relocalisation in around 50% of the progeria population. A key question is whether the loss of lamin B1 is a cause or consequence of progeria. The way forward is to investigate the pattern of lamin B1 expression in nuclei from *Zmpste24* mosaic mice, whose features are phenotypically normal. The rationale is to compare mosaic cells with complete *Zmpste24*$^{-/-}$ cells. Features that are present in the complete KO cells but not in the mosaic cells will be of special interest, as they might be important features that contribute to ageing.

Transcriptome-wide, *Zmpste24*$^{-/-}$ cells were profiled at the single-cell level to understand cellular heterogeneity in progeria. I observed transcriptional differences between WT and progeria cells, with genes such as *Fgf2* and *Ngf* being highly expressed in progeria cells, and associated them to the G2/M phase of the cell cycle. At first glance, this might appear counter-intuitive as high expression of growth factors are often linked to increased rates of cellular proliferation and growth, while progeria cells are senescent-like.

One study correspondingly found that expression of FGF2 in mouse cell lines prevented cell proliferation and induced a G2/M arrest in the context of malignant cells transformed by the *Ras* oncogene (Salotti et al., 2013). Given that the majority of progeria cells were in the G1 state, it is tempting to speculate that progeria cells are more prone to damage and, therefore, G1 arrest than WT cells are. Through a compensatory response or (epi)genetic selection, some progeria cells with high levels of *Fgf2* may escape the G1 phase and are driven into the G2/M phase [Figure 5.10].

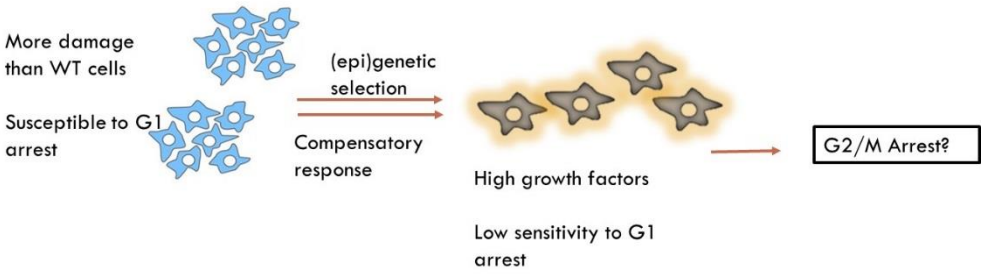

Figure 5.8: Schematic Diagram for a Model of Progeria Cell Cycle.

5.6 Summary

The characterisation of morphological features and biochemical assays of *Zmpste24-/-* cells indicated that the progeria phenotype is heterogeneous, with certain portions of progeria cells showing abnormalities, in contrast to the classical view that the cells are severely compromised in their entirety. Next, single-cell RNA sequencing data presented the starting point for the revelation of cell-to-cell transcriptional heterogeneity between WT and progeria cells. Cell cycle analysis suggested that a greater proportion of progeria cells cycled in the G2/M phase, which could be explained by a scenario in which progeria cells had undergone a compensatory or selection process and been forced to enter the G2/M arrest.

Chapter 6: Conclusions and Future Directions

6.1 Single-Cell Transcriptomics in OIS

Oncogene-induced senescence (OIS) represents a tumour-suppressive response to oncogenic insults and is transmissible through secreted factors of the senescence-associated secretory phenotype (SASP). As a result and considered as a secondary event, primary OIS cells can induce the neighbouring cells to become senescent in a paracrine fashion. The current and predominant view holds that primary and secondary senescent cells are not functionally distinct endpoints.

The first research project of this thesis explored the use of single-cell technologies, the Smart-Seq2 and the 10X Chromium Genomics, in deciphering molecular endpoints in OIS. Single-cell transcriptome analyses revealed two distinct transcriptional endpoints, a primary endpoint characterised by the Ras oncogene activation, and a secondary endpoint marked by Notch signalling activation.

Subsequent *in vitro* and *in vivo* experiments showed that secondary-induced senescence is dependent on Notch, rather than on SASP alone, as previously believed. Furthermore, in secondary senescence, SASP was weakened, but not abolished, by Notch signalling. This Notch-dominant and SASP-suppressive event also occurred in parallel with a failure to downregulate fibrillar collagens. Together, the global transcriptomic differences, the blunted SASP response, and the maintenance of fibrillar collagens in secondary senescence support the role of Notch as an essential driver of secondary senescence and point towards a functional diversification between secondary and primary senescence.

Despite the abundance of evidence uncovering a clear distinction between primary OIS and secondary senescence, one fundamental and intriguing question that has emerged and awaits further investigation is whether secondary senescence per se bears any significant biological function and physiological relevance. Assessing the functional role of secondary senescence remains an open question in the research field. The specific upregulation of Jagged1 in the primary OIS population seems to hint at the function of secondary senescence in containing the effects of senescence within a local microenvironment to pave the way for

efficient immune clearance. Future studies will need to focus on testing the proposed mechanism and linking it to a meaningful biological interpretation.

A pilot study has already been underway to decipher transcriptional differences between SAHF-positive and SAHF-negative cells in OIS. This can be achieved by the recently developed approach to isolating single cells, known as the Vycap Puncher platform, which allows live multi-coloured fluorescent images of cells to be captured at the same time as the selection of live cells that pass defined criteria for downstream single-cell analysis. In tandem with an *in vivo* model designed to test the physiological role of secondary senescence, a better understanding of the putative relationship between SAHF formation and secondary senescence will provide the basis for subsequent studies aiming to determine the function of secondary senescence.

Another important experiment that has already begun in the lab revolves around the genome-wide chromatin landscape data of OIS, both in monoculture and in co-culture using the ATAC-Seq technology, which is commonly used to detect nucleosome-free regions of the genome. The mapping and analysis of chromatin accessible sites in OIS will allow transcription factors and regulatory elements playing a part in OIS to be discovered and characterised at the single-base pair resolution. This, in turn, presents a new opportunity to describe the variability of chromatin accessibility and classification of senescent cells based on their chromatin architecture.

In summary, the molecular mechanisms underlying OIS are beginning to be revealed, subject to intense investigation achievable by single-cell technologies. The functional and molecular diversification of OIS endpoints is a relatively new concept in the field of senescence, but could bear significant implications on the role of OIS *in vivo*, given the firmly established evidence of its tumour-suppression and tumour-promotion effects. Predominantly, this is largely mediated by the transmission of senescence through SASP, which is thought to govern cell communication within the tissue microenvironment. As shown in this thesis, Notch signalling has emerged as an important regulator of lateral facilitation of secondary senescence. Since Notch ligands are often overexpressed in cancer cells, the significance of Notch-mediated senescence may not just represent a phenomenon with no physiological relevance. Deciphering the nature and meaning of juxtacrine senescence is likely to offer scientists with promising exploitation in cancer therapy.

6.2 Single-Cell Transcriptomics in Progeria

Single-cell sequencing technologies are a valuable tool for addressing the long-standing question of what causes ageing and senescence. Clearance of senescent cells has been shown to improve age-related dysfunctions and extend healthy lifespan in mammals, implicating senescent cells in promoting an ageing environment that leads to the demise of neighbouring cells and, ultimately, whole organisms. In the second research project, I applied the 10X single-cell technology and molecular phenotyping techniques to dissect cellular heterogeneity of progeria cells, which serve as a model system for studying ageing, with the aim to understand how many of them were functionally compromised and how progeria conditions could drive the ageing phenotype.

Preliminary observations on the morphology of *Zmpste24-/-* nuclei suggested that only a very small proportion of progeria nuclei showed gross nuclear lobulation or invagination, as opposed to this being a common feature attributed to classical progeria. This led to the investigation of other morphological features, which are thought to be characteristic of the progeria phenotype. The results indicate that progeria cells are phenotypically heterogeneous with a substantial proportion of cells appearing to be normal and unaffected by the genetic defect. This unexpected finding seems to fit well with the toxic ageing model, as it would explain how a small proportion of dysfunctional cells could exert toxic effects on other functionally normal cells and drive organismal ageing.

At the transcriptome level, single-cell analyses shed light into the genes that are differentially expressed between normal and progeria cells and identified upregulation of growth factor genes in such as *Fgf2* and *Ngf* in a progeria sub-population whose cell cycle profiles corresponded to the G2/M phase. Accordingly, it has been hypothesised that since progeria cells are more susceptible to damage and cell cycle arrest than normal cells are, some progeria cells would be subjected to (epi)genetic selection or a compensatory mechanism, with cells that highly express growth factors being able to escape the G1 phase and enter the G/M arrest.

Therefore, to test this hypothesis, one can enforce *Fgf2* expression in normal and progeria cells and assess if more of them undergo a G2/M arrest. Additional work will include downstream analyses of differentially expressed genes and associated regulatory pathways in which those genes are involved. A treasure trove of marker genes identified and how they are

linked to cell-fate decisions will provide guidance for carrying out more thorough downstream analyses and to understand how and why progeria cells are largely heterogeneous.

Finally, efforts should be directed at characterising different subpopulations of cells based on their transcriptomes and cell cycle stage and to determine the number of cells that belong to each subpopulation. Foreseeably, new insights into the heterogeneity of progeroid syndromes through single-cell analyses will help to elucidate which of the numerous pathways are compromised, most relevant for and causally linked to the pathologies. This will entail wide-ranging implications for understanding cellular heterogeneity in ageing and offer new avenues for therapeutic applications in promoting healthy lifespan.

References

Acosta, Juan C., Ana O'Loghlen, Ana Banito, Maria V. Guijarro, Arnaud Augert, Selina Raguz, Marzia Fumagalli, et al. 2008a. "Chemokine Signaling via the CXCR2 Receptor Reinforces Senescence." *Cell* 133 (6): 1006–18. https://doi.org/10.1016/j.cell.2008.03.038.

———. 2008b. "Chemokine Signaling via the CXCR2 Receptor Reinforces Senescence." *Cell* 133 (6): 1006–18. https://doi.org/10.1016/j.cell.2008.03.038.

Acosta, Juan Carlos, Ana Banito, Torsten Wuestefeld, Athena Georgilis, Peggy Janich, Jennifer P Morton, Dimitris Athineos, et al. 2013. "A Complex Secretory Program Orchestrated by the Inflammasome Controls Paracrine Senescence." *Nature Cell Biology* 15 (8): 978–90. https://doi.org/10.1038/ncb2784.

Anders, Simon, Paul Theodor Pyl, and Wolfgang Huber. 2015. "HTSeq--a Python Framework to Work with High-Throughput Sequencing Data." *Bioinformatics (Oxford, England)* 31 (2): 166–69. https://doi.org/10.1093/bioinformatics/btu638.

Baker, Darren J., Bennett G. Childs, Matej Durik, Melinde E. Wijers, Cynthia J. Sieben, Jian Zhong, Rachel A. Saltness, et al. 2016. "Naturally Occurring P16Ink4a-Positive Cells Shorten Healthy Lifespan." *Nature* 530 (7589): 184–89. https://doi.org/10.1038/nature16932.

Baker, Darren J., Tobias Wijshake, Tamar Tchkonia, Nathan K. LeBrasseur, Bennett G. Childs, Bart van de Sluis, James L. Kirkland, and Jan M. van Deursen. 2011. "Clearance of P16Ink4a-Positive Senescent Cells Delays Ageing-Associated Disorders." *Nature* 479 (7372): 232–36. https://doi.org/10.1038/nature10600.

Bartkova, Jirina, Nousin Rezaei, Michalis Liontos, Panagiotis Karakaidos, Dimitris Kletsas, Natalia Issaeva, Leandros-Vassilios F. Vassiliou, et al. 2006a. "Oncogene-Induced Senescence Is Part of the Tumorigenesis Barrier Imposed by DNA Damage Checkpoints." *Nature* 444 (7119): 633–37. https://doi.org/10.1038/nature05268.

———. 2006b. "Oncogene-Induced Senescence Is Part of the Tumorigenesis Barrier Imposed by DNA Damage Checkpoints." *Nature* 444 (7119): 633–37. https://doi.org/10.1038/nature05268.

Bergo, Martin O., Bryant Gavino, Jed Ross, Walter K. Schmidt, Christine Hong, Lonnie V. Kendall, Andreas Mohr, et al. 2002. "Zmpste24 Deficiency in Mice Causes Spontaneous Bone Fractures, Muscle Weakness, and a Prelamin A Processing Defect." *Proceedings of the National Academy of Sciences of the United States of America* 99 (20): 13049–54. https://doi.org/10.1073/pnas.192460799.

Bird, Thomas G., Miryam Müller, Luke Boulter, David F. Vincent, Rachel A. Ridgway, Elena Lopez-Guadamillas, Wei-Yu Lu, et al. 2018. "TGFβ Inhibition Restores a Regenerative Response in Acute Liver Injury by Suppressing Paracrine Senescence." *Science Translational Medicine* 10 (454): eaan1230. https://doi.org/10.1126/scitranslmed.aan1230.

Bischoff, Claus, Hans Christian Petersen, Jesper Graakjaer, Karen Andersen-Ranberg, James W Vaupel, Vilhelm A Bohr, Steen Kølvraa, and Kaare Christensen. 2006. "No

Association between Telomere Length and Survival among the Elderly and Oldest Old." *Epidemiology (Cambridge, Mass.)* 17 (2): 190–94. https://doi.org/10.1097/01.ede.0000199436.55248.10.

Braig, Melanie, Soyoung Lee, Christoph Loddenkemper, Cornelia Rudolph, Antoine H F M Peters, Brigitte Schlegelberger, Harald Stein, Bernd Dörken, Thomas Jenuwein, and Clemens A Schmitt. 2005. "Oncogene-Induced Senescence as an Initial Barrier in Lymphoma Development." *Nature* 436 (7051): 660–65. https://doi.org/10.1038/nature03841.

Butler, Andrew, Paul Hoffman, Peter Smibert, Efthymia Papalexi, and Rahul Satija. 2018. "Integrating Single-Cell Transcriptomic Data across Different Conditions, Technologies, and Species." *Nature Biotechnology* 36 (5): 411–20. https://doi.org/10.1038/nbt.4096.

Campisi, Judith. 2013. "Aging, Cellular Senescence, and Cancer." *Annual Review of Physiology* 75: 685–705. https://doi.org/10.1146/annurev-physiol-030212-183653.

Cawthon, Richard M, Ken R Smith, Elizabeth O'Brien, Anna Sivatchenko, and Richard A Kerber. 2003. "Association between Telomere Length in Blood and Mortality in People Aged 60 Years or Older." *The Lancet* 361 (9355): 393–95. https://doi.org/10.1016/S0140-6736(03)12384-7.

Chandra, Tamir, and Kristina Kirschner. 2016. "Chromosome Organisation during Ageing and Senescence." *Current Opinion in Cell Biology* 40 (June): 161–67. https://doi.org/10.1016/j.ceb.2016.03.020.

Chang, E, and C B Harley. 1995. "Telomere Length and Replicative Aging in Human Vascular Tissues." *Proceedings of the National Academy of Sciences of the United States of America* 92 (24): 11190–94. https://doi.org/10.1073/pnas.92.24.11190.

Chen, Zhenbang, Lloyd C Trotman, David Shaffer, Hui-Kuan Lin, Zohar A Dotan, Masaru Niki, Jason A Koutcher, et al. 2005. "Crucial Role of P53-Dependent Cellular Senescence in Suppression of Pten-Deficient Tumorigenesis." *Nature* 436 (7051): 725–30. https://doi.org/10.1038/nature03918.

Chicas, Agustin, Xiaowo Wang, Chaolin Zhang, Mila McCurrach, Zhen Zhao, Ozlem Mert, Ross A. Dickins, Masashi Narita, Michael Zhang, and Scott W. Lowe. 2010. "Dissecting the Unique Role of the Retinoblastoma Tumor Suppressor during Cellular Senescence." *Cancer Cell* 17 (4): 376–87. https://doi.org/10.1016/j.ccr.2010.01.023.

Cipriano, Rocky, Charlene E Kan, James Graham, David Danielpour, Martha Stampfer, and Mark W Jackson. 2011. "TGF-Beta Signaling Engages an ATM-CHK2-P53-Independent RAS-Induced Senescence and Prevents Malignant Transformation in Human Mammary Epithelial Cells." *Proceedings of the National Academy of Sciences of the United States of America* 108 (21): 8668–73. https://doi.org/10.1073/pnas.1015022108.

Collado, Manuel, Jesús Gil, Alejo Efeyan, Carmen Guerra, Alberto J. Schuhmacher, Marta Barradas, Alberto Benguría, et al. 2005. "Senescence in Premalignant Tumours." *Nature* 436 (7051): 642–642. https://doi.org/10.1038/436642a.

Coppé, Jean-Philippe, Christopher K Patil, Francis Rodier, Yu Sun, Denise P Muñoz, Joshua Goldstein, Peter S Nelson, Pierre-Yves Desprez, and Judith Campisi. 2008. "Senescence-Associated Secretory Phenotypes Reveal Cell-Nonautonomous Functions of Oncogenic RAS and the P53 Tumor Suppressor." Edited by Julian Downward. *PLoS*

Biology 6 (12): e301. https://doi.org/10.1371/journal.pbio.0060301.

Couso, J P, S A Bishop, and A Martinez Arias. 1994. "The Wingless Signalling Pathway and the Patterning of the Wing Margin in Drosophila." *Development (Cambridge, England)* 120 (3): 621–36. https://doi.org/8223268.

Dankort, David, David P Curley, Robert A Cartlidge, Betsy Nelson, Anthony N Karnezis, William E Damsky Jr, Mingjian J You, Ronald A DePinho, Martin McMahon, and Marcus Bosenberg. 2009. "BrafV600E Cooperates with Pten Loss to Induce Metastatic Melanoma." *Nature Genetics* 41 (5): 544–52. https://doi.org/10.1038/ng.356.

Denoyelle, Christophe, George Abou-Rjaily, Vladimir Bezrookove, Monique Verhaegen, Timothy M. Johnson, Douglas R. Fullen, Jenny N. Pointer, et al. 2006. "Anti-Oncogenic Role of the Endoplasmic Reticulum Differentially Activated by Mutations in the MAPK Pathway." *Nature Cell Biology* 8 (10): 1053–63. https://doi.org/10.1038/ncb1471.

Deursen, Jan M van. 2014. "The Role of Senescent Cells in Ageing." *Nature* 509 (7501): 439–46. https://doi.org/10.1038/nature13193.

Dreesen, Oliver, Alexandre Chojnowski, Peh Fern Ong, Tian Yun Zhao, John E. Common, Declan Lunny, E. Birgitte Lane, et al. 2013. "Lamin B1 Fluctuations Have Differential Effects on Cellular Proliferation and Senescence." *The Journal of Cell Biology* 200 (5). http://jcb.rupress.org/content/200/5/605.

Eggert, Tobias, Katharina Wolter, Juling Ji, Chi Ma, Tetyana Yevsa, Sabrina Klotz, José Medina-Echeverz, et al. 2016. "Distinct Functions of Senescence-Associated Immune Responses in Liver Tumor Surveillance and Tumor Progression." *Cancer Cell* 30 (4): 533–47. https://doi.org/10.1016/j.ccell.2016.09.003.

Eriksson, Maria, W. Ted Brown, Leslie B. Gordon, Michael W. Glynn, Joel Singer, Laura Scott, Michael R. Erdos, et al. 2003. "Recurrent de Novo Point Mutations in Lamin A Cause Hutchinson–Gilford Progeria Syndrome." *Nature* 423 (6937): 293–98. https://doi.org/10.1038/nature01629.

Fagagna, Fabrizio d'Adda di, Philip M. Reaper, Lorena Clay-Farrace, Heike Fiegler, Philippa Carr, Thomas von Zglinicki, Gabriele Saretzki, Nigel P. Carter, and Stephen P. Jackson. 2003. "A DNA Damage Checkpoint Response in Telomere-Initiated Senescence." *Nature* 426 (6963): 194–98. https://doi.org/10.1038/nature02118.

Garrison, Erik, and Gabor Marth. 2012. "Haplotype-Based Variant Detection from Short-Read Sequencing," July. http://arxiv.org/abs/1207.3907.

Hande, M. Prakash, Enrique Samper, Peter Lansdorp, and María A. Blasco. 1999. "Telomere Length Dynamics and Chromosomal Instability in Cells Derived from Telomerase Null Mice." *The Journal of Cell Biology* 144 (4): 589–601. https://doi.org/10.1083/jcb.144.4.589.

Harley, Calvin B., A. Bruce Futcher, and Carol W. Greider. 1990. "Telomeres Shorten during Ageing of Human Fibroblasts." *Nature* 345 (6274): 458–60. https://doi.org/10.1038/345458a0.

Hastie, Nicholas D., Maureen Dempster, Malcolm G. Dunlop, Alastair M. Thompson, Daryll K. Green, and Robin C. Allshire. 1990. "Telomere Reduction in Human Colorectal Carcinoma and with Ageing." *Nature* 346 (6287): 866–68. https://doi.org/10.1038/346866a0.

Hayflick, L., and P.S. Moorhead. 1961. “The Serial Cultivation of Human Diploid Cell Strains.” *Experimental Cell Research* 25 (3): 585–621. https://doi.org/10.1016/0014-4827(61)90192-6.

Hoare, Matthew, Yoko Ito, Tae-Won Kang, Michael P. Weekes, Nicholas J. Matheson, Daniel A. Patten, Shishir Shetty, et al. 2016a. “NOTCH1 Mediates a Switch between Two Distinct Secretomes during Senescence.” *Nature Cell Biology* 18 (9): 979–92. https://doi.org/10.1038/ncb3397.

Hoare, Matthew, Yoko Ito, Tae-Won Kang, Michael P Weekes, Nicholas J Matheson, Daniel A Patten, Shishir Shetty, et al. 2016b. “NOTCH1 Mediates a Switch between Two Distinct Secretomes during Senescence.” *Nature Cell Biology* 18 (9): 979–92. https://doi.org/10.1038/ncb3397.

Hoare, Matthew, and Masashi Narita. 2017. “NOTCH and the 2 SASPs of Senescence.” *Cell Cycle* 16 (3): 239–40. https://doi.org/10.1080/15384101.2016.1248730.

Hubackova, Sona, Katerina Krejcikova, Jiri Bartek, and Zdenek Hodny. 2012. “IL1- and TGFβ-Nox4 Signaling, Oxidative Stress and DNA Damage Response Are Shared Features of Replicative, Oncogene-Induced, and Drug-Induced Paracrine ‘Bystander Senescence.’” *Aging* 4 (12): 932–51. https://doi.org/10.18632/aging.100520.

Iannello, Alexandre, Thornton W. Thompson, Michele Ardolino, Scott W. Lowe, and David H. Raulet. 2013. “P53-Dependent Chemokine Production by Senescent Tumor Cells Supports NKG2D-Dependent Tumor Elimination by Natural Killer Cells.” *The Journal of Experimental Medicine* 210 (10): 2057–69. https://doi.org/10.1084/jem.20130783.

Ito, Yoko, Matthew Hoare, and Masashi Narita. 2017. “Spatial and Temporal Control of Senescence.” *Trends in Cell Biology* 27 (11): 820–32. https://doi.org/10.1016/j.tcb.2017.07.004.

Kamijo, T, F Zindy, M F Roussel, D E Quelle, J R Downing, R A Ashmun, G Grosveld, and C J Sherr. 1997. “Tumor Suppression at the Mouse INK4a Locus Mediated by the Alternative Reading Frame Product P19ARF.” *Cell* 91 (5): 649–59. https://doi.org/10.1016/s0092-8674(00)80452-3.

Kharchenko, Peter V, Lev Silberstein, and David T Scadden. 2014a. “Bayesian Approach to Single-Cell Differential Expression Analysis.” *Nature Methods* 11 (7): 740–42. https://doi.org/10.1038/nmeth.2967.

———. 2014b. “Bayesian Approach to Single-Cell Differential Expression Analysis.” *Nature Methods* 11 (7): 740–42. https://doi.org/10.1038/nmeth.2967.

Kim, Daehwan, Ben Langmead, and Steven L Salzberg. 2015. “HISAT: A Fast Spliced Aligner with Low Memory Requirements.” *Nature Methods* 12 (4): 357–60. https://doi.org/10.1038/nmeth.3317.

Kiselev, Vladimir Yu, Kristina Kirschner, Michael T Schaub, Tallulah Andrews, Andrew Yiu, Tamir Chandra, Kedar N Natarajan, et al. 2017. “SC3: Consensus Clustering of Single-Cell RNA-Seq Data.” *Nature Methods* 14 (5): 483–86. https://doi.org/10.1038/nmeth.4236.

Kuilman, Thomas, Chrysiis Michaloglou, Liesbeth C.W. Vredeveld, Sirith Douma, Remco van Doorn, Christophe J. Desmet, Lucien A. Aarden, Wolter J. Mooi, and Daniel S. Peeper. 2008a. “Oncogene-Induced Senescence Relayed by an Interleukin-Dependent

Inflammatory Network." *Cell* 133 (6): 1019–31. https://doi.org/10.1016/j.cell.2008.03.039.

———. 2008b. "Oncogene-Induced Senescence Relayed by an Interleukin-Dependent Inflammatory Network." *Cell* 133 (6): 1019–31. https://doi.org/10.1016/j.cell.2008.03.039.

la Rosa, Jorge de, José M P Freije, Rubén Cabanillas, Fernando G Osorio, Mario F Fraga, M Soledad Fernández-García, Roland Rad, et al. 2013. "Prelamin A Causes Progeria through Cell-Extrinsic Mechanisms and Prevents Cancer Invasion." *Nature Communications* 4: 2268. https://doi.org/10.1038/ncomms3268.

Laberge, Remi-Martin, Yu Sun, Arturo V. Orjalo, Christopher K. Patil, Adam Freund, Lili Zhou, Samuel C. Curran, et al. 2015. "MTOR Regulates the Pro-Tumorigenic Senescence-Associated Secretory Phenotype by Promoting IL1A Translation." *Nature Cell Biology* 17 (8): 1049–61. https://doi.org/10.1038/ncb3195.

Lange, T. de. 2005. "Shelterin: The Protein Complex That Shapes and Safeguards Human Telomeres." *Genes & Development* 19 (18): 2100–2110. https://doi.org/10.1101/gad.1346005.

Lee, Han-Woong, Maria A. Blasco, Geoffrey J. Gottlieb, James W. Horner, Carol W. Greider, and Ronald A. DePinho. 1998. "Essential Role of Mouse Telomerase in Highly Proliferative Organs." *Nature* 392 (6676): 569–74. https://doi.org/10.1038/33345.

Lee, Soyoung, and Clemens A. Schmitt. 2019. "The Dynamic Nature of Senescence in Cancer." *Nature Cell Biology* 21 (1): 94–101. https://doi.org/10.1038/s41556-018-0249-2.

Lee, Su-Jin, Youn-Sang Jung, Min-Ho Yoon, So-Mi Kang, Ah-Young Oh, Jee-Hyun Lee, So-Young Jun, et al. 2016. "Interruption of Progerin-Lamin A/C Binding Ameliorates Hutchinson-Gilford Progeria Syndrome Phenotype." *The Journal of Clinical Investigation* 126 (10): 3879–93. https://doi.org/10.1172/JCI84164.

Lesina, Marina, Sonja Maria Wörmann, Jennifer Morton, Kalliope Nina Diakopoulos, Olga Korneeva, Margit Wimmer, Henrik Einwächter, et al. 2016. "RelA Regulates CXCL1/CXCR2-Dependent Oncogene-Induced Senescence in Murine Kras-Driven Pancreatic Carcinogenesis." *Journal of Clinical Investigation* 126 (8): 2919–32. https://doi.org/10.1172/JCI86477.

Love, Michael I, Wolfgang Huber, and Simon Anders. 2014. "Moderated Estimation of Fold Change and Dispersion for RNA-Seq Data with DESeq2." *Genome Biology* 15 (12): 550. https://doi.org/10.1186/s13059-014-0550-8.

Lu, Wei-Yu, Thomas G. Bird, Luke Boulter, Atsunori Tsuchiya, Alicia M. Cole, Trevor Hay, Rachel V. Guest, et al. 2015. "Hepatic Progenitor Cells of Biliary Origin with Liver Repopulation Capacity." *Nature Cell Biology* 17 (8): 971–83. https://doi.org/10.1038/ncb3203.

Malaquin, Nicolas, Chantal Vercamer, Fatima Bouali, Sébastien Martien, Emeric Deruy, Nicolas Wernert, Maggy Chwastyniak, Florence Pinet, Corinne Abbadie, and Albin Pourtier. 2013. "Senescent Fibroblasts Enhance Early Skin Carcinogenic Events via a Paracrine MMP-PAR-1 Axis." *PloS One* 8 (5): e63607. https://doi.org/10.1371/journal.pone.0063607.

Martin-Ruiz, Carmen M., Jacobijn Gussekloo, Diana Heemst, Thomas Zglinicki, and Rudi G. J. Westendorp. 2005. “Telomere Length in White Blood Cells Is Not Associated with Morbidity or Mortality in the Oldest Old: A Population-Based Study.” *Aging Cell* 4 (6): 287–90. https://doi.org/10.1111/j.1474-9726.2005.00171.x.

McCarthy, Davis J., Kieran R. Campbell, Aaron T. L. Lun, and Quin F. Wills. 2017. “Scater: Pre-Processing, Quality Control, Normalization and Visualization of Single-Cell RNA-Seq Data in R.” *Bioinformatics* 33 (8): btw777. https://doi.org/10.1093/bioinformatics/btw777.

McHugh, Domhnall, and Jesús Gil. 2018. “Senescence and Aging: Causes, Consequences, and Therapeutic Avenues.” *The Journal of Cell Biology* 217 (1): 65–77. https://doi.org/10.1083/jcb.201708092.

Micco, Raffaella Di, Marzia Fumagalli, Angelo Cicalese, Sara Piccinin, Patrizia Gasparini, Chiara Luise, Catherine Schurra, et al. 2006. “Oncogene-Induced Senescence Is a DNA Damage Response Triggered by DNA Hyper-Replication.” *Nature* 444 (7119): 638–42. https://doi.org/10.1038/nature05327.

Michaloglou, Chrysiis, Liesbeth C. W. Vredeveld, Maria S. Soengas, Christophe Denoyelle, Thomas Kuilman, Chantal M. A. M. van der Horst, Donné M. Majoor, Jerry W. Shay, Wolter J. Mooi, and Daniel S. Peeper. 2005. “BRAFE600-Associated Senescence-like Cell Cycle Arrest of Human Naevi.” *Nature* 436 (7051): 720–24. https://doi.org/10.1038/nature03890.

Mosteiro, Lluc, Cristina Pantoja, Alba de Martino, and Manuel Serrano. 2018. “Senescence Promotes in Vivo Reprogramming through P16INK4a and IL-6.” *Aging Cell* 17 (2). https://doi.org/10.1111/acel.12711.

Muñoz-Espín, Daniel, and Manuel Serrano. 2014. “Cellular Senescence: From Physiology to Pathology.” *Nature Reviews. Molecular Cell Biology* 15 (7): 482–96. https://doi.org/10.1038/nrm3823.

Nardella, Caterina, John G Clohessy, Andrea Alimonti, and Pier Paolo Pandolfi. 2011. “Pro-Senescence Therapy for Cancer Treatment.” *Nature Reviews. Cancer* 11 (7): 503–11. https://doi.org/10.1038/nrc3057.

Narita, Masashi, Sabrina Nũnez, Edith Heard, Masako Narita, Athena W Lin, Stephen A Hearn, David L Spector, Gregory J Hannon, and Scott W Lowe. 2003. “Rb-Mediated Heterochromatin Formation and Silencing of E2F Target Genes during Cellular Senescence.” *Cell* 113 (6): 703–16. http://www.ncbi.nlm.nih.gov/pubmed/12809602.

Nelson, Glyn, James Wordsworth, Chunfang Wang, Diana Jurk, Conor Lawless, Carmen Martin-Ruiz, and Thomas von Zglinicki. 2012. “A Senescent Cell Bystander Effect: Senescence-Induced Senescence.” *Aging Cell* 11 (2): 345–49. https://doi.org/10.1111/j.1474-9726.2012.00795.x.

Njajou, Omer T., Wen-Chi Hsueh, Elizabeth H. Blackburn, Anne B. Newman, Shih-Hsuan Wu, Rongling Li, Eleanor M. Simonsick, et al. 2009. “Association Between Telomere Length, Specific Causes of Death, and Years of Healthy Life in Health, Aging, and Body Composition, a Population-Based Cohort Study.” *The Journals of Gerontology: Series A* 64A (8): 860–64. https://doi.org/10.1093/gerona/glp061.

Oh, Juhyun, Yang David Lee, and Amy J Wagers. 2014. “Stem Cell Aging: Mechanisms, Regulators and Therapeutic Opportunities.” *Nature Medicine* 20 (8): 870–80.

https://doi.org/10.1038/nm.3651.

Olovnikov, A.M. 1973. “A Theory of Marginotomy.” *Journal of Theoretical Biology* 41 (1): 181–90. https://doi.org/10.1016/0022-5193(73)90198-7.

Osorio, F. G., C. Barcena, C. Soria-Valles, A. J. Ramsay, F. de Carlos, J. Cobo, A. Fueyo, J. M. P. Freije, and C. Lopez-Otin. 2012. “Nuclear Lamina Defects Cause ATM-Dependent NF- B Activation and Link Accelerated Aging to a Systemic Inflammatory Response.” *Genes & Development* 26 (20): 2311–24. https://doi.org/10.1101/gad.197954.112.

Pankotai, Tibor, Anne Sophie Hoffbeck, Charlene Boumendil, and Evi Soutoglou. 2009. “DNA Damage Response in the Absence of DNA Lesions Continued….” *Cell Cycle* 8 (24): 4023–28. https://doi.org/10.4161/cc.8.24.10564.

Parry, Aled J., Matthew Hoare, Dóra Bihary, Robert Hänsel-Hertsch, Stephen Smith, Kosuke Tomimatsu, Elizabeth Mannion, et al. 2018. “NOTCH-Mediated Non-Cell Autonomous Regulation of Chromatin Structure during Senescence.” *Nature Communications* 9 (1): 1840. https://doi.org/10.1038/s41467-018-04283-9.

Pazhanisamy, Senthil Kumar. 2009. “Stem Cells, DNA Damage, Ageing and Cancer.” *Hematology/Oncology and Stem Cell Therapy* 2 (3): 375–84. https://doi.org/10.1016/S1658-3876(09)50005-2.

Pendás, Alberto M., Zhongjun Zhou, Juan Cadiñanos, José M.P. Freije, Jianming Wang, Kjell Hultenby, Aurora Astudillo, et al. 2002. “Defective Prelamin A Processing and Muscular and Adipocyte Alterations in Zmpste24 Metalloproteinase–Deficient Mice.” *Nature Genetics* 31 (1): 94–99. https://doi.org/10.1038/ng871.

Pérez-Mancera, Pedro A., Andrew R. J. Young, and Masashi Narita. 2014. “Inside and out: The Activities of Senescence in Cancer.” *Nature Reviews Cancer* 14 (8): 547–58. https://doi.org/10.1038/nrc3773.

Picelli, Simone, Omid R Faridani, Åsa K Björklund, Gösta Winberg, Sven Sagasser, and Rickard Sandberg. 2014. “Full-Length RNA-Seq from Single Cells Using Smart-Seq2.” *Nature Protocols* 9 (1): 171–81. https://doi.org/10.1038/nprot.2014.006.

Pospelova, Tatyana V., Zoya N. Demidenko, Elena I. Bukreeva, Valery A. Pospelov, Andrei V. Gudkov, and Mikhail V Blagosklonny. 2009. “Pseudo-DNA Damage Response in Senescent Cells.” *Cell Cycle* 8 (24): 4112–18. https://doi.org/10.4161/cc.8.24.10215.

Qiu, Xiaojie, Qi Mao, Ying Tang, Li Wang, Raghav Chawla, Hannah A Pliner, and Cole Trapnell. 2017a. “Reversed Graph Embedding Resolves Complex Single-Cell Trajectories.” *Nature Methods* 14 (10): 979–82. https://doi.org/10.1038/nmeth.4402.

———. 2017b. “Reversed Graph Embedding Resolves Complex Single-Cell Trajectories.” *Nature Methods* 14 (10): 979–82. https://doi.org/10.1038/nmeth.4402.

Ramsköld, Daniel, Shujun Luo, Yu-Chieh Wang, Robin Li, Qiaolin Deng, Omid R Faridani, Gregory A Daniels, et al. 2012. “Full-Length MRNA-Seq from Single-Cell Levels of RNA and Individual Circulating Tumor Cells.” *Nature Biotechnology* 30 (8): 777–82. https://doi.org/10.1038/nbt.2282.

Rayess, Hani, Marilene B. Wang, and Eri S. Srivatsan. 2012. “Cellular Senescence and Tumor Suppressor Gene P16.” *International Journal of Cancer* 130 (8): 1715–25. https://doi.org/10.1002/ijc.27316.

Ritchie, Matthew E., Belinda Phipson, Di Wu, Yifang Hu, Charity W. Law, Wei Shi, and Gordon K. Smyth. 2015. “Limma Powers Differential Expression Analyses for RNA-Sequencing and Microarray Studies.” *Nucleic Acids Research* 43 (7): e47–e47. https://doi.org/10.1093/nar/gkv007.

Rossi, L., R. Manfredini, F. Bertolini, D. Ferrari, M. Fogli, R. Zini, S. Salati, et al. 2007. “The Extracellular Nucleotide UTP Is a Potent Inducer of Hematopoietic Stem Cell Migration.” *Blood* 109 (2): 533–42. https://doi.org/10.1182/blood-2006-01-035634.

Rousseeuw, Peter J. 1987. “Silhouettes: A Graphical Aid to the Interpretation and Validation of Cluster Analysis.” *Journal of Computational and Applied Mathematics* 20 (November): 53–65. https://doi.org/10.1016/0377-0427(87)90125-7.

Rudolph, K. L., S Chang, M Millard, N Schreiber-Agus, and R A DePinho. 2000. “Inhibition of Experimental Liver Cirrhosis in Mice by Telomerase Gene Delivery.” *Science* 287 (5456): 1253–58. https://doi.org/10.1126/science.287.5456.1253.

Rudolph, K L, S Chang, H W Lee, M Blasco, G J Gottlieb, C Greider, and R A DePinho. 1999. “Longevity, Stress Response, and Cancer in Aging Telomerase-Deficient Mice.” *Cell* 96 (5): 701–12. https://doi.org/10.1016/s0092-8674(00)80580-2.

Salotti, Jacqueline, Matheus H. Dias, Marianna M. Koga, Hugo A. Armelin, and IH Kang. 2013. “Fibroblast Growth Factor 2 Causes G2/M Cell Cycle Arrest in Ras-Driven Tumor Cells through a Src-Dependent Pathway.” Edited by Antimo Migliaccio. *PLoS ONE* 8 (8): e72582. https://doi.org/10.1371/journal.pone.0072582.

Sandre-Giovannoli, A. De, Rafaëlle Bernard, Pierre Cau, Claire Navarro, Jeanne Amiel, Irène Boccaccio, Stanislas Lyonnet, et al. 2003. “Lamin A Truncation in Hutchinson-Gilford Progeria.” *Science* 300 (5628): 2055–2055. https://doi.org/10.1126/science.1084125.

Scaffidi, Paola, and Tom Misteli. 2008. “Lamin A-Dependent Misregulation of Adult Stem Cells Associated with Accelerated Ageing.” *Nature Cell Biology* 10 (4): 452–59. https://doi.org/10.1038/ncb1708.

Serrano, M, A W Lin, M E McCurrach, D Beach, and S W Lowe. 1997. “Oncogenic Ras Provokes Premature Cell Senescence Associated with Accumulation of P53 and P16INK4a.” *Cell* 88 (5): 593–602. http://www.ncbi.nlm.nih.gov/pubmed/9054499.

Sinha, Jitendra Kumar, Shampa Ghosh, and Manchala Raghunath. 2014. “Progeria: A Rare Genetic Premature Ageing Disorder.” *The Indian Journal of Medical Research* 139 (5): 667–74. http://www.ncbi.nlm.nih.gov/pubmed/25027075.

Soria-Valles, Clara, Fernando G. Osorio, Ana Gutiérrez-Fernández, Alejandro De Los Angeles, Clara Bueno, Pablo Menéndez, José I. Martín-Subero, George Q. Daley, José M. P. Freije, and Carlos López-Otín. 2019. “Retraction Note: NF-KB Activation Impairs Somatic Cell Reprogramming in Ageing.” *Nature Cell Biology* 21 (3): 410–410. https://doi.org/10.1038/s41556-018-0259-0.

Subramanian, A., P. Tamayo, V. K. Mootha, S. Mukherjee, B. L. Ebert, M. A. Gillette, A. Paulovich, et al. 2005. “Gene Set Enrichment Analysis: A Knowledge-Based Approach for Interpreting Genome-Wide Expression Profiles.” *Proceedings of the National Academy of Sciences* 102 (43): 15545–50. https://doi.org/10.1073/pnas.0506580102.

Sullivan, T, D Escalante-Alcalde, H Bhatt, M Anver, N Bhat, K Nagashima, C L Stewart, and B Burke. 1999. “Loss of A-Type Lamin Expression Compromises Nuclear Envelope

Integrity Leading to Muscular Dystrophy." *The Journal of Cell Biology* 147 (5): 913–20. http://www.ncbi.nlm.nih.gov/pubmed/10579712.

Taimen, Pekka, Katrin Pfleghaar, Takeshi Shimi, Dorothee Möller, Kfir Ben-Harush, Michael R Erdos, Stephen A Adam, et al. 2009. "A Progeria Mutation Reveals Functions for Lamin A in Nuclear Assembly, Architecture, and Chromosome Organization." *Proceedings of the National Academy of Sciences of the United States of America* 106 (49): 20788–93. https://doi.org/10.1073/pnas.0911895106.

Teo, Yee Voan, Nattaphong Rattanavirotkul, Nelly Olova, Angela Salzano, Andrea Quintanilla, Nuria Tarrats, Christos Kiourtis, et al. 2019. "Notch Signaling Mediates Secondary Senescence." *Cell Reports* 27 (4): 997-1007.e5. https://doi.org/10.1016/j.celrep.2019.03.104.

Ventura, Andrea, David G. Kirsch, Margaret E. McLaughlin, David A. Tuveson, Jan Grimm, Laura Lintault, Jamie Newman, Elizabeth E. Reczek, Ralph Weissleder, and Tyler Jacks. 2007. "Restoration of P53 Function Leads to Tumour Regression in Vivo." *Nature* 445 (7128): 661–65. https://doi.org/10.1038/nature05541.

Wang, Jing, Suhas Vasaikar, Zhiao Shi, Michael Greer, and Bing Zhang. 2017. "WebGestalt 2017: A More Comprehensive, Powerful, Flexible and Interactive Gene Set Enrichment Analysis Toolkit." *Nucleic Acids Research* 45 (W1): W130–37. https://doi.org/10.1093/nar/gkx356.

Watson, J D. 1972. "Origin of Concatemeric T7 DNA." *Nature: New Biology* 239 (94): 197–201. http://www.ncbi.nlm.nih.gov/pubmed/4507727.

Witten, Daniela M., and Robert Tibshirani. 2010. "A Framework for Feature Selection in Clustering." *Journal of the American Statistical Association* 105 (490): 713–26. https://doi.org/10.1198/jasa.2010.tm09415.

Xue, Wen, Lars Zender, Cornelius Miething, Ross A Dickins, Eva Hernando, Valery Krizhanovsky, Carlos Cordon-Cardo, and Scott W Lowe. 2007. "Senescence and Tumour Clearance Is Triggered by P53 Restoration in Murine Liver Carcinomas." *Nature* 445 (7128): 656–60. https://doi.org/10.1038/nature05529.

Zhuang, D, S Mannava, V Grachtchouk, W-H Tang, S Patil, J A Wawrzyniak, A E Berman, et al. 2008. "C-MYC Overexpression Is Required for Continuous Suppression of Oncogene-Induced Senescence in Melanoma Cells." *Oncogene* 27 (52): 6623–34. https://doi.org/10.1038/onc.2008.258.

Herbig et al., 2004; Beauséjour et al., 2003

Lee By: Senescence-associated beta-galactosidase is lysosomal beta-galactosidase.

Takaoka et al., 2004 Ha-RasG12V induces senescence in primary and immortalized human esophageal keratinocytes with p53 dysfunction

Rapisarda V, Borghesan M, Miguela V, Encheva V, Snijders AP, Lujambio A, O'Loghlen A. Integrin Beta 3 regulates cellular senescence by activating the TGF-beta pathway. Cell Rep 2017; 18:2480-93;

PMID:28273461; http://dx.doi.org/10.1016/j.celrep.2017.02.012 [PMC free article] [PubMed] [CrossRef] [Google Scholar]

High-level expression of Mastermind-like 2 contributes to aberrant activation of the NOTCH signaling pathway in human lymphomas

Appendix

Table S1: Presence of Construct and qPCR Primer.

https://www.ncbi.nlm.nih.gov/pmc/articles/PMC6486482/bin/mmc4.xlsx

Table S2: Alignment Rates and Quality Control of RNA Sequencing Data.

https://www.ncbi.nlm.nih.gov/pmc/articles/PMC6486482/bin/mmc2.xlsx

Table S3: Differential Expression of RNA Sequencing Data.

https://www.ncbi.nlm.nih.gov/pmc/articles/PMC6486482/bin/mmc3.xlsx

Table S4: Genes for Venn Diagrams.

https://www.ncbi.nlm.nih.gov/pmc/articles/PMC6486482/bin/mmc5.xlsx